*Ai miei genitori.*

# Ringraziamenti

*Queste poche righe che ho scritto non possono certo racchiudere tutte le soddisfazioni, le esperienze ed i momenti che ho passato in questi tre anni. Tuttavia, posso cercare di ringraziare tutte le persone che mi hanno fatto crescere e che mi hanno dato una mano per affrontare al meglio le sfide che mi si sono poste davanti. Come d'obbligo, è giusto partire dal ringraziare i miei superiori, il Prof. Benedetto Allotta ed il Dott. Ing. Andrea Rindi, dato che se loro non avessero creduto in me all'inizio probabilmente non avrei intrapreso il dottorato di ricerca. Sono loro che mi hanno permesso di accrescere il mio bagaglio di esperienze sia professionali che personali. Un altro ringraziamento particolare lo devo al mio co-tutor di dottorato, il Dott. Ing. Enrico Meli, che è stato sempre un esempio da seguire e che mi ha fatto apprezzare la ricerca con la "R" maiuscola. Infine, l'ultimo ringraziamento che voglio fare non è ad una persona, ma ad un gruppo: il gruppo di lavoro in cui sono stato accolto tre anni fà. Questo gruppo è mutato negli anni e molti colleghi che c'erano all'inizio adesso non ci sono più. Esso è composto da persone molto diverse tra loro che, tuttavia, hanno unito le loro competenze e professionalità per la riuscita dei progetti di robotica sottomarina che sono finiti, stanno procedendo o che sono in fase di partenza. Di tutti, quelli che mi sento di ringraziare uno per uno perchè oltre che colleghi sono anche amici con cui ho condiviso più esperienze sono Alessandro Ridolfi, Enrico Meli e Riccardo Costanzi. Al loro aiuto devo anche la riuscita delle esperienze che ho riportato in questa tesi.*

# Contents

# Introduction

This chapter introduces the issues characterizing the underwater autonomous manipulation performed by Intervention-Autonomous Underwater Vehicles (I-AUVs). This Ph.D. dissertation will explicitly deal with the development and control of a small AUV for inspection and cooperative tasks in which the sensors for the localization and communication are relatively low cost.
As concerns the research activity, the thesis is mainly focused on the analysis of cooperative control strategy for I-AUVs; however, the study started from the idea to reduce the general complexity of the system. This concept is highly applied to the development of the innovative cooperative mobile manipulation architecture.
Therefore, this research study consists of two main contributions: in the first part, the development and testing of the real small AUV of the MDM Lab (University of Florence) are shown and, in the second part, a cooperative control strategy for I-AUVs is presented and simulated.
To highlight the importance of this research topic, a brief state of the art of the AUVs and of the I-AUVs is presented. Then, the formulation of the problem statement and the structure of the thesis are carried out.

**State of the art:**

In the last decades, the interest in the underwater environment is rapidly increased due to the commercial and military fields [1],[6]; many research efforts have been devoted to the development of underwater robotics [1],[3],[5] because of the need for exploring and preserving the oceanic environments. The Unmanned Underwater Vehicles (UUVs) can be divided in:

- Remotely Operated Vehicles (ROVs): they are tele-operated vehicles, that can be used to perform underwater inspection and intervention missions (being a mobile platform for sensors and manipulators);

- Autonomous Underwater Vehicles (AUVs): they are autonomous vehicles, which are used as mobile platforms that can undertake underwater survey and inspection missions without human interaction.

The classical ROV system is a very complex system [3],[5] because different

parts are strictly connected: the pilot controls the ROV from the control station which is installed on the mother ship (with the necessity of the dynamical positioning of the ship), the Launch And Recovery System (LARS) is used to immerse the ROV, the cage is where the ROV is located during the diving, and finally, the ROV (see Figure 1). The main motivations to reduce the use of ROVs are mainly the following:

- high operational costs (approximatively 8000 euro per day);
- large crew and specialized mother vessel (dynamical positioning);
- operator fatigue (even with auto-heading, auto-depth, etc.);
- time-delay in human-machine interaction (loss of precision).

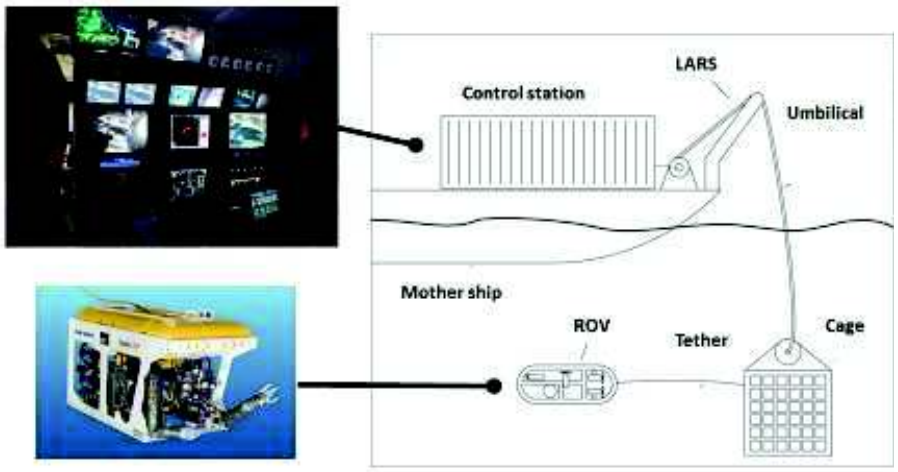


Figure 1: Complete architecture of the ROV system

The other UUVs are the Autonomous Underwater Vehicles. Also in this case, AUVs can be substantially divided into two main classes: observation and intervention. Currently, the observation AUVs are the major part of the operating vehicles, classically used for the recognition, the exploration and the patrolling. The observation AUV is provided of cameras and acoustic sensors able to localize itself and to navigate. The main applications of these robotic systems are deep water (adverse conditions for communication to surface), under ice (inaccessible area for surface vehicles) or nuclear plant fuel rod storage tanks (hazardous environment).

The AUVs for intervention, usually called Intervention-AUVs (I-AUV) or Autonomous Underwater Vehicle-Manipulator System (A-UVMS), are robotic systems in which a robotic manipulator is installed on an autonomous vehicle. These kinds of systems, which are usually characterized by a high degree of


Figure 2: Commercial AUVs

redundancy, combine the manipulability of a fixed-base manipulator with the mobility of a mobile platform. Such systems allow the most usual missions of robotic systems which require both motion and manipulation abilities.
An underwater vehicle equipped with manipulator system is particularly useful and plays an important role in most of the underwater manipulation tasks, such as underwater pipeline welding, mining, drilling, underwater cable burial, and military applications. Its application has intensified the research interest in the development of the control systems for A-UVMS. However, the presence of hydrodynamic effects makes the control problem of A-UVMS a challenging task. Particularly, modelling of the A-UVMS can be found in [2],[4] and [7]. In [8], a control law for tracking of a desired motion trajectory for an A-UVMS has been proposed, where an observer has been designed to provide estimation of velocities used by the control law. Several force control schemes for A-UVMS have been presented in [9] and [10]. In [11], a solution to the problem of redundancy solution and motion coordination between vehicle and manipulator by using fuzzy technique has been presented. In [4],[12], feedback linearization control has been proposed for an underwater vehicle-manipulator systems, where the exact dynamical model is assumed to be known. In [13], the underwater vehicle-manipulator system has been partially decoupled and the control scheme compensates only part of the nonlinear coupling effects. Although the control complexity was reduced, partial knowledge of dynamical model is still required. To overcome parametric uncertainties on the UVMS, adaptive controllers have been introduced in [14]. However, these controllers require a regressor of the dynamical model which includes the inertia matrix, Coriolis and centrifugal forces, hydrodynamic damping, gravity and buoyancy force. In underwater applications, the number of the dynamical parameters of the UVMS to be updated by the adaptive law is very large and hence is too complex to be implemented.
In the same direction, coordinated control of multiple mobile manipulators has attracted the attention of many researchers [20],[21] (Figure 3). The interest in such systems stems from the capability for carrying out complex and dexterous

tasks which cannot be simply made using a single robot. Main coordination schemes for multiple mobile manipulators in the literature are: Leader–follower control and hybrid position–force one. The leader–follower control for mobile manipulator is the approach where one, or a group, of mobile manipulators plays the role of a leader (which tracks a preplanned trajectory) and the rest of the mobile manipulators forms the follower group which move in conjunction with the leader [23],[24]. In [25], a leader-follower type formation control is designed for a group of mobile manipulators. To overcome parameter uncertainties in the model of the robot, a decentralized control law is applied to individual robots, in which an adaptive model is used to online model robot dynamics. The hybrid position–force control can use both decentralized and

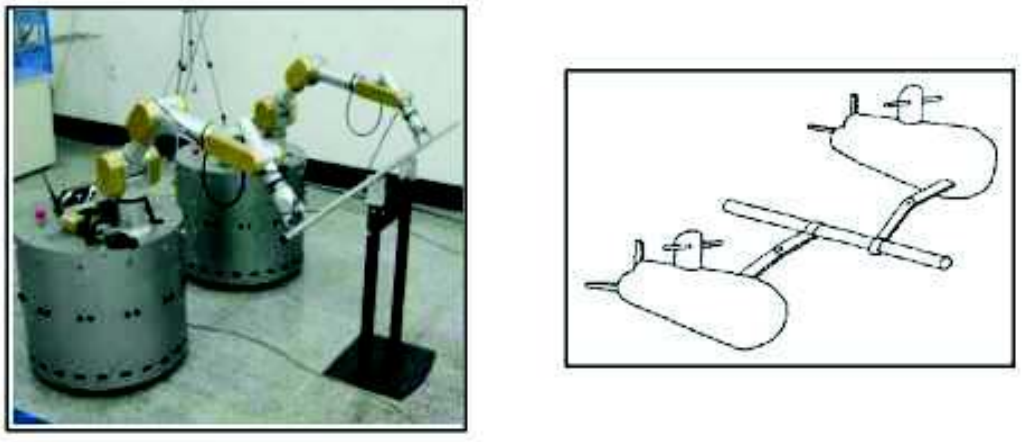

Figure 3: Application of Cooperative Mobile Manipulation for terrestrial robots and UVMSs

centralized scheme; the position of the object is controlled in a certain direction of the workspace and the internal forces of the object are controlled in a small workspace [20], [21]. In [26], robust adaptive controls of multiple mobile manipulators carrying a common object in a cooperative manner have been investigated with unknown inertial parameters and disturbances. At first, a concise dynamics consisting of the dynamics of mobile manipulators and the geometrical constraints between the end-effectors and the object is developed for coordinated multiple mobile manipulators. In [27] coupled dynamics are presented for two cooperating mobile manipulators manipulating an object with relative motion in the presence of uncertainties and external disturbances. Centralized robust adaptive controls are introduced to guarantee the motion and force trajectories of the constrained object. A simulation study to the decentralized dynamical control for a robot collective (consisting of non-holonomic wheeled mobile manipulators) is performed in [28], by tracking the trajectories of the load, where two reference signals are used for each

robot, one for the mobile platform and another for the end-effector.
According to the state of the art presented for cooperative mobile manipulators, cooperative manipulation of A-UVMS is another new and important capability for extending the domain of underwater robotics applications. This research interest stems great benefits and advantages when multiple A-UVMS are used to perform cooperative tasks. For example, multiple cooperative small A-UVMS can be used to move objects easily and conveniently, action that cannot be performed by a single A-UVMS (due to the object size and weight constraints). Cooperative A-UVMS can also be used in various underwater assembly tasks such as underwater structure construction and maintenance; underwater pipeline and cable transportation can be easily carried out by multiple cooperative A-UVMS; underwater search and rescue tasks shall be more efficient and effective if multiple A-UVMS are used.

**Problem statement:**

Underwater robotics is an interesting and challenging field in which many problems including navigation, guidance and control are strictly connected. This research activity focuses on the development and control of a small AUV for inspection and cooperative tasks; in addition, an innovative control architecture for cooperative mobile manipulation is proposed. Both these studies involve different problems:

- guidance and control: the AUV/I-AUV has to autonomously operate considering the dynamical effects of the interactions between vehicle and manipulator;
- cooperation: the cooperation between vehicles can be faced off through a centralized or a decentralized approach;
- communication: in the underwater environment, the acoustic communication between vehicles is quite complex and can introduce delays, disturbances and low efficiency;
- localization: the localization task among vehicles is onerous in terms of necessary sensors (e.g. Long Base Line, Ultra Short Base Line, etc.) and can introduce drift effects.

The projects which actually deal with the A-UVMS development and control use centralized approach, starting from the idea of a single I-AUV in which all the sensors and the dexterous capacities are centralized. The concept behind our research activity is the reduction of the single I-AUV characteristics and performance thanks to the implementation of an I-AUV swarm.
The study about the development and control of AUVs for inspection tasks and cooperative mobile manipulation can be divided in two main phases:

1. development and testing of a small AUV able to communicate with other AUVs and to operate observation tasks: in this phase all the aspects of the vehicle are involved, from the design to the control architecture;

2. modelling and analysis of cooperative I-AUVs: in this part the innovative control architecture based on the potential field method will be presented and simulated.

In the following, the structure of the research activity is described:

- chapter 1: it deals with the modelling techniques used for Autonomous Underwater Vehicle particularly focused on the specific designed vehicle;

- chapter 2: the main design phases of the real small AUV of the MDM Lab are described;

- chapter 3: it is focused on the control architecture implemented on board of the vehicle. In addition, both the computer vision algorithm and the acoustic localization system are deeply explained;

- chapter 4: the numerical simulations and the experimental results obtained for the AUV during the Student Autonomous Underwater vehicle Challenge Europe 2013 (SAUC-e) competition are shown. The tasks are simulated both in the Matlab environment and in the ROS-UWSim one.

As concerns the second part of the thesis:

- chapter 5: it introduces the state of the art of the I-AUVs and of the cooperative mobile manipulation. In this chapter also the modelling techniques used for I-AUV and the control strategies implemented are deeply described;

- chapter 6: the innovative cooperative control architecture based on potential field method is described;

- chapter 7: it shows the preliminar results in terms of numerical simulations for the proposed control strategy.

# Chapter 1

# Feelhippo AUV: Analytical model

Modelling of underwater vehicles involves the analysis of kinematics and dynamics of the rigid body in the underwater environment. This study deals the motion of underwater vehicles in 6 degrees of freedoms (DOFs) since 6 independent coordinates are necessary to determine the position and orientation of a rigid body. In the following sections, using the classical SNAME (Society of Naval Architects and Marine Engineers) notation, the description of the kinematical and the dynamical equations is carried out.
The kinematical and dynamical models are then applied to MDM AUV, considering all the characteristics of the vehicle (geometry, masses, inertias, etc.).

## 1.1 AUV kinematic model

The kinematical analysis of an underwater vehicle can be based on the definition of two reference frames (Figure 1.1):

- **"Body" frame** $< b >$ **:** reference frame with its origin $O^b$ in the center of mass of the vehicle (body) and axes aligned with the inertia principle axes of the body itself. $x^b$ axis is the longitudinal one, positive according to the vehicle advancement, $z^b$ axis vertical and pointing down and $y^b$ axis to compose with the others a dexterous reference frame;

- **"Fixed" frame** $< n >$**:** inertial reference frame, with its origin $O^n$ on the surface and axes aligned with the ones of a NED (North-East-Down) frame. $x^n$ axis points North, $y^n$ axis points Est and $z^n$ Down.

According to SNAME nomenclature the underwater motion of the vehicle can be described using:

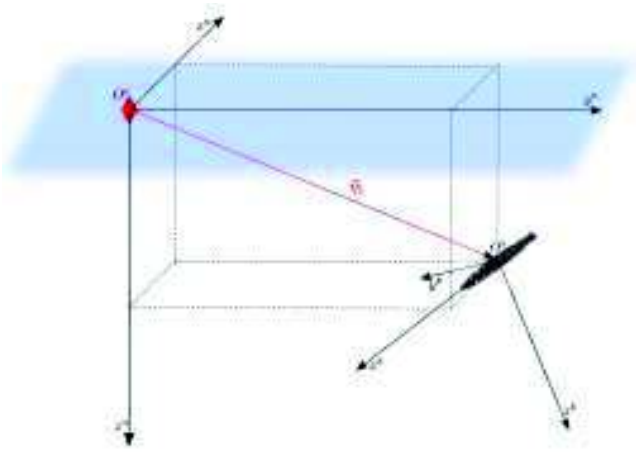

Figure 1.1: Body frame $< b >$ and fixed frame $< n >$

$$\begin{aligned}
\vec{\eta} &= \left[\vec{\eta}_1^{\top}\ \vec{\eta}_2^{\top}\right]^{\top} \quad \text{with} \quad \vec{\eta}_1 = [x\ y\ z]^{\top} \quad \vec{\eta}_2 = [\varphi\ \vartheta\ \psi]^{\top} \\
\vec{\nu} &= \left[\vec{\nu}_1^{\top}\ \vec{\nu}_2^{\top}\right]^{\top} \quad \text{with} \quad \vec{\nu}_1 = [u\ v\ w]^{\top} \quad \vec{\nu}_2 = [p\ q\ r]^{\top} \\
\vec{\tau} &= \left[\vec{\tau}_1^{\top}\ \vec{\tau}_2^{\top}\right]^{\top} \quad \text{with} \quad \vec{\tau}_1 = [X\ Y\ Z]^{\top} \quad \vec{\tau}_2 = [K\ M\ N]^{\top},
\end{aligned} \tag{1.1}$$

where $\vec{\eta}$ represents the position ($\vec{\eta}_1$) and orientation ($\vec{\eta}_2$) vector with respect to the fixed frame$< n >$, $\vec{\nu}$ components are the linear ($\vec{\nu}_1$) and angular ($\vec{\nu}_2$) speeds as to the body frame $< b >$, while $\vec{\tau}$ is the vector of the linear forces ($\vec{\tau}_1$) and the torques ($\vec{\tau}_2$) applied to the vehicle as to the body frame $< b >$. The vehicle's coordinates relative to the earth-fixed coordinate system is given by a velocity transformation:

$$\dot{\vec{\eta}}_1 = R_b^n\left(\vec{\eta}_2\right)\ \vec{\nu}_1\ , \tag{1.2}$$

where $R_b^n\left(\vec{\eta}_2\right)$ is the transformation matrix between $< b >$ and $< n >$. This matrix is function of the Euler angles RPY $[\varphi, \vartheta, \psi]^T$ and can be expressed in:

$$R_b^n\left(\vec{\eta}_2\right) = \begin{bmatrix} c_\psi c_\vartheta & -s_\psi c_\varphi + c_\psi s_\vartheta s_\varphi & s_\psi s_\varphi + c_\psi c_\varphi s_\vartheta \\ s_\varphi c_\vartheta & c_\psi c_\varphi + s_\psi s_\vartheta s_\varphi & -c_\psi s_\varphi + s_\psi c_\varphi s_\vartheta \\ -s_\vartheta & s_\varphi c_\vartheta & c_\varphi c_\vartheta \end{bmatrix}\ , \tag{1.3}$$

where, for simplicity,

$$c_\alpha = cos\left(\alpha\right)\ ,\ s_\alpha = sin\left(\alpha\right)\ . \tag{1.4}$$

As regards the orientation part, the relation between $< b >$ and $< n >$ is the following:

$$\dot{\vec{\eta}}_2 = T_b^n\left(\vec{\eta}_2\right)\ \vec{\nu}_2\ , \tag{1.5}$$

where the transformation matrix $T_b^n(\vec{\eta_2})$ is defined in terms of Euler angles:

$$T_b^n(\vec{\eta_2}) = \frac{1}{c_\vartheta}\begin{bmatrix} c_\vartheta & s_\varphi s_\vartheta & c_\varphi s_\vartheta \\ 0 & c_\varphi c_\vartheta & -c_\vartheta s_\varphi \\ 0 & s_\varphi & c_\varphi \end{bmatrix}. \tag{1.6}$$

It is worth to note in (1.6) the presence of a singularity for $\vartheta = (2n+1)\frac{\pi}{2}$, with $n \in \mathbb{N}$ . This problem can be solved using a redundant representation of the orientation, e.g. the quaternions.
Finally, it is possible to describe the relation between $\dot{\vec{\eta}}$ and $\vec{\nu}$ using the following expression:

$$\dot{\vec{\eta}} = J_b^n(\vec{\eta_2})\ \vec{\nu}\ , \tag{1.7}$$

where

$$J_b^n(\vec{\eta_2})\ = \begin{bmatrix} R_b^n(\vec{\eta_2}) & 0_{3\times3} \\ 0_{3\times3} & T_b^n(\vec{\eta_2}) \end{bmatrix}. \tag{1.8}$$

Through the Equation (1.7), the relations can be written in that terms:

$$\begin{aligned} \dot{\vec{\eta}} &= J_b^n\,\vec{\nu} && \Leftrightarrow \quad \vec{\nu} = (J_b^n)^{-1}\ \dot{\vec{\eta}} \\ \ddot{\vec{\eta}} &= J_b^n\,\dot{\vec{\nu}} + \dot{J}_b^n\,\vec{\nu} && \Leftrightarrow \quad \dot{\vec{\nu}} = (J_b^n)^{-1}\ \left(\ddot{\vec{\eta}} - \dot{J}_b^n\,(J_b^n)^{-1}\,\dot{\vec{\eta}}\right)\ . \end{aligned} \tag{1.9}$$

## 1.2 AUV dynamical model

In the following section, we will show that the 6 DOF nonlinear dynamic equations of motion can be conveniently expressed as:

$$M\dot{\vec{\nu}} + C(\vec{\nu})\,\vec{\nu} + D(\vec{\nu})\,\vec{\nu} + \vec{g}(\vec{\eta}) = \vec{\tau} + \vec{\tau}_E\ , \tag{1.10}$$

where

- $\mathbf{M}$ = inertia matrix;
- $\mathbf{C}(\tilde{\nu})$ = matrix of Coriolis and centripetal terms;
- $\mathbf{D}(\tilde{\nu})$ = damping matrix;
- $\mathbf{g}(\tilde{\eta})$ = vector of gravitational forces and torques;
- $\tilde{\tau}$ = vector of control inputs;
- $\tilde{\tau}_{\mathbf{E}}$ = vector of environmental terms;

Particularly, this equation is the result of the superposition effect between the hydrodynamic damping, the buoyancy forces and added inertia matrix because:

$$M = M_{RB} + M_A \tag{1.11}$$

$$C = C_{RB} + C_A \quad , \tag{1.12}$$

where $M_A$ and $C_A$ are the inertia and the Coriolis matrix due to the surrounding fluid and $M_{RB}$ and $C_{RB}$ are related to the rigid body.
According to the hypothesis that the center of gravity $CG$ is coincident with the origin $O^b$ in the body frame $< b >$, the inertia matrix $M_{RB}$ is equal to:

$$M_{RB} = \begin{bmatrix} m & 0 & 0 & & & \\ 0 & m & 0 & & 0_{3\times3} & \\ 0 & 0 & m & & & \\ & & & I_{xx} & 0 & 0 \\ & 0_{3\times3} & & 0 & I_{yy} & 0 \\ & & & 0 & 0 & I_{zz} \end{bmatrix}, \tag{1.13}$$

where $m$ is the vehicle mass and $I_{ii}$ is the inertia moment with respect to the $i$-th axes. With the same hypothesis, also for the $C_{RB}$ matrix it is possible to obtain a simplified form:

$$C_{RB} = \begin{bmatrix} 0 & -mr & mq & & & \\ mr & 0 & -mp & & 0_{3\times3} & \\ -mq & mp & 0 & & & \\ & & & 0 & I_{zz}r & -I_{yy}q \\ & 0_{3\times3} & & -I_{zz}r & 0 & I_{xx}p \\ & & & I_{yy}q & -I_{xx}p & 0 \end{bmatrix}. \tag{1.14}$$

The hydrodynamical effects applied on a rigid body mainly consist in two contributions:

- Added masses and inertias: this contribute is related to the inertia of the fluid which is accelerated together with the vehicle;
- Hydrodynamical resistance: this contribute deals with the forces due to the viscosity of the fluid.

As regards the statical effects that are caused both by the gravity and the buoyancy effects, they are usually called *restoring forces*.
The concept of added mass is usually misunderstood to be a finite amount of water connected to the vehicle such that the vehicle and the fluid represents a new system with mass larger than the original system. This is not true since the vehicle motion will force the whole fluid to oscillate with different fluid particle amplitudes in phase with the forced harmonic motion of the vehicle. However, the amplitudes will decay far away from the body and may therefore be negligible. Added mass should be understood as pressure induced forces and moments due to to the acceleration of the body.
According to the hypothesis that the vehicle is completely submerged and it

has three planes of symmetry, it is possible to neglect the contribution from the off-diagonal elements in the added mass matrix. The following simple expressions for $M_A$ and $C_A$ are obtained:

$$M_A = -\text{diag}\left\{X_{\dot{u}}, Y_{\dot{v}}, Z_{\dot{w}}, K_{\dot{p}}, M_{\dot{q}}, N_{\dot{r}}\right\} \ , \tag{1.15}$$

where the hydrodynamic force of the added mass $Y_A$ along the $y$ axes is caused by an acceleration $\dot{u}$ in the $x$ direction:

$$Y_A = Y_{\dot{u}}\dot{u} \ , \quad \text{con} \quad Y_{\dot{u}} = \frac{\partial Y}{\partial \dot{u}} \ . \tag{1.16}$$

$M_A$ is strictly positive since the rigid boy is completely submerged.
The $C_A$ matrix is antisymmetrical and function of the velocity:

$$C_A = \begin{bmatrix} 0 & 0 & 0 & 0 & -Z_{\dot{w}}w & Y_{\dot{v}}v \\ 0 & 0 & 0 & Z_{\dot{w}}w & 0 & -X_{\dot{u}}u \\ 0 & 0 & 0 & -Y_{\dot{v}}v & X_{\dot{u}}u & 0 \\ 0 & -Z_{\dot{w}}w & Y_{\dot{v}}v & 0 & -N_{\dot{r}}r & M_{\dot{q}}q \\ Z_{\dot{w}}w & 0 & -X_{\dot{u}}u & N_{\dot{r}}r & 0 & -K_{\dot{p}}p \\ -Y_{\dot{v}}v & X_{\dot{u}}u & 0 & -M_{\dot{q}}q & K_{\dot{p}}p & 0 \end{bmatrix} \ . \tag{1.17}$$

**Hydrodynamical resistance**
As regard the hydrodynamical resistance, the viscosity of the the fluid imposes a resultant force during a relative motion between rigid body and surrounding fluid, whose intensity depends on many factors (the relative speed, the shape and the sizes of the body, the fluid characteristics). This contribution is traditionally divided in the parallel component to the direction of motion (Drag force) and in the orthogonal component (Lift force). Both Drag and Lift forces are calculated integrating the stress on the wall caused by the viscosity (friction contribution) and by the local pressure of the fluid (shape contribution). In the case of small autonomous robots, assuming motions along the principal axes directions, lift forces can be reasonably neglected (even by the absence of control surfaces, e.g. wings or rudders).
The damping effect caused by the Drag forces is significant for the study of the dynamical behaviour of an underwater vehicle. The reason is the important contribution on the non-linearity part in the equations of motion. Usually, a simplification hypothesis is made: the considered forces are only with the addiction of linear and quadratic speed. That case, for a totally submerged body and characterized by three planes of symmetry, the Hydrodynamic damping matrix $D\left(\vec{\nu}\right)$ is diagonal and defined positive, given by:

$$\begin{aligned} D = &- \text{diag}\left\{X_u, Y_v, Z_w, K_p, M_q, N_r\right\} + \\ &- \text{diag}\left\{X_{u|u|}\left|u\right|, Y_{v|v|}\left|u\right|, Z_{w|w|}\left|w\right|, K_{p|p|}\left|p\right|, M_{q|q|}\left|q\right|, N_{r|r|}\left|r\right|\right\} \ . \end{aligned} \tag{1.18}$$

Assuming a diagonal form for the damping matrix means neglecting the coupling of the dissipative terms: this is reasonable if the speeds are not high as in the case of small autonomous robots, typically lower than 4 knots.

**Restoring forces**

The $\vec{g}(\vec{\eta})$ term that appears in the equation of motion (1.10) is the result of a combination of gravity and buoyancy forces. The buoyancy force is the vertical contribute agenting on an immersed body (the pressure resultant acting on its surface) and it is independent from the relative motion between the vehicle and the fluid (hydrostatic effect). It is possible to define the vector $\vec{g}^n$ as the gravitational acceleration expressed according to the vector:

$$\vec{g}^n = [0 \;\; 0 \;\; 9.81]^\top \, \mathrm{m/s^2} \; . \tag{1.19}$$

Assuming that $V_{rb}$ is the vehicle volume (totally surrounded), $m$ is the mass and $\rho_a$ is the local density of water, the module of the weight force is $\left\|\vec{W}\right\|$ and the module of the buoyancy force $\left\|\vec{B}\right\|$ are given by:

$$\begin{aligned} W &= \left\|\vec{W}\right\| = m \left\|\vec{g}^n\right\| \\ B &= \left\|\vec{B}\right\| = \rho_a V_{rb} \left\|\vec{g}^n\right\| \; , \end{aligned} \tag{1.20}$$

with both forces directed along the axis $z^n$ in opposite way. The weight force $\vec{f}_G^b$ expressed in the $< b >$ tern, applied in the center of mass of the vehicle coincides with the origin of $< b >$ obtaining:

$$\vec{f}_G^b = R_n^b \begin{bmatrix} 0 \\ 0 \\ W \end{bmatrix} \; , \tag{1.21}$$

where $R_n^b$ is the inverse transformation compared with (1.3) equal to $R_n^b = (R_b^n)^\top$.
The buoyancy force $\vec{f}_B^b$ defined in the body reference frame $< b >$ is:

$$\vec{f}_B^b = -R_n^b \begin{bmatrix} 0 \\ 0 \\ B \end{bmatrix} \; . \tag{1.22}$$

That force is applied to center of buoyancy defined as $\vec{r}_B^b$:

$$\vec{r}_B^b = \begin{bmatrix} x_B^b & y_B^b & z_B^b \end{bmatrix}^\top \; . \tag{1.23}$$

Then, the vector $\vec{g}(\vec{\eta})$ assumes the following form:

$$\vec{g}(\vec{\eta}) = \begin{bmatrix} \vec{f}_G^b + \vec{f}_B^b \\ \vec{r}_B^b \times \vec{f}_B^b \end{bmatrix} \; , \tag{1.24}$$

where "$\times$" is the vector product.
Specifying the $\vec{g}(\vec{\eta})$ vector in the $< b >$ reference frame, the following expression is obtained:

$$\vec{g}(\vec{\eta}) = \begin{bmatrix} \left(||\vec{W}|| - ||\vec{B}||\right) s_\vartheta \\ -\left(||\vec{W}|| - ||\vec{B}||\right) c_\vartheta s_\varphi \\ -\left(||\vec{W}|| - ||\vec{B}||\right) c_\vartheta c_\varphi \\ y_B^b \, ||\vec{B}|| \, c_\vartheta c_\varphi - z_B^b ||\vec{B}|| \, c_\vartheta s_\varphi \\ -z_B^b \, ||\vec{B}|| \, s_\vartheta - x_B^b ||\vec{B}|| \, c_\vartheta c_\varphi \\ x_B^b \, ||\vec{B}|| \, c_\vartheta s_\varphi + y_B^b ||\vec{B}|| \, s_\vartheta \end{bmatrix} , \tag{1.25}$$

**Environmental effects**
An important factor which is necessary to take into account to obtain a realistic vehicle simulation is the modelling of the environmental effects, e.g. marine currents. The currents are generated by several factors (including the wind, the heat exchange near to the free surface and the Earth's rotation) can be a significant problem in the small AUV navigation. The problem is the high velocities of the ocean currents, able to reach up to $2 \div 3\,\mathrm{m/s}$, compared with the vehicle velocities that rarely exceeds $0.4 \div 0.5\,\mathrm{m/s}$.
To include the marine current effects in the equation of motion (1.10), it is assumed that the same equation can be rewritten in terms of relative velocity $\vec{\nu_r}$:

$$\vec{\nu_r} = \vec{\nu} - \vec{\nu}_c \quad . \tag{1.26}$$

where $\vec{\nu}_c = [u_c, v_c, w_c, 0, 0, 0]^T$ is the relative velocity (supposed irrotational)expressed in the $< b >$ body reference frame.
This vector can be calculated from the decomposition of the marine current velocity expressed in the $< n >$ fixed term, $\vec{\mathrm{V}}_c = \left[u_c^E, v_c^E, w_c^E\right]^T$ where "E" is referred to *Earth*) through the rotation matrix $R_n^b$ (1.3):

$$\begin{bmatrix} u_c \\ v_c \\ w_c \end{bmatrix} = R_n^b \begin{bmatrix} u_c^E \\ v_c^E \\ w_c^E \end{bmatrix} \quad . \tag{1.27}$$

Making the hypothesis of slow variable marine current velocities:

$$\dot{\vec{\nu}}_c = \vec{0} \quad \Rightarrow \quad \dot{\vec{\nu}}_r = \dot{\vec{\nu}} \quad , \tag{1.28}$$

the equation of motion expressed in marine current reference frame are obtained.

$$M\dot{\vec{\nu}}_r + C(\vec{\nu}_r)\,\vec{\nu}_r + D(\vec{\nu}_r)\,\vec{\nu}_r + \vec{g}(\vec{\eta}) = \vec{\tau} \, . \tag{1.29}$$

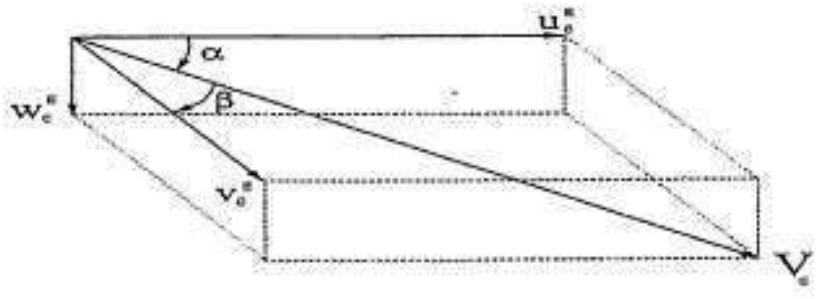


Figure 1.2: Decomposition of the marine current velocity in the NED reference frame $x^n$, $y^n$, $z^n$

## 1.3 MDM AUV model

In this section, the main kinematical and dynamical characteristics for the MDM AUV vehicle (presented in the Chapter 2) are described. This part is very important to correctly correlate the real AUV and the AUV model. Moreover, this was an iterative process in order to in parallel proceed with the prototype building and the AUV model.

Figure 1.3: FeelHippo vehicle: model and real vehicle

### 1.3.1 Vehicle characteristics

The vehicle is approximatively a cylinder and its sizes are the following:

- L=350 [mm]
- R=105 [mm]

The mass vehicle is obtained starting from the hypothesis of 1% hydrostatically positive (emerging) and the inertia matrix is calculated from the CAD software for that specific mass:

$$\begin{aligned} I_x &= 0.6832\ [kgm^2] \\ I_y &= 0.5707\ [kgm^2] \\ I_z &= 1.1413\ [kgm^2] \end{aligned} \tag{1.30}$$

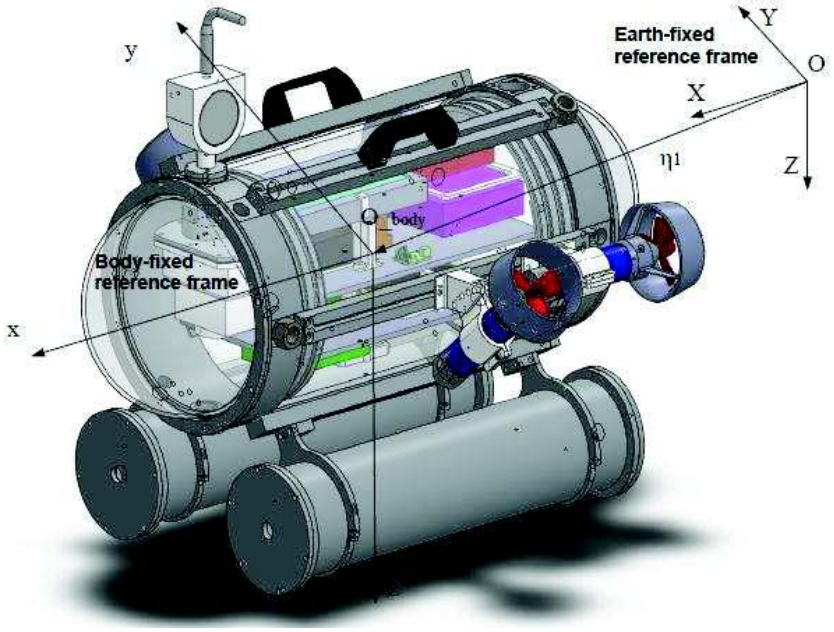


Figure 1.4: Vehicle reference frames

### 1.3.2 Propeller models

The vehicle has four brushless motors Maxon EC motor with a power of 100 W able to perform 4 DOFs (x,y,z,yaw). The characteristics of the motor define a rated speed of 28600 rpm/min with a maximum torque of 43, 6 mNm. Two of these motors are arranged in the vehicle rear part and they are used to move the vehicle both in the longitudinal and in the yaw directions. The other two engines are laterally installed with an inclination of 30 degrees with respect to the horizontal plane; that way, they permit both the lateral and the vertical movement. Usually, defining for an under-actuated 4DOFs vehicle, the vector $\vec{\tau}_L = [F_x\ F_y\ F_z\ M_x\ M_y\ M_z]^T$ containing the forces and the torques applied on the vehicle in the body reference frame $< b >$ and the thruster vector $\vec{S} = [S_1\ S_2\ S_3\ S_4]^T$, it is possible to define the relations between these generalized forces and the thruster vector:

$$\vec{\tau}_L = B\vec{S} \tag{1.31}$$

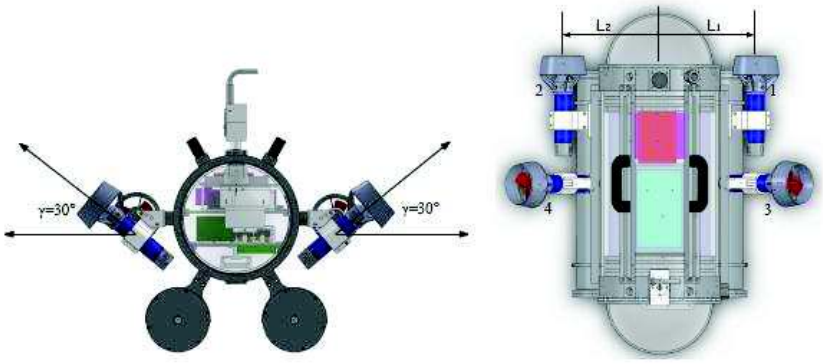


Figure 1.5: Vehicle frontal and lateral views

with the propeller matrix is

$$B = \begin{bmatrix} \vec{v}_1 & \vec{v}_2 & \vec{v}_3 & \vec{v}_4 \\ \vec{P}_{m1} \times \vec{v}_1 & \vec{P}_{m2} \times \vec{v}_2 & \vec{P}_{m3} \times \vec{v}_3 & \vec{P}_{m4} \times \vec{v}_4 \end{bmatrix} \tag{1.32}$$

where $\vec{P}_{mi}$ for $i = 1$ *to* 4 is the propeller position vector in body reference frame and $v_i$ for $i = 1$ *to* 4 is the unitary vector of the thrust directions.

### 1.3.3 Camera models

In this part, the main models used for the camera modelling are presented. A camera can be seen as a device that maps the 3D Euclidean space into a 2D image. This mathematical relation is characteristic for every camera and permits to connect input and output of the sensor. Usually, the main models to simulate a camera are the following:
**Pinhole model**: this model is based on the principle in which the image of a generic point $\vec{P}$ is transformed into an image on the screen plane only through a single ray of light which crosses a small hole. The main drawbacks of this simplified model are the high sensitivity to the hole size and the low quality of the image. where $z_c$ is the optical axes of the camera, $f$ is the focal distance, $O_c$ is the camera reference system, $O_m$ is the image reference frame, $\vec{P} = [x_c y_c z_c]^T$ is the point in the 3D space and $\vec{p} = [xy]^T$ is the projection of the point on the camera reference frame. The analytical relation between the 3D space and the 2D one is performed by the Calibration matrix $K$:

$$\tilde{p} = \begin{bmatrix} fX_c \\ fY_c \\ Z_c \end{bmatrix} = \begin{bmatrix} f & 0 & 0 \\ 0 & f & 0 \\ 0 & 0 & 1 \end{bmatrix} \begin{bmatrix} X_c \\ Y_c \\ Z_c \end{bmatrix} = K\vec{P} \tag{1.33}$$

where $K$ depends on real characteristics of the sensor.
**CCD Full perspective model**: this accurate model introduces many pa-

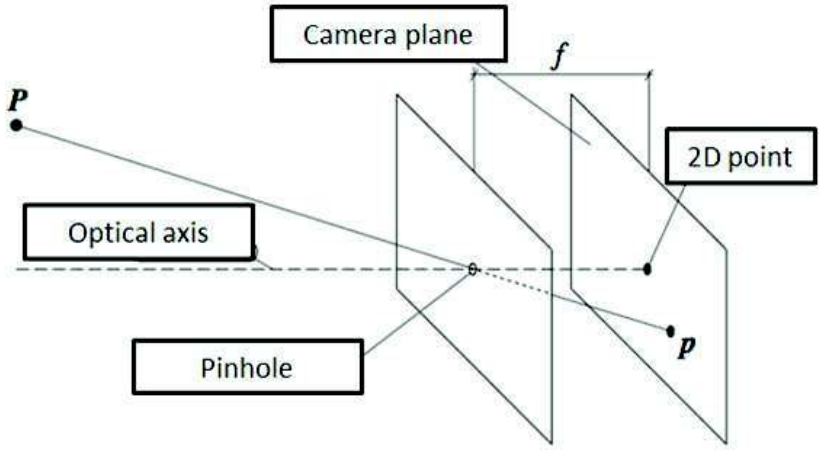


Figure 1.6: Basic pinhole model

rameters in order to better simulate the camera behaviour:

$$\tilde{p} = \begin{bmatrix} f\alpha_x & f\alpha_x \cot(\phi) & x_0 \\ 0 & f\alpha_x / \sin(\phi) & y_0 \\ 0 & 0 & 1 \end{bmatrix} \vec{P} \tag{1.34}$$

where $\alpha_x$ and $\alpha_y$ is the number of pixel per unity, $\phi$ is the pixel angle, $\alpha_x \cot(\phi)$ is the skew parameter and $\alpha_x/\alpha_y$ is the aspect ratio.
After a brief description of the main camera models, it is necessary to find the camera characteristics parameters to correctly model the Philips SPZ 5000 camera (Calibration phase). Usually, the calibration techniques consist to find the proper correspondence between a rigid grid points and their position on the camera plane. Considering a 3D point $\vec{P}_0$ of the calibration grid fixed to the $< o >$ reference frame, it is possible to describe the transformation through:

$$\begin{bmatrix} \vec{P} \\ 1 \end{bmatrix} = \begin{bmatrix} R_0^C & \vec{t}_0^C \\ 0^T & 1 \end{bmatrix} \begin{bmatrix} \vec{P}_0 \\ 1 \end{bmatrix} \tag{1.35}$$

where $R_0^C$ and $\vec{t}_0^C$ are respectively the rotation matrix and the translation vector from the $< o >$ reference frame to the $< c >$ camera frame. Using the full perspective model it is possible to define:

$$\vec{p} = K \begin{bmatrix} R_0^C & \vec{t}_0^C \end{bmatrix} \begin{bmatrix} \vec{P}_0 \\ 1 \end{bmatrix} = Q \begin{bmatrix} \vec{P}_0 \\ 1 \end{bmatrix} \tag{1.36}$$

where $\vec{p}$ is the $\vec{P}_0$ projection on the camera frame. The $Q$ matrix is defined as *camera projection matrix*. The calibration problem is replaced by the calculation of the $Q$ matrix: using the correspondence between the grid points

and the camera plane ones, it is possible to define the following homogeneous linear system:

$$L_1 \vec{A} = 0, \tag{1.37}$$

where the coefficient matrix $L \in \Re^{2x12}$ and the vector $\vec{A}$ are:

$$\vec{L_1} = \begin{bmatrix} X_0 & Y_0 & Z_0 & 1 & 0 & 0 & 0 & 0 & -uX_0 & -uY_0 & -uZ_0 & -u \\ 0 & 0 & 0 & 0 & X_0 & Y_0 & Z_0 & 1 & -vX_0 & -vY_0 & -vZ_0 & -v \end{bmatrix}, \tag{1.38}$$

$$\vec{A} = \begin{bmatrix} q_{11} & q_{12} & q_{13} & q_{14} & q_{21} & q_{22} & q_{23} & q_{24} & q_{31} & q_{32} & q_{33} & q_{34} \end{bmatrix}. \tag{1.39}$$

Using a grid with a point number $N >> 6$, it is possible to define a homogeneous linear system:

$$\vec{L}\vec{A} = 0, \tag{1.40}$$

with a coefficient matrix $\vec{L} \in \Re^{2N*12}$. The linear system can be solved using optimization techniques (Singular Value Decomposition).
Particularly, after a brief description on the theoretical approach, the camera calibration phase of the AUV is carried out with the MATLAB®Camera Calibration toolbox. The phases realized to calibrate the camera can be synthesized in the following steps: firstly, a grid is built and then twenty photos are acquired. Then, starting from the acquired photos, the number of points

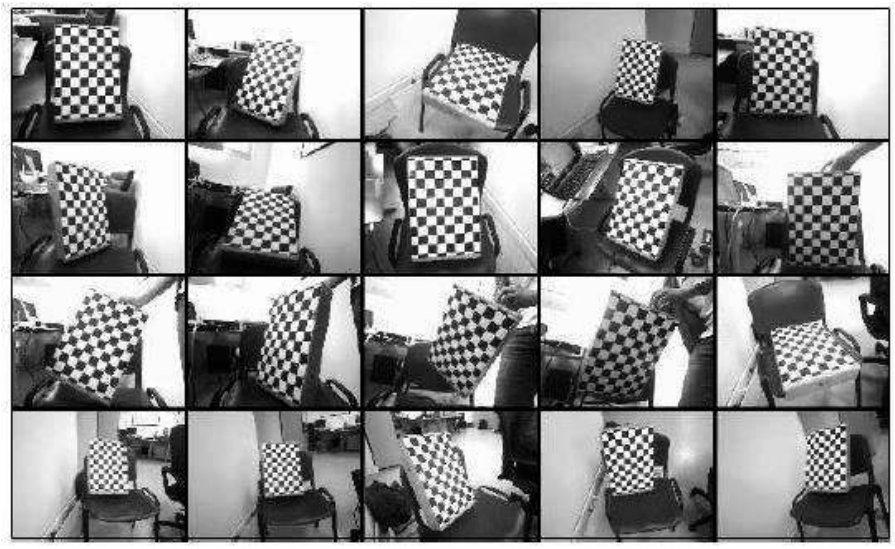

Figure 1.7: Grid for the calibration phase

of interests are compared among the real grid and the camera image grid (Figure 1.7-1.8). The calibration procedure allows ,through an optimization method, the finding of the camera characteristic parameters able to exactly coincide each grid point with the grid point on the camera image. The real characteristic parameters of the SPZ5000 camera are described in Table 1.1.

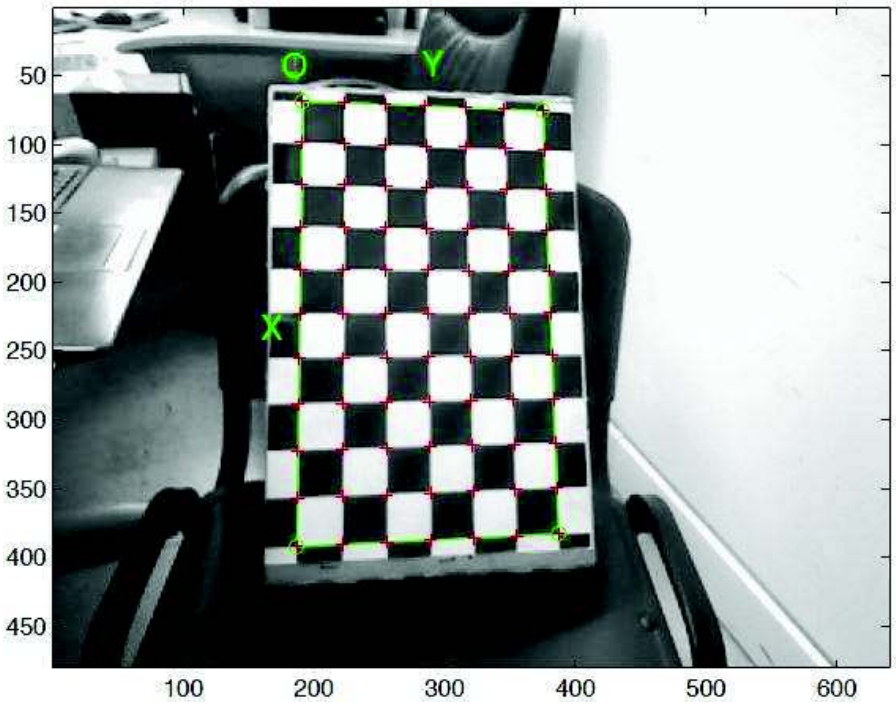


Figure 1.8: Points of interest

| **Parameters** | **Value** |
|---|---|
| $f\alpha_x$ | 492 pixel |
| $f\alpha_y$ | 493 pixel |
| $x_0$ | 323 pixel |
| $y_0$ | 243 pixel |
| $\phi$ | 90 degree |

Table 1.1: Characteristics camera parameters

# Chapter 2

# Feelhippo AUV: Design

In this chapter, the main design phases of the MDM Lab AUV (internally called Feelhippo) are presented. The design of the whole vehicle deals two main parts: the mechanical design part and the electronic one. The mechanical design phase faces the problems due to the required watertightness of the vehicle; as concern the electronic part, the main issues are related to the electrical scheme building and the connection of the electronic devices. The project of the new Autonomous Underwater Vehicle (AUV) is strictly connected to the attending to the European competition SAUC-e 2013 and it started at the end of the summer 2012. Both the experience acquired by the University of Florence team during the SAUC-e 2012 and the 2013 competition rules suggested the following main key points for the new vehicle:

- easiness of assembly;
- easiness of access to the internal instruments;
- electrical safe solution, thanks to the 24V supply;
- high number of sensors to acquire many different variables;
- acoustic modem inside, in order to cooperate with vehicle.

These key points allow the use of the new AUV in many different applications from the classical inspection phase in harbours to complex tasks in cooperation with other vehicles. In addition, the development of this low-cost vehicle is carried out considering the possibility to build other AUVs to create a swarm of homogeneous vehicles to perform cooperation tasks.

## 2.1 Mechanical design

The design phase of the mechanical parts starts with the description of the maximum sizes of the vehicle and the list of the sensors to be implemented. The main sensors to be introduced are:

- cameras: one or more cameras to perform visual tasks;
- Inertial Measurement Unit (IMU) with gyroscopes to properly evaluate the acceleration and the orientation of the vehicle;
- acoustic hydrophones to evaluate the distance from acoustic pinger;
- depth sensor;
- echo-sounder, an acoustic device measuring the distance from object.

AUV's central body (Figure 2.1) is a plexiglass pipe that contains the instrumental hardware, except for the batteries that are located inside the two Al pipes under the main body. At the ends of the plexiglass body there are two domes, made in plexiglass too, connected with the first one by structural Al parts. These parts are connected together with six Al profiles that work as tie rods, to get a compact frame. The profiles also connect all the external parts with the main body. The Al pipes, representing the "feets" of the vehicle, are welded with two aluminium flanges; these pipe ends are enclosed by two Al circular caps, connected with 6 screws. Each "foot" is supported by two Al semicircles that connect it to a tie rod. Other parts, e.g. the propellers, the depth sensor and LED illuminators, are connected to the main structure by specific plastic (ABS) supports obtained with the 3D printer for rapid prototyping of the MDM Lab. The main components of the vehicle (the plexiglass pipe and the tie rods) are verified through the Finite Element Methods (Figure 2.2-2.3) and the results in terms of deformations and stresses are lower than the material and the project limits. The internal arrangement of the electronic components is evaluated in terms of static stability of the vehicle (Archimede effect). The internal balancing is made to obtain the center of gravity (CG) lower than the center of thrust. The vehicle has two plexiglass shelves to increase the easiness of intervention and to reduce the Electro-Magnetics (EM) disturbances between the sensors and the motor drivers (Figure 2.4-2.5).
The 4 LiPo batteries are placed inside the "feet" to obtain a low center of gravity and to facilitate their extraction for charging: this is possible only by removing one of the end caps.

As concerns the other devices, in the front part of the vehicle there is an echo-sounder sensor. Close to the echo there are 3 LEDs able to illuminate the water; this solution allows the front camera to get good pictures. In the rear part of the vehicle there are, instead, the depth sensor, the strobe light (required by the rules) and another LED light, that illuminates the seabed so that the other camera pointing down can work well. Next to the strobe light there is the acoustic modem.
The external components of the vehicle are: the propellers, the echo-sounder, the depth sensor, the acoustic idrophones, the acoustic modem emitter and the LEDs. In Figure 2.6, the propeller, the echo-sounder and the acoustic modem


Figure 2.1: Vehicle parts

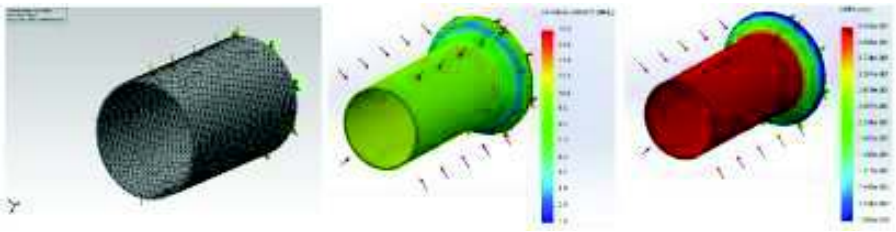

Figure 2.2: pipe FEM test

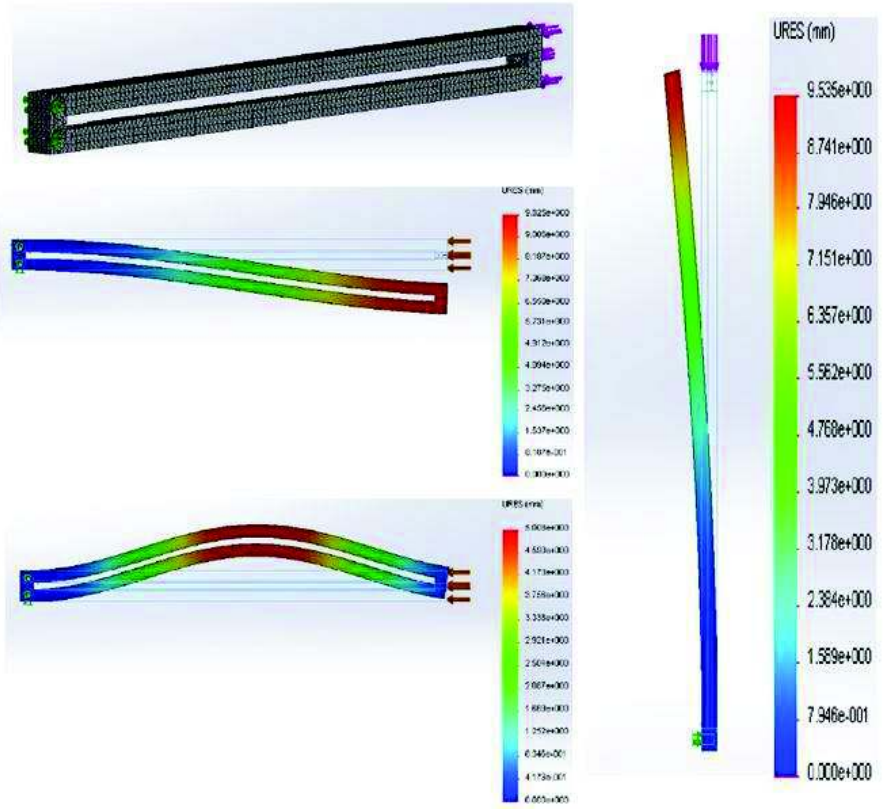


Figure 2.3: rod FEM test

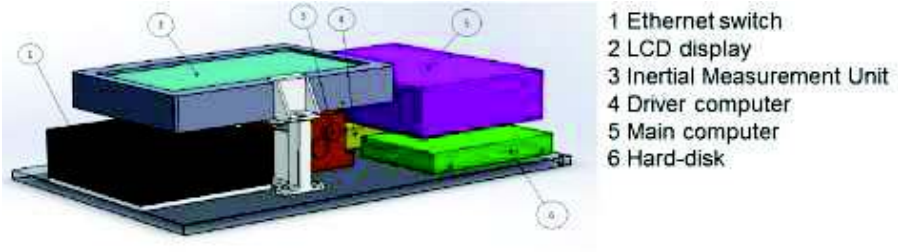


Figure 2.4: Upper shelf

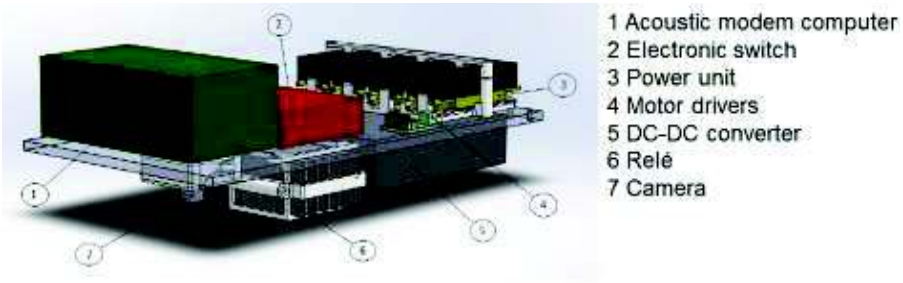


Figure 2.5: Lower shelf

emitter are shown. The echo-sounder is installed on a rotating shaft controlled by a servomotor; this way, the echo-sounder can acquire with a 360° range. The acoustic emitter is placed in upper part of the vehicle. In Figure 2.7, the arrangement of the leds and of the hydrophones are shown. In the following,

Figure 2.6: External components: propeller, echo-sounder and acoustic modem emitter

a list of the components installed in the vehicle is made:

- Xsens IMU;
- Netgear switch;
- LCD display;
- Micro Maestro electronic board for motor control;

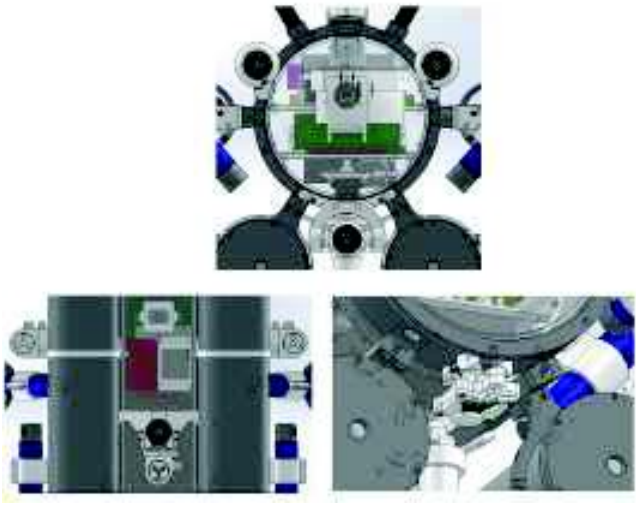

Figure 2.7: External components: leds and hydrophones

- Commell SBC;
- Raspberry Pi;
- Flex board.

And, on the bottom plate there are, instead:

- acoustic modem board;
- DC-DC converter (24V-12V);
- relay;
- motor drivers;
- lower camera.

In Figure 2.8, the whole 3D CAD of the vehicle with the final arrangement is shown. The motion of the AUV is given by 4 propellers controlling 4 DOFs of the vehicle (x-y-z-yaw):

- two of these are mounted like a V-engine, to mainly control the depth and the lateral movement;
- the other two are horizontal, one per side, to control the longitudinal advancing direction and the yaw angle.

The structure of the vehicle guarantees:

- the lower parts already guarantee with their shape stability to roll;

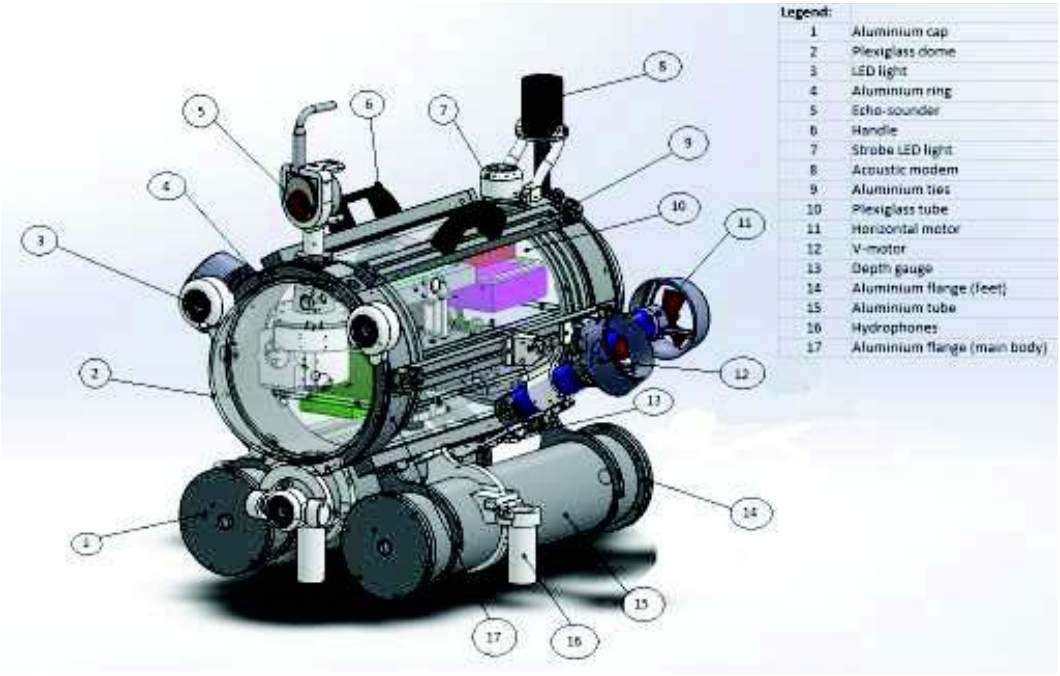


Figure 2.8: Vehicle CAD design

- low weight (about 25 kg);
- low cost.

The wet tests for the external components are evaluated at the MDM Lab pool. The results of these tests shown the watertightness of the whole body and the electrical connections between the outside and the inside of the vehicle (see Figure 2.9-2.10).

Figure 2.9: External view of the vehicle

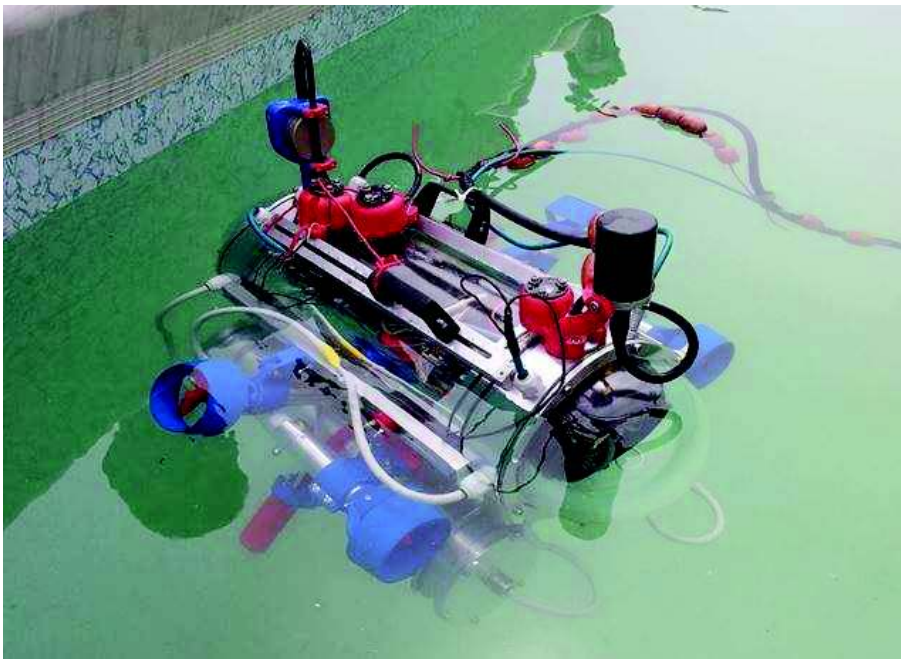

Figure 2.10: Vehicle in MDM Lab pool

## 2.2 Electronics design

The vehicle is equipped with four 22.2V LiPo batteries placed in the vehicle feet and connected in parallel before the entrance in the main hull. Each battery can deliver 8Ah for a total onboard energy of about 710 Wh. All the onboard modules are supplied by this voltage bus, directly or after a suitable DC-DC converter. The present voltage levels are two, the main one at 24V and the derived one at 12V. The devices working at 5V (XSens, USB cameras, hyrophones, etc.) are connected to proper output pins of the Commell SBC. The four batteries can be disconnected through a contact controlled by a magnetic switch. It is thus possible to turn on and off the AUV just touching the hull with a magnet.
Some of the AUV devices are managed by the onboard Raspberry Pi. Through a program running on it, the status of the GPIO is managed to control the illuminators and the strobe light. The Raspberry Pi is also used as interface with the LCD screen that shows the values of FeelHippo status variables (Figure 2.11). The Raspberry Pi is integrated in the overall vehicle architecture, from a hardware point of view, by means of an ethernet connection. Whereas, from a software point of view, the ROS system on Raspberry Pi works with the ROScore on the Commell board, the main PC, that represents the master machine. The motor drivers control is performed through the Micro Maestro control board.

Figure 2.11: Internal view of the vehicle

### 2.2.1 Propelling system

The AUV has 4 electric brushless Maxon motors. The chosen model is the sensorless, EC 22 brushless 100 Watt (Figure 2.12). Despite its small dimensions and low weight this motor provides quite a high torque, also through a

Maxon Planetary Gearhead (reduction 3.8:1). Each motor is controlled by a ROXXY BL 940-6 controller. The control signal is provided to each controller by the Micro Maestro control board, converting the PC output into the motor command. As regard the mechanical part of the propeller,a dedicated software to design the propellers is used. The blade profiles have been drawn starting from the desired thrust as a function of the motor angular speed.

Figure 2.12: Vehicle propeller

### 2.2.2 Sensors

In the following, a list of the components installed on the vehicle is carried out.

#### 2.2.2.1 AHRS - Xsens MTi

The MTi Xsens contains 3D gyroscopes, accelerometers and magnetometer (Figure 2.13). The internal low-power digital signal processor runs a real-time proprietary sensor fusion algorithm providing drift-free 3D orientation data. The sensor datasheet ensures a RMS dynamic accuracy of 2 degrees. Additionally, 3D dynamic data are given by the gyroscopes, accelerometers and magnetometer, so that it will be possible during experimental phases to compare the performances of the proprietary algorithm with the algorithms implemented by the team. This will allow to verify the validity of the results of simulations carried out by the team. The sensor is plugged to the main PC through a USB port for both data exchange and power supply. An on site calibration procedure will be necessary for the characterization of the local magnetic field disturbances and, compensating them, to work properly. The MTi Xsens is already equipped with a software tool for this procedure.


Figure 2.13: Inertial Measurement Unit

#### 2.2.2.2 Pressure sensor - MS5535-CM

To measure the local pressure, the MS5535-CM sensor from Measurement Specialties Inc. has been chosen (Figure 2.14). The MS5535-CM is a 16bit digital sensor with an operating range up to 14 bar. The sensor is soldered on a little board built by the team and drowned in the resin with the board itself to isolate all the electric contacts from the water. The sensor communicates through a serial protocol via USB with the main PC. The sensor is also equipped with a temperature sensor to compensate the pressure measurement error.

Figure 2.14: Pressure sensor

#### 2.2.2.3 Webcam - Philips SPZ5000

One webcam is mounted inside the frontal transparent dome, another one is instead placed in the lower part of the main hull, pointing down. All the tasks can be faced thanks to this position of the optical sensors. The cameras are the SPZ5000 by PHILIPS, chosen especially for its brightness (maximum aperture is F:2.6), for its wide angle of 80 degrees in air (water will reduce it) and for its resolution of 1.3 MP (Figure 2.15). The cameras are plugged to the main PC through a USB connection for both data transmission and power supply.

#### 2.2.2.4 Echo Sounder - Imagenex 852

An Imagenex 852 is mounted on the front part of the vehicle, able of rotating around its vertical axis, used to measure the distance of the vehicle from

Figure 2.15: Camera sensor

obstacles and for localization purposes. It will have a basic role during all the competition time slot for real-time localization based on wall detection. The localization will be particularly useful in the intermediate stages between a task and the following one when no references in the environment, such as buoys or the structure, may be unidentifiable. This will be also useful in the wall survey sub-task where the distance (>2 m) to be kept between the vehicle and the wall is enough to make impossible the use of cameras. The sensor is characterized by a conical transducer with a 10° beam width, a 8bit resolution and an adjustable maximum range between 5 m and 50 m (Figure 2.16). The sensor is plugged to the main PC via RS232 port, whereas the power is supplied by the battery bus (22-30 VDC required).

Figure 2.16: Imagenex echo-sounder

#### 2.2.2.5 Acoustic Modem - SeaModem by AppliCon

The vehicle has the AppliCon acoustic modems as mean of communication to perform cooperation tasks. The modems are cheaper than all the other mar-

ket available solutions of comparable performance evaluated in other vehicles. The dimensions of the electronic board are quite small, a basic feature for the integration on board the AUV (Figure 2.17). Despite of the tiny dimensions and the low cost, the data bit rate is quite high. The modems work with the FSK technique up to 8 tones to increase the data bit rate (up to 2250 bits/sec). The working frequency of the transducer is 40 kHz.

Figure 2.17: Seamodem by Applicon

# Chapter 3

# Feelhippo AUV: Control architecture

In this chapter the general architecture of the AUV control system is shown. In the following, a detailed description of the architecture main functions will be explained. At the end, the chapter will introduce the computer vision part and the localization algorithm.

## 3.1 Control architecture

The operating system of the vehicle is Robot Operating System (ROS), which is a meta-operating system based on Linux core. The software runs on two Linux based machines (the Commell SBC and the Raspberry Pi) and, in order to simplify the programming activity, it is split in several applications linked together through the ROS operating system. This approach offers some advantages: first of all debugging is easier because the code is divided in small and focused modules, and, last but not least, it is available online a lot of code developed by the ROS community, also for the interface with several devices, e.g. the XSens IMU. In figure 3.1, the general architecture is shown. The software is organized in levels; starting from the top, the highest level deals with communication and decision management issues. It is mainly composed of a node for the acoustic modem and a mission selector node that basically is a state machine that chooses the sub-task to be performed on the basis of the inputs coming from the external environment through the on board sensors. The intermediate level contains a node for each competition task; these nodes select the more suitable trajectory generator and controller nodes for the related task. The low level contains, instead, nodes that work between control and hardware driver nodes. These are, e.g., algorithms for the position estimation, target finding and thrust distribution among the FeelHippo propellers. Finally, at the lowest level there are all the driver nodes that act as interface between the system and the various devices. This architecture represents the

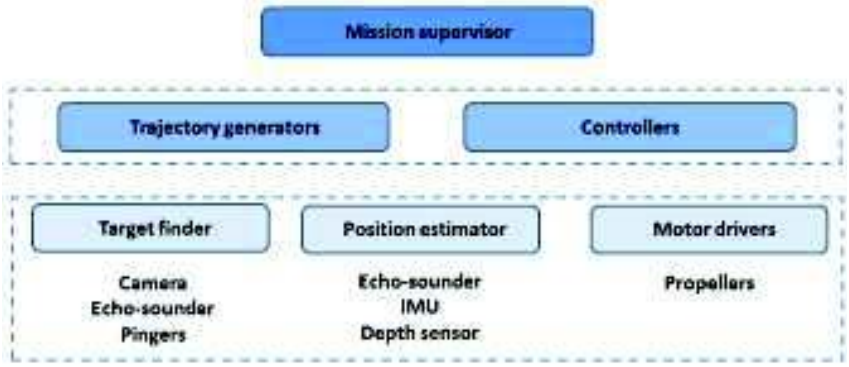


Figure 3.1: Control architecture scheme

system core as concerns the modules essential to face the task issues; in addiction there are more nodes that operate across the various software levels, for instance the logging node and the watchdog node. The first one logs every message exchanged between processes, whereas the watchdog supervises the status of all nodes and reboots them in case of potential crash. Another important node, which is not running on the vehicle, is the remote control interface. It is a QT based ROS node executed on a remote PC, connected to Hippo via an Ethernet cable. It is very useful to drive FeelHippo in ROV mode, especially during the testing and the debugging phases.
This control architecture is completely developed in ROS and, through the Underwater Simulator environment (created by the ROS community), the single nodes are preliminarily tested and simulated to reduce the debugging phase.

### 3.1.1 Computer Vision algorithm

The computer vision software is based on the open source OpenCv libraries and on the framework Qt4. The use of customized algorithms permits to maximize the information coming from the cameras and to easily change the task performed.
The development of a customizable visual software is one of the key points necessary to perform different tasks in observation mode; in addition, a particular algorithm able to individuate underwater structures is implemented (to participate with this AUV to the European competition SAUC-e 2013). The algorithm used to determine underwater structures is based on the the analysis of the Hue Saturation Value (HSV) color space: the ratio of a particular color presents in the image is as a discriminant of the presence of the object (see Figure 3.2). The libraries used to recognize the buoys are the cvBlob which are very well optimized to determine the shapes with high contrast. In order to monitor the frequency of the light source is possible to reduce the size of the analyzed image and increasing the frame rate. This algorithm based on

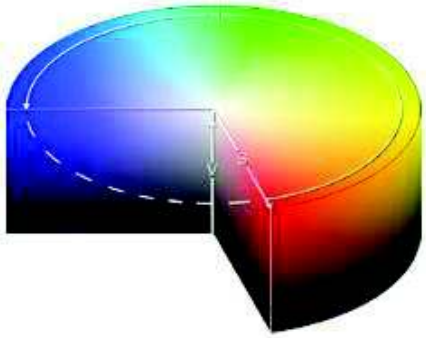

Figure 3.2: Hue Saturation Value color space

the HSV analysis is used to execute different tasks:

- Underwater structure inspection: the vehicle starts the inspection when the desired percentage of yellow is reached. The maintenance of the desired distance is also based on this quantity of yellow.
- Underwater anomaly identification: for the detection of the anomaly and the gate buoys, the HSV method is again used, considering their red color (see Figure 3.3). The algorithm is tuned up to eliminate the whole area in the frequency domain excepted the small area containing the anomaly. The size of this area, determines the sensitivity to the anomaly, which can be detected by counting the white pixels in the image.

Figure 3.3: Underwater anomaly

According to the hypothesis of a single camera control strategy, the main errors used in the control algorithms are:

- Yellow ratio error: this error is defined to easily evaluate the distance from the object. Supposing to know the object sizes and the RGB camera matrix, it is possible to define a ratio between the yellow part of the image (the target) and the blue one (the rest of the image) that is proportional to a well defined camera-object distance. Therefore, this ratio is defined reference ratio. The yellow ratio error is the error between the reference ratio and the actual ratio.

- Image centering error: this error is used to maintain the frontal direction of the vehicle pointed toward the object; for this error, it is necessary to find the coordinates of the Center of Mass of the yellow shape in the camera reference frame. These information provide the indications to move the vehicle in the lateral direction and in the yaw one.

## 3.2 Acoustic localization system

The acoustic localization system for an AUV is one of the most critical part of the vehicle, because it is usually based on very expensive sensors (USBL, LBL, DVL, etc.). The development of an acoustic localization system using a rotating single beam echo-sounder, allows the vehicle localization in structured environments (such as harbours, shipwrecks, etc.) but reduces the cost of the vehicle. Part of the on board hardwares has been designed and built to be suitable for the data acquisition and for the on-line estimation of the vehicle position.
In particular, the vehicle is equipped with an Imagenex 852 ultra-miniature echo-sounder; the angular position of the sensor, around its vertical axis, can be controlled through a servo motor mounted inside the vehicle hull (see Figure 3.4). The Imagenex 852 is an active SONAR sensor with a piezoelectric transducer that is used both to generate the acoustic pulse and to receive the echo. The acoustic pulse generated by the piezoelectric transducer is a sine wave at a frequency of 675 kHz for a duration of 1-150 microseconds. The form of the beam is conical with an amplitude of 10 °. The sensor samples the received echo in 250 samples related to 250 relative distances, the measurement noise is due to multiple causes:

- quantization error;
- measurement noise of the piezoelectric transducer;
- intrinsic noise of the environment.

The noise level has to be considered in relation to the intensity echo return through the signal to noise ratio SNR(Signal Noise Ratio). The attenuation of the echo is only minimally due to attenuation of the acoustic waves ($2.17 * 10^{-3}$ dB/m); in case of maximum range of 50 m, you should have an attenuation of $-0.217$ dB: from this point on it is assumed that the wave attenuation is negligible and therefore that the energy is constant. The obtained system is comparable to a normal mechanical scanning sonar but its total price is much lower. In Figure 3.4 the final prototype carried out by MDM Lab is shown. The compact motor chosen is the Dynamixel AX-18. The shown solution, with limited sizes, does not permit to house the whole device outside the vehicle hull. Thus, the final prototype of the echo-sounder is located in part inside the


Figure 3.4: The rotating echo-sounder

hull, but, nevertheless, it is easily adaptable to different vehicles. The support is composed of three parts: one Al pipe, to fix the sonar to the vehicle and containing two oil seals to prevent the water coming into the hull; one Al plate, screwed to the pipe, and one plastic (ABS) cap where the motor is fixed. The system is watertight thanks to the oil seals, further flat gaskets and ad hoc profiled plates in Tufnol. Finally, it is worth to note that the sonar support is used also to held the frontal camera.
As regards the localization algorithm, the continuous rotation of the echo-sounder head acquires the echo coming from all directions around the vehicle. The generation of SONAR images is possible when the following information are available: the direction of the echo and the sampling echoes recorded by a SONAR sensor. The echo direction is usually measured through an inertial measurement unit (in this case the Xsens MTi), while the echo is sampled by the Imagenex echo-sounder. The acquired data can be collected in an image (figure 3.5), where, according to a gray scale from black to white, the color of each pixel is proportional to the strength of the echo coming from the related point. The analysis of this image is quite onerous, but it simplifies if is based on a prototype searching strategy, possible if the environment is well-known and steady in time. In the proposed localization algorithm, the Hough transform is used to individuate the points belonging to the basin edge. Generally, the Hough transform is a feature extraction technique used in image analysis. The object of the technique is to find imperfect instances of objects within a certain class of shapes by a voting procedure. This voting procedure is carried out in a parameter space, from which object candidates are obtained as local maxima in a so-called accumulator space that is explicitly constructed by the algorithm for computing the Hough transform.
The implemented case of Hough transform is the linear transform for detecting straight lines. In the image space, the straight line can be described as

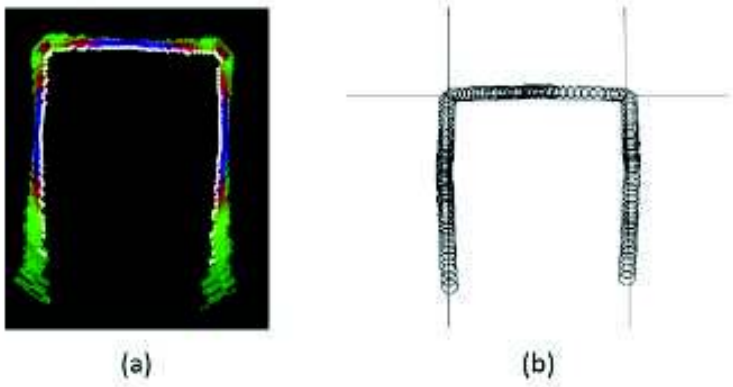


Figure 3.5: Echosounder image of the basin: (a) row image (b) prototype-based image

$y = mx + b$ where the parameter $m$ is the slope of the line, and $b$ is the intercept (y-intercept). In the Hough transform, the main idea is to consider the characteristics of the straight line not as discrete image points (x1, y1), (x2, y2), etc., but instead, in terms of its parameters according to the slope-intercept model, i.e., the slope parameter $m$ and the intercept parameter $b$.For computational reasons, the use of a different pair of parameters denoted $r$ and $\theta$ (polar coordinates) for the lines in the Hough transform is implemented (see Figure 3.6). The main image processing phases are three: in the first pro-

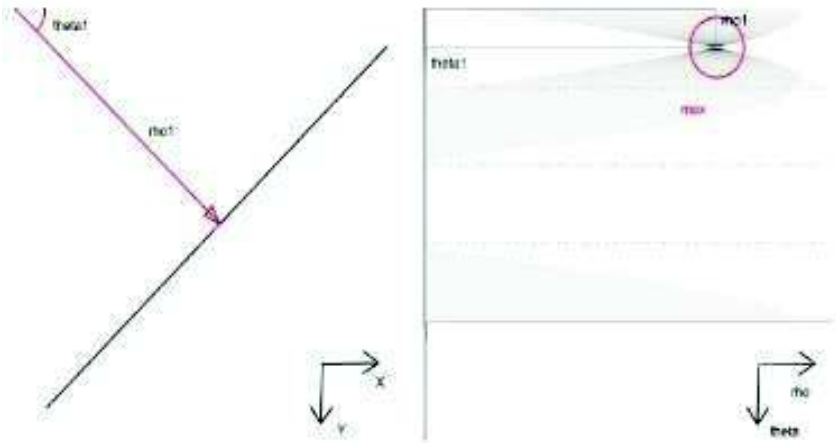

Figure 3.6: A straight line expressed in the Hough transform: the highlighted maximum exactly corresponds to the polar coordinates of the straight line

cessing phase an image whose pixels are black or white according to whether they are, probabilistically, belonging to the arena borders or not is carried out. The distinction will be performed with an algorithm based on the cross-correlation of the sent signal and the received one or on the gradient of the

echo strength along each direction. The second phase of the data process is the Hough transform of the image to identify the straight lines that should represent the arena borders (to determine the vehicle position in the basin). The a priori knowledge about the environment, and, particularly, about the directions of the three arena walls, is exploited to reduce the searching area, on the Hough distance-angle plane, where to find the points corresponding to probable boarders (Figure 3.7). To summarize, the localization algorithm,

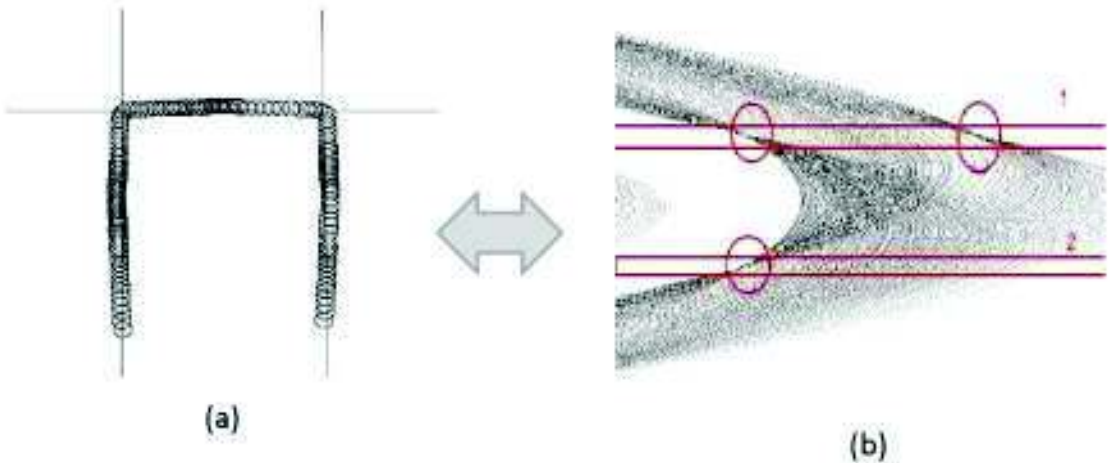


Figure 3.7: Hough Transform of the basin

interfaced with the ROS overall system, is based on a heuristic filter composed of two main steps:

1. distance estimation: in this part, the distance between vehicle and wall is calculated. The estimates is based on the cross-correlation between the characteristics shape of the wall echo and the received echo.

2. position estimation: the position is firstly estimated through the Hough transform and, then, a Kalman filter is applied to a simplified AUV kinematical model.

**Distance estimation:**
The main phase of the distance estimation is related to the data acquisition: the echo-sounder data and the related echo-sounder yaw angle are collected in a data structure and sent to a specific ROS topic; then, the algorithm operates a feature extraction and outliers elimination. The real distance estimation is based on the calculation of the cross-correlation function between echo received and echo of wall: experimental tests have highlighted the characteristics shape of the received wall echo in terms of squared wave with $t_1 - t_2$ parameters.

$$R_{fg}(t) = \int_{-\infty}^{\infty} f(\tau)g(t-\tau)d\tau \tag{3.1}$$

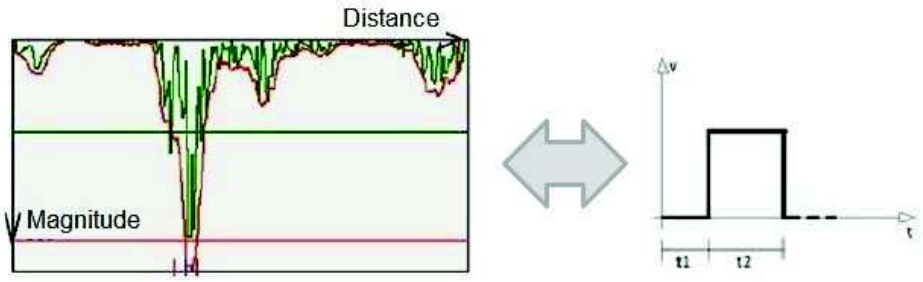


Figure 3.8: Characteristics shape of a wall echo and its square wave representation

The heuristic philter is used to determine the real wall-vehicle distance. The philosophy is to eliminate all doubtful cases and focus on a few reliable measurements. The filtering is based on the following hypothesis: no echo after the wall and the echo of a wall is equivalent to a square wave (see Figure 3.8). The cross-correlation function is analyzed starting from the farest sample to the closest; the first sample that satisfies all the listed below conditions probably corresponds to the real vehicle-wall distance:

- the intensity of the cross-correlation must be higher than a predetermined threshold (threshold 2);
- There must be no peaks beyond the wall above a predetermined threshold (threshold 1).

The definition of these two thresholds is based on experimental tests directly carried out at the basin. The success of this phase is strongly constrained to the width of these two thresholds. According to Figure 3.9, the green signal is obtained through the cross-correlation between the real echo and the square wave. The two threshold are set after an experimental phase and they allow the determination of the proper echo; in this case, the signal does not correspond with the proper echo because the peak 2 (which for the threshold is correct) is above another peak 1, and this is physically unacceptable. After

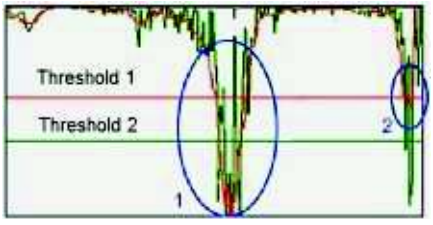


Figure 3.9: Wrong echo-signal

these two phases, the data acquired and filtered are allocated into a buffer in

order to be used from the position estimation algorithm.
The output is a vector of $N$-echoes containing both the proper distance $d_n$ and the direction of the echo $\theta_n$. The vector containing these information can be plotted as an image in which each circle is localized by the distance and by the direction. The generated image is easily understandable and can be used

Figure 3.10: Representation of the allocated buffer

in the algorithm setting phase.
**Position estimation:**
In the position estimation, the algorithm performs the determination of the maximum cross-correlation points and Hough transform of the generated image. The determination of the maximum points on the Hough transform in limited areas of the Hough distance-angle plane allows the individuation of the real wall with respect to the vehicle (see Figure 3.10). Finally, the measurements are filtered by an Extended Kalman Filter based on the kinematic model of the vehicle.
The Hough transform is widely described in the previous part and its advantages with respect to a geometrical method are mainly the high robustness and the reduced sensitivity to measurement noises. The Extended Kalman Filter is the last step of the algorithm and it allows the improving of the localization capacity of the vehicle. The state of the system is the position of the vehicle and the vehicle velocity:

$$\hat{X}_k = \begin{bmatrix} \hat{x}_k \\ \hat{y}_k \\ |v_k| \end{bmatrix} \tag{3.2}$$

where the pedix $k$ indicates the time instant. The simplifying hypothesis is that the velocity is slow-time variable and it can be assumed as constant $|v_k| = |v_{k+1}|$.
The kinematical model of the system can be described by this matrix:

$$\begin{bmatrix} \hat{x}_{k+1} \\ \hat{y}_{k+1} \\ |v_{k+1}| \end{bmatrix} = \begin{bmatrix} 1 & 0 & \cos(\theta_k) \\ 0 & 1 & \sin(\theta_k) \\ 0 & 0 & 1 \end{bmatrix} \begin{bmatrix} \hat{x}_k \\ \hat{y}_k \\ |v_k| \end{bmatrix} + \begin{bmatrix} q_k \\ w_k \\ 0 \end{bmatrix} \tag{3.3}$$

where $q_k = N(0, \sigma_q^2)$ and $w_k = N(0, \sigma_w^2)$ and $\theta$ is the vehicle yaw angle. The measurement equations are described by the following system:

$$m_k = \begin{bmatrix} x_k \\ y_k \end{bmatrix} + \begin{bmatrix} u_k \\ r_k \end{bmatrix} \tag{3.4}$$

where $u_k = N(0, \sigma_u^2)$ and $r_k = N(0, \sigma_r^2)$ are orthogonal.
The upgrading equations and the measurement ones can be rewritten into:

$$\begin{aligned} K_k &= \hat{P}_{k|k-1} C' \left( C \hat{P}_{k|k-1} C' + R \right)^{-1} \\ \hat{X}_{k|k} &= \hat{X}_{k|k-1} + K_k \left( m_k - C \hat{X}_{k|k-1} \right) \\ \hat{P}_{k|k} &= \hat{P}_{k|k-1} - K_k \left( C \hat{P}_{k|k-1} C' + R \right) K_k' \end{aligned} \tag{3.5}$$

and

$$\begin{aligned} \hat{x}_{k+1|k} &= F_k \hat{x}_k \\ \hat{P}_{k+1|k} &= F_k \hat{P}_k F_k' + Q \\ &. \end{aligned} \tag{3.6}$$

where the constitutive matrices are:

$$\begin{aligned} Q &= \begin{bmatrix} \sigma_q & 0 \\ 0 & \sigma_w \end{bmatrix} \qquad R = \begin{bmatrix} \sigma_u & 0 \\ 0 & \sigma_r \end{bmatrix} \qquad F_k = \begin{bmatrix} 1 & 0 & \cos(\theta_k) \\ 0 & 1 & \sin(\theta_k) \\ 0 & 0 & 1 \end{bmatrix} \\ P_k &= \begin{bmatrix} {p^k}_{1,1} & {p^k}_{1,2} \\ {p^k}_{2,1} & {p^k}_{2,2} \end{bmatrix} \quad C = \begin{bmatrix} 1 & 0 & 0 \\ 0 & 1 & 0 \end{bmatrix} \end{aligned} \tag{3.7}$$

The localization algorithm is tested both in simulations and in experimental tests; the system is able to work both with a fixed vehicle or with a moving one. The distortion of the images due to the vehicle movement is not a problem considering the low vehicle speed (small if compared to wall dimensions).

# Chapter 4

# Feelhippo AUV: Simulations and experimental results

In this chapter, the numerical simulations and the experimental results describing the real behaviour of the AUV during the SAUC-e 2013 competition are shown. The implemented control algorithms are developed for the European competition SAUC-e 2013. Therefore, this competition is used as benchmark case both in terms of hardware parts and control architecture. The numerical simulations are tested into two environments:

- MATLAB®- Simulink environment: the AUV modelling is based on the equations described in Chapter 1. This environment is mainly used to develop all the control strategies of the vehicle.
- ROS - UWSim environment: In parallel the control architecture described in Chapter 3 is developed into the ROS environment, in order to verify the interconnections between the high, medium and low levels. In addition, an especially developed underwater simulator (UWSim) completely based on ROS is used.

As regards the Eurpoean competition SAUC-e 2013, the tasks of the competition are four and all the tasks have to be completely performed in autonomous way (without any external intervention):

- Task 1: control the vehicle to pass through an underwater validation gate at an assigned depth;
- Task 2: the vehicle has to inspect an underwater structure in an unknown position;
- Task 3: the vehicle has to individuate an anomaly during the wall tracking. Then, the vehicle 1 has to contact the vehicle 2 trough the acoustic modem passing it the position of the anomaly;

- Task 4: the vehicle has to determine and reach the unknown position of an acoustic pinger.

All these tasks have been firstly proved both in MATLAB®- Simulink environment and in ROS - UWSim one.

## 4.1 ROS-UWSim

The Robot Operating System (ROS) is a computer environment based on Linux for the development of software to control robots. ROS provides the standard services of an operative system: abstraction hardware, low level control of devices, implementation of the common functionalities such as the management both of the information and of the related packages. It is based on an graph architecture where each process is represented by a node, programmed in C + + or Python, which carries out functions and exchanges messages with other nodes trough the topics. Underwater Simulator (UWSim) is a ROS-


Figure 4.1: Robot Operating System and UWSim logos

based software developed for viewing and simulating underwater robots. The main features of this software are the possibility to be easily integrable with existing control architectures (Control algorithms are external to the simulator that in many cases just works as a visualization of the output computed by external algorithms), to be general and easily customizable, to include support for underwater manipulators, thus allowing simulating underwater intervention missions (kinematic chains can be created and controlled) and, finally, to be visually realistic (permitting the configuration of several parameters such as water color, visibility, floating particles, etc.). UWSim is implemented in C++ and it uses the *OpenSceneGraph* (OSG) and the *OSGOcean* libraries. Therefore, before the beginning of the competition, the tasks are partially simulated in the ROS environment through UWSim which allows the modelling

of a virtual environment (in this case, the pool and the obstacle), the simulation of the sensors and the testing of different control strategies. In UWSim it is possible to simulate a 3D environment which models the dynamics of an underwater vehicle, the obstacle and the sensors (called virtual sensors such as camera, depth gauge or Inertial Measurement Unit). The acquisition node takes information from the sensor installed on the vehicle model; these virtual sensors publish information on a topic that communicates with the acquisition node. This node processes the RGB data from the camera, the depth information from the depth gauge and the yaw angle provided by the IMU sensor in order to provide the proper information to the controller node. Controller node uses these information to modify the AUV dynamics to maintain stable the vehicle and to complete the tasks.

## 4.2 SAUC-e 2013 competition

In this section, the SAUC-e 2013 competition and the tasks are in detail analysed. According to a specific task, the main control strategy developed to deal are described and simulated. The simulation environments are both MATLAB®- Simulink and ROS - UWSim. At the end of each task, the results obtained during the competition are shown and commented.
The SAUC-e 2013 competition mainly consists in four different task to execute only in autonomous way. The competition arena is the basin of the NATO Centre for Maritime Research and Experimentation (CMRE) near La Spezia, Italy (see Figures 4.2- 4.3).

Figure 4.2: CMRE basin

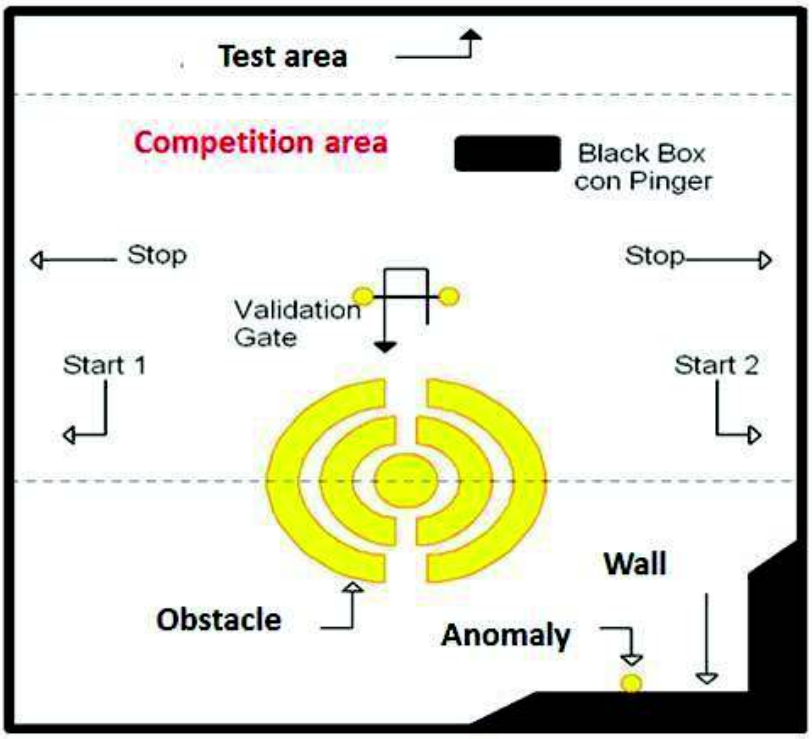


Figure 4.3: Competition arena scheme

### 4.2.1 Task 1

The goal of this task (SAUC-e Mission and Rules, Task 1) is to control the vehicle to proceed on a straight line from a starting point, maintaining a constant depth, turning for 90 degrees when the underwater structure is individuated, and continuing along a straight direction to pass through the validation gate.
The vehicle navigation exploits on-board sensor measurements:

- orientation and angular velocity, using the Xsens sensor;
- depth estimation, given by the pressure sensor;
- position of the underwater structure obtained by the camera image processing.

The motion strategy is the following one: the vehicle is submerged till the desired depth and it has to proceed from the start point with an open-loop advancing thrust profile and a closed-loop orientation control. The target is obtained with a simple PID regulator with a feed-forward compensation of buoyancy and gravity effects. Advancing thrust profile is thought to a vehicle speed initially quite high, about 0.3 m/s, and a lower one (0.1 m/s) when it is expected to be near the underwater structure. PID regulator controls yaw and pitch angles with respect to a desired reference: for yaw angle it is a constant zero value, for pitch angle it can be deduced from a high level kinematic controller. Briefly, its value is chosen to correct vehicle depth using advancing thrusters. When the camera approaches the underwater structure (this event can be recognized by constantly monitoring the yellow pixel percentage in the captured image) a reference distance can be used within a PID regulator in order to place the vehicle over the desired trajectory corner point. When the vehicle is positioned approximately stationary over the underwater structure, it is controlled to rotate around its vertical axis to line its bow up to the validation gate. This rotation follows a trapezoidal angular velocity profile. Finally, when the vehicle angular position is correct, it can advance again with an open-loop thrust profile and a closed-loop orientation control, as described in the first point.
**MATLAB®- Simulink environment:**
This control procedure has been preliminary tested in the MATLAB®- Simulink environment. The results are shown in figure 4.4: according to that, the vehicle centers the middle of the gate and maintains its depth quite well.

### 4.2.2 Task 2

The objective of the 2nd task is to carry out an inspection of an underwater structure in which the AUV has to avoid and to circumnavigate a yellow obstacle placed in the basin. The obstacle consists of several cylinders, arranged

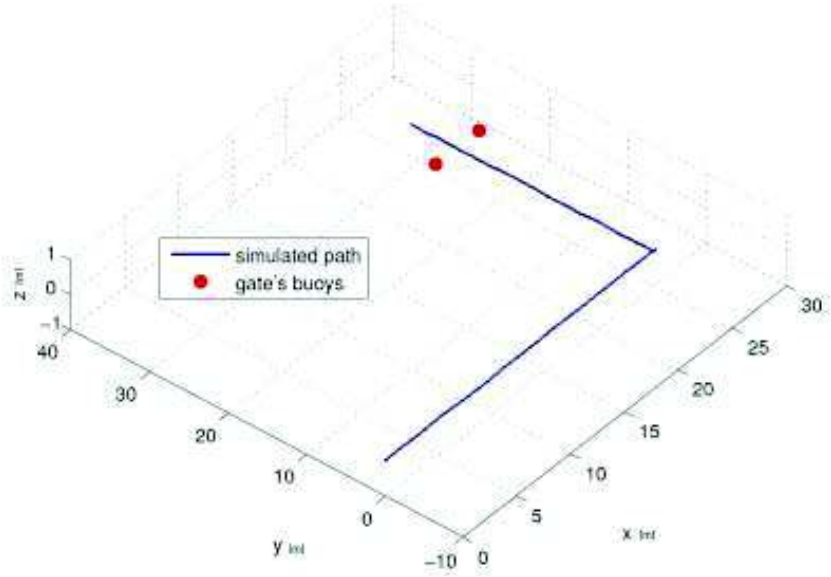


Figure 4.4: Validation test: simulation results

in concentric circles, with different diameters (0.5 m - 1.5 m) to simulate a pipeline-like structure; in addition, at the bottom of the structure, several tori are placed to increase the height of the whole structure. The steps of the task are the following: the vehicle stars from a generic point of the bottom side of the underwater structure. The AUV has to maintain a well defined distance from it and, using the camera, perform several circles around the landmark to different depths.
The adopted control strategy to complete the mission is based on the Potential Field Method; in this strategy, the AUV is considered as an immersed particle that moves in a potential field produced by a generator (the goal to reach). The generator creates an attractive potential field and each obstacle generates a repulsive one. This way, the potential field can be defined as an energy field where its gradient is the generated force. The AUV immersed in the potential field is subjected to different actions (produced by the forces) that drives the vehicle in the environment, keeping it away from the obstacles; therefore, this method can be interpreted as the motion of a particle in a gradient vector field generated by electrically positive and negative particles. The AUV is a positive charge, the goal is a negative charge and the obstacles are a set of positive charges (to generate the repulsive forces keeping away the vehicle). After a brief explanation of the method, as concerns the task, this method is used to maintain the proper distance from the obstacle: the AUV circumnavigates the obstacle basing on the amount of yellow on the camera screen. If the quantity of yellow overcomes the desired value, the obstacle generates a repulsive force that keeps away the robot; on the other side, if the AUV is too much distant from the obstacle, it generates an attractive force to maintain the desired value

of yellow. The vehicle has 4 controlled DOFs (longitudinal, lateral and vertical directions and the yaw angle) and the control actions are directly generated through PID controllers: the first one controls the longitudinal distance from the obstacle (based on the amount of yellow); the second PID is used to correct the yaw angle to keep centered the camera image. This control is based on the estimation of the obstacle Center of Gravity provided by the visual processing of the image. Finally, the last PID is used as a depth controller that permits to keep the desired depth during the circumnavigation of the obstacle (figure 4.14, UWSim).

**MATLAB®- Simulink environment:**

In MATLAB®, the AUV model and the main sensor ones (camera, IMU, depth sensor) are implemented. The initial position of the vehicle is far from the yellow underwater structure. The main errors used for this task (accurately described in Chapter 1) are the yellow ratio (ratio between the desired quantity and the real quantity of yellow in the image), the image CM centering error (the error between the Center of Mass of the acquired yellow image and the center of the camera) and the depth error.

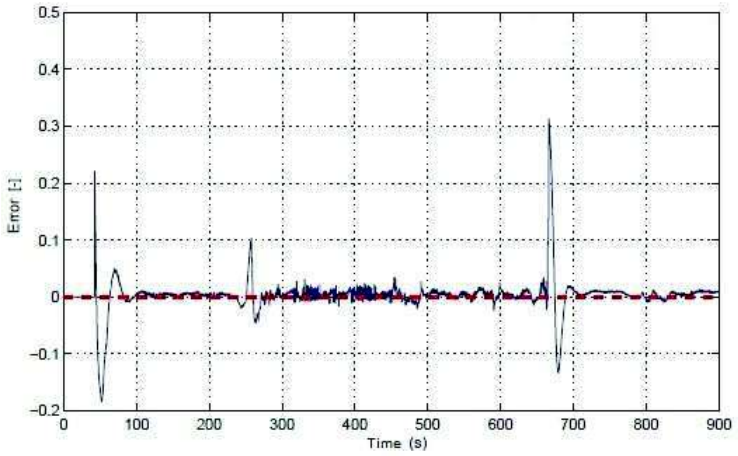


Figure 4.5: Yellow ratio error

In Figures 4.5-4.6, the yellow ratio and the Image CM centering error are respectively shown. It is worth to note the initial part of the graphics where the errors are completely zero: these parts correspond at the absence of the the object from the camera. In Figure 4.7, the depth error is shown. The errors after a short transient reach the desired values. The peaks depend on the changes of depth to complete the inspection of the whole structure. In Figure 4.8, the whole trajectory of the vehicle around the yellow underwater structure is represented.

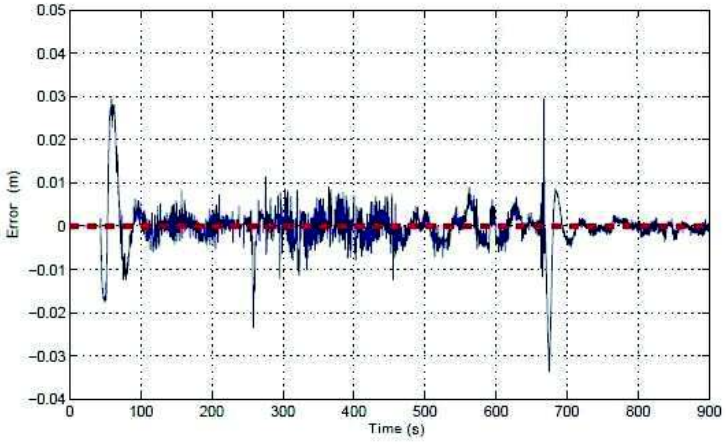


Figure 4.6: Image CM centering error

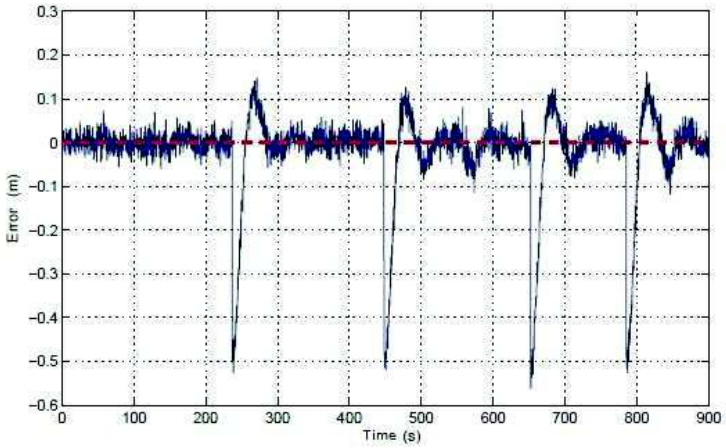


Figure 4.7: Depth error

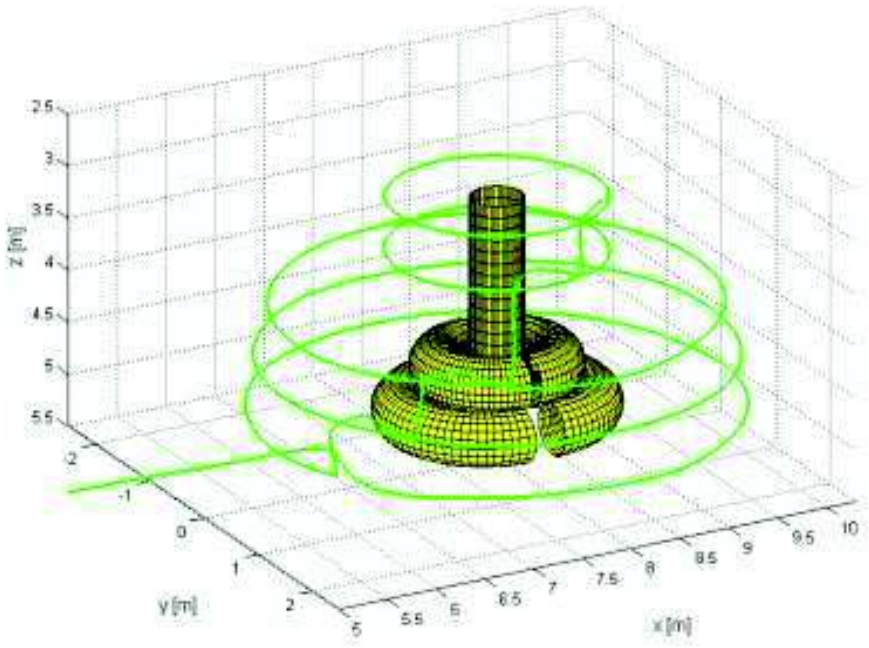


Figure 4.8: Trajectory of the AUV

**ROS - UWSim environment:**
The task has been completely simulated in the ROS environment through UWSim which allows the whole ROS architecture and the testing of different control strategies. The initial position of the vehicle is far from the underwater structure position. In UWSim, also a 'Lawn mover' strategy for the looking for of the underwater structure is implemented. The errors analysed in this part are the same of the MATLAB®ones: the yellow ratio, the image CM centering error and the depth error. In addition, also the behaviour of the yaw angle is shown.

In Figure 4.10, the error is quite low ($< 0.04$) which defines a distance error lower than 0.1 m. The nervous behaviour of the central part of the graphic depends on the presence in the camera both of the toroidal parts and of the cylinder one. In the last part, when the vehicle is stable at the final depth, the behaviour is more stable because in the camera plane there is only the cylinder part. In Figures 4.11-4.12, the Image CM centering error and the depth one are respectively shown. in both cases, it is possible to individuate short transients when the vehicle changes its depth, but the behaviour is globally stable. Finally, in Figure 4.13, the behaviour of the yaw angle compared to the reference value during the initial part of the object searching is shown. In Figure 4.14, the whole task is represented using the UWSim representation.

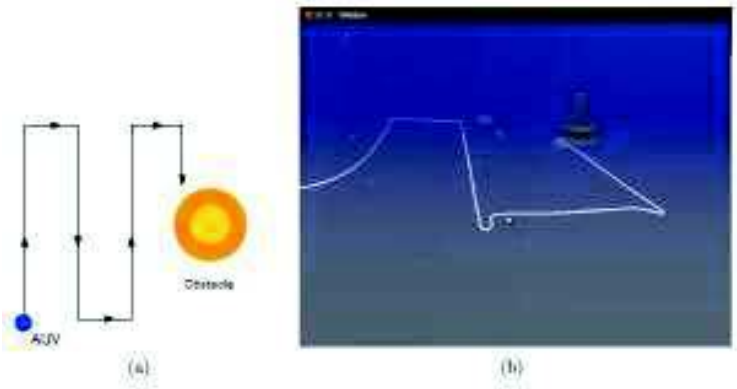


Figure 4.9: (a) Lawn mover strategy (b) UWSim simulation: searching the obstacle

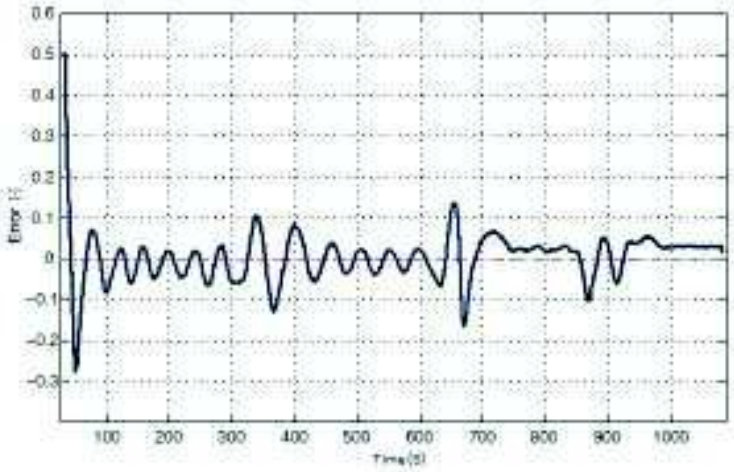


Figure 4.10: Yellow ratio error

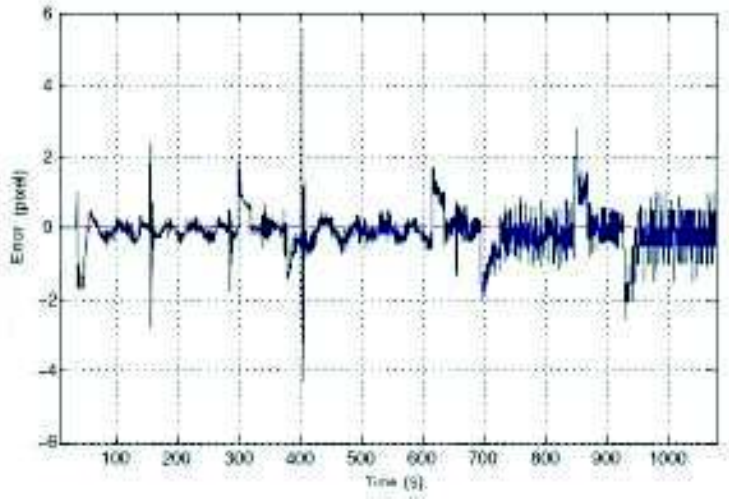


Figure 4.11: Image CM centering error

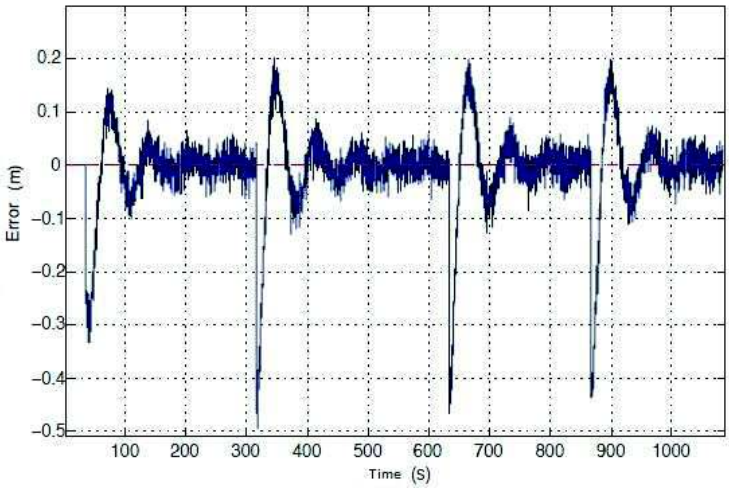


Figure 4.12: Depth error

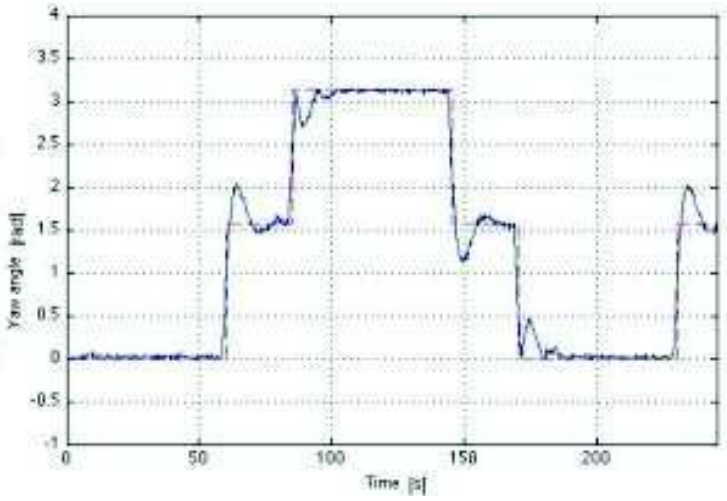


Figure 4.13: Yaw behaviour during the first phase of 'lawn mover'

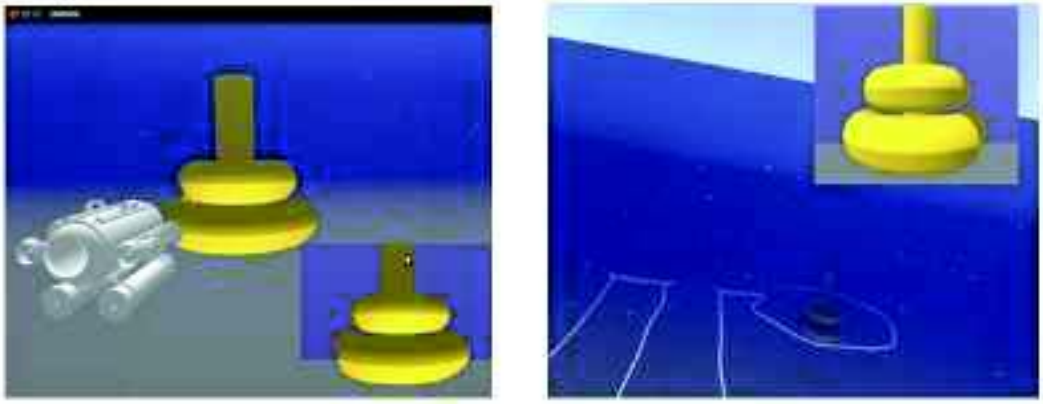

Figure 4.14: Simulated mission with UWSim: the obstacle and the vehicle

### 4.2.3 Task 3

The object of the 3rd task is articulated in various phases and involves cooperation between two vehicles: a search AUV and an inspection AUV. After a first phase of a wall survey where the search AUV has to keep a constant distance from the wall and a defined depth, the vehicle has also to identify an anomaly. The anomaly is a yellow object placed along the wall which has a light. The search AUV has to communicate its position to the inspection vehicle and the inspection vehicle has to reach this position refinding the anomaly. In the survey phase, the vehicle has to track a non-straight wall maintaining a defined distance. This part can be evaluated using two different strategies for the estimation of the wall distance: a single orthogonal beam used to evaluate the distance from the wall and multiple measurements of the echo-sounder using its rotating support. Both the strategies use the capacity of the vehicle to translate along its lateral direction thanks to the V-propeller configuration. This way, the vehicle moves along the wall with the camera oriented toward the wall. The first strategy is based on the same idea used during the SAUC-e 2012 competition. It is based on a single measure of the wall distance along a well-known direction with respect to the vehicle. The error with respect to the reference distance is translated by the motion control in a compensating force along the lateral degree of freedom. The second strategy is based on two measurements of the distance in two orthogonal directions. The MATLAB®simulations results have shown the main advantages and drawbacks of these two strategies: the first strategy is more robust than the second one because is not depending from the echo-sounder motion (that could introduce delays in the distance estimation).
The anomaly identification is the second part of the task. The control strategy developed for this aim has to be very robust and to cover both the low and the medium range from the wall: the idea is to use both the echo-sounder and the camera sensors to evaluate the presence of the anomaly. As regards the echo-sounder part, which is probably better for the reduced visibility condition, the anomaly individuation is based on the discontinuity evaluation of the distance (the presence of the anomaly probably introduces a peak in the distance measurement). For the camera part, which is probably better for reduced distances, it is performed through the computational vision algorithms, described in the dedicated section, based on the optical images acquired by the frontal camera.
In this part, the main simulations performed are referred to the search AUV role, because it is most critical part. It is supposed that both the search AUV and the inspection AUV use the localization algorithm to individuate their position respect to the basin. Therefore, for the inspection AUV the functioning is based on the estimation of the position through the localization algorithm and on the anomaly identification just explained.

The vehicle is carried out to perform both the two roles described in the rule document: the survey role and the inspection one. This phase is strongly based on the vehicle cooperation and acoustic communication. The communication is based on the SeaModem acoustic modems.

**MATLAB®- Simulink environment:**

In MATLAB®- Simulink environment, the testing of the proposed control strategies for the wall tracking and for the anomaly identification has been carried out. The initial condition of the search AUV is supposed to be at the beginning of the wall. The errors analysed in this part are the distance error

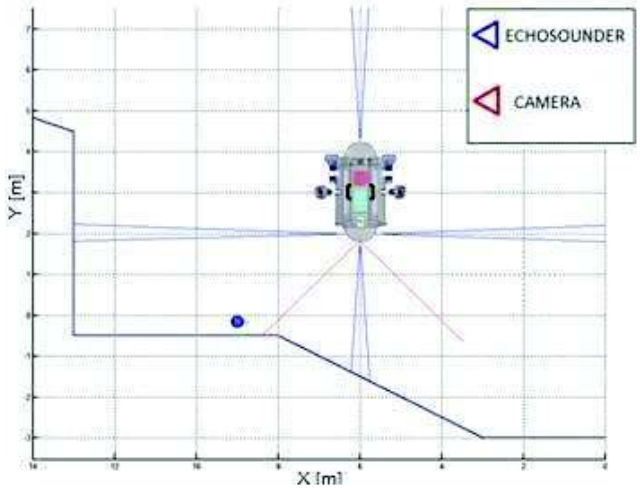


Figure 4.15: The initial condition of the simulation: wall, vehicle and anomaly

(measured from the echo-sounder), the yaw error, the depth error, the yellow ratio error and the image CM centering error (both measured by the camera).

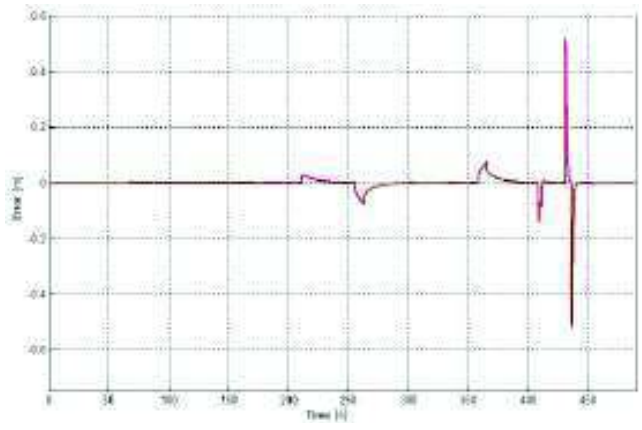

Figure 4.16: Distance error from the desired distance from the wall

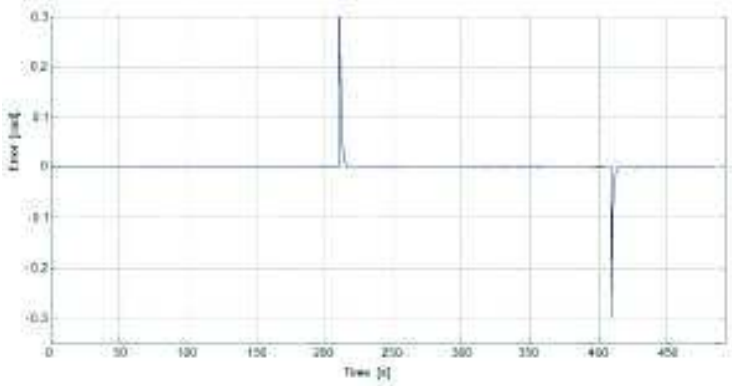

Figure 4.17: Yaw error

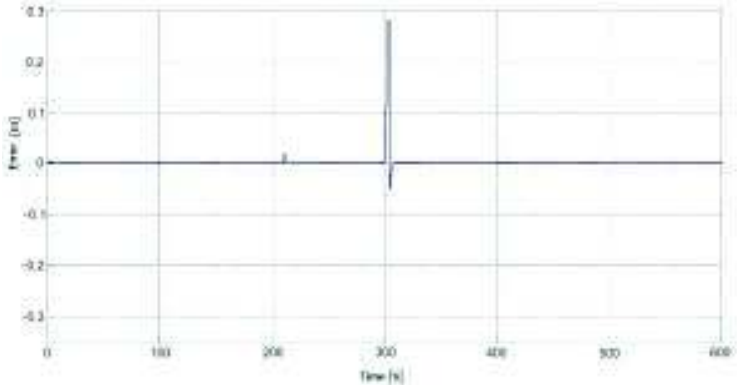

Figure 4.18: Depth error

In Figures 4.16-4.17-4.18, the behaviour of the distance, yaw and depth errors are respectively shown. The peaks in the distance error graphic depends on the changes of the wall angle: the vehicle has to reject this disturbances and after a short transient the error result stable. The big peak at the end of the graphics is rather than referred to the anomaly individuation. As regards the yaw error graphic, also in this case there are some peaks: they depend on the changes of the desired yaw angle in order to maintain along all the wall the front of the vehicle in the orthogonal direction compared with the wall. Finally, for the depth error graphic, the peaks are referred to the depth changes necessary to explore the wall also in the vertical direction.

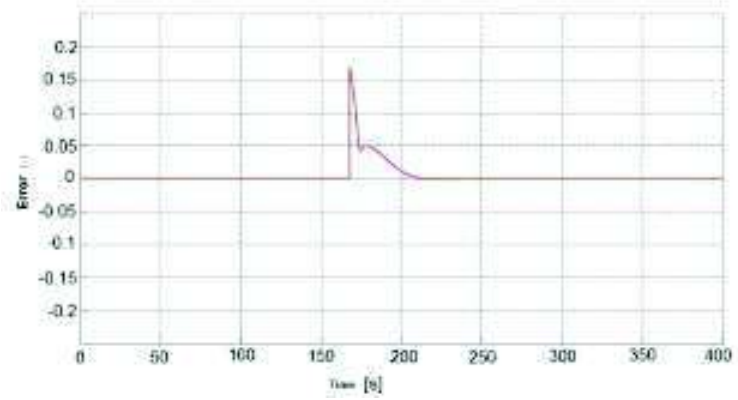


Figure 4.19: Yellow ratio error

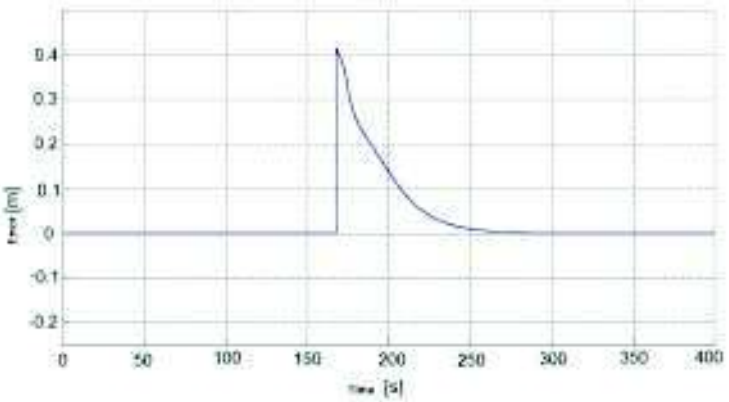


Figure 4.20: Image CM centering error

For the anomaly identification, it is possible to observe in Figures 4.19-4.20 the behaviour of the camera error indexes. They permit to keep the vehicle in front of the anomaly at a defined distance. The initial part of the graphics are zero because the anomaly is not acquired from the camera; when

the object appears in camera plane, the computation vision algorithm allows the maintaining of the anomaly position. Also in these case, the behaviour is stable after a short transient. In Figure 4.21, the whole task 3 for the search AUV is simulated.

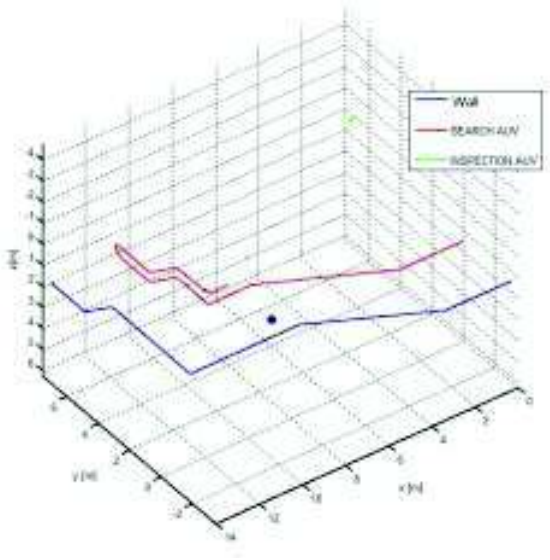

Figure 4.21: Task 3 simulation: search AUV

**ROS - UWSim environment:**
The third task has been partially simulated also in the ROS environment through UWSim; in this case the control of the vehicle is guaranteed by the coupled camera and echo-sounder strategy. The initial position of the vehicle is at the beginning of the wall; in addition, it is supposed to find the anomaly at the end of the wall in order to show the behaviour of the vehicle during the turning of the corner. In Figure 4.22 the initial conditions of the vehicle are shown; it is worth to note in the upper part of the image the camera output. The errors analysed in this part are the same of the MATLAB®ones: the distance error, the yellow ratio, the image CM centering error and the depth error.
Figure 4.23 shows the distance error: in the first part, from 0 to 20 s, the vehicle is moving along the first part of the wall. At 20 s, the vehicle turns the corner of the wall and, after a short transient, the error tends to zero. After 80 s, the distance error presents two peaks: these are referred to the transition from the vehicle control based on echo-sounder to the vehicle control based on camera. These effects can be seen also in Figures 4.24-4.25, where after atwo transitions between echo-sounder control and camera one, the vehicle reaches

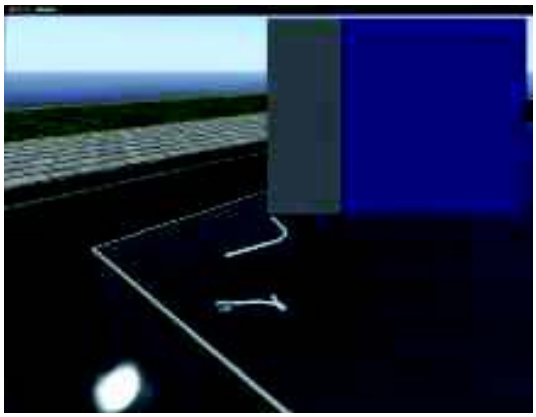

Figure 4.22: Initial conditions of the task 3

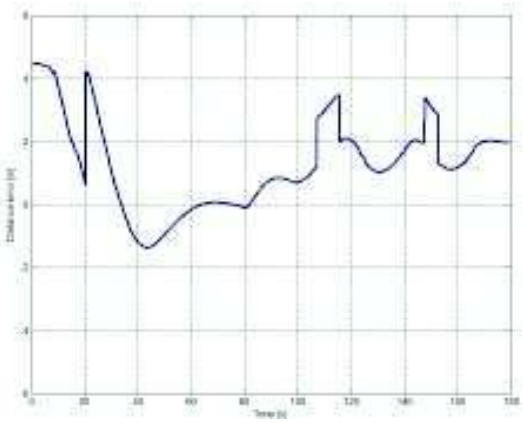

Figure 4.23: Distance error

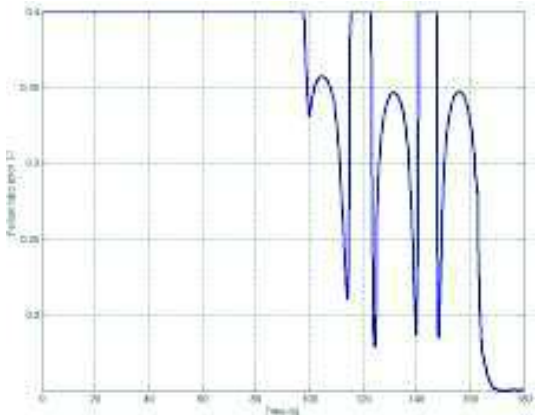

Figure 4.24: Yellow ratio error

its stable configuration in front of the anomaly. In fact, both the yellow ratio error and the Image CM centering error converges to zero, while the distance error remains stable at 2 m.

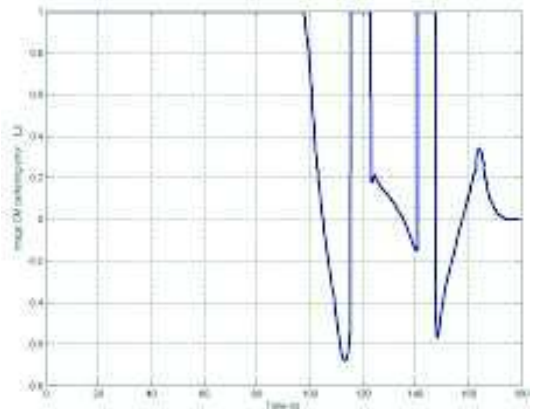

Figure 4.25: Image CM centering error

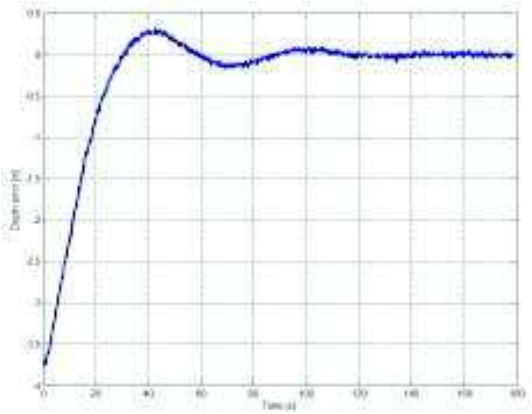

Figure 4.26: Depth error

In Figure 4.26, the depth error is displayed. The PID controllers guarantee the reaching of the desired depth. In conclusion, in Figure 4.27, two phases of the transition between echo-sounder and camera controllers are represented.

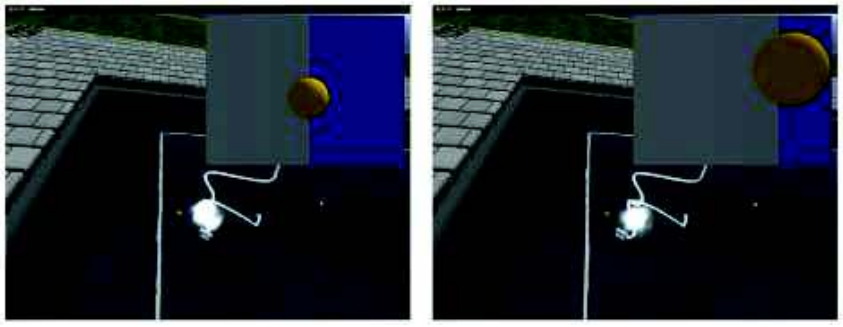

Figure 4.27: Simulated mission with UWSim: the vehicle during the approaching to the anomaly

### 4.2.4 Task 4

The aim of the task is to localize and to move towards a pinger. A fixed pinger is placed on a buoy positioned in an unknown point of the basin and it generates a signal with a frequency of 15 kHz.
The control strategy to carry out the task is based on 4 hydrophones able to receive signals from outside and, using a multi lateration algorithm based on the differences among the flight times (TDOA - Time Difference Of Arrival), calculates the direction and the position of the pinger. Through the TDOA it is possible to localize the position of the vehicle with respect to the pinger. To this goal, it is necessary to introduce an amplification circuit and the filtering of the received signals, which will be sent to a Digital Signal Processing (DSP) containing the localization algorithm.
The control strategies used in this task are mainly the classical motion control algorithms described and implemented in the previous tasks; for this reason the simulations of the task 4 are not shown.
In this part, there are mainly described the electronic building of the filtering system. The amplification stage consists of an inverting configuration with single supply 0V /+ 5 V with a suitable gain. The use of capacitors in the Input-Output and a voltage divider in the input to the non-inverting amplifier lead permitted to have an output signal characterized by a zero mean value, as required by the filtering circuit. The amplifier has been placed near the microphone capsule, because otherwise it would amplify also the noise picked up by the cables from the hydrophones and the processing board. The filtering stage consists of a 6th order band-pass filter at a frequency of 15khz (frequency emitted by the fixed pinger). Three amplifiers in inverting configuration cascade, in a single power supply, are placed in the filter. This way only the signal from the pinger gets to the DSP , eliminating additional external signals.
The localization procedure is made up of a set of algorithms which calculate the distance from the pinger; according to the algorithm outputs, the control system produces proper forces and torques to control the vehicle dynamics.

The three-dimensional position is identified through the multi-lateration algorithm in the vehicle reference frame. To estimate the vehicle orientation, four on-board hydrophones are fixed to the vehicle to allow the system to successfully work in all operative conditions.

## 4.3 Experimental results of the tasks

The preliminary validation tests, performed at SAUC-e 2013, have been very encouraging, confirming that FeelHippo, although equipped with a very inexpensive set of sensors, has the potentiality to work autonomously, taking advantages of the information about the surrounding environment. The visual data acquiring system, integrated into the vehicle hull, has proven to be capable of capturing clear images of the submerged structures to be monitored or inspected. Moreover, the control strategies based on the ratio and the CM errors (defined in Section 3.1.1) have shown high robustness compared to the external disturbances.
These tests were performed at the SAUC-e competition where, each year, the competition proposes a series of tasks for the participating vehicles to evaluate the AUVs capabilities to face realistic missions. The AUV demonstrates to be able to identify, completely autonomously, the submersed structure placed in the competition field and to take an inspection video of it. Some frames, taken from the competition log, are shown in Fig. 4.28. These frames represent the submersed structure placed in the middle of the basin at 2.5 meters of depth; in addition, also the frames representing the anomaly are shown (Fig. 4.29).

One of the innovative FeelHippo feature is the acoustic localization system; the tests performed during the competition are used to proven the efficiency of this system. Therefore, it has been possible to get a preliminary validation of the localization system, designed for FeelHippo, based on the single beam echo-sounder. One of the most important result was the possibility to compare the acoustic images obtained from the echo-sounder data (through the procedure explained in Sect. 3.2) with the acoustic images, kindly provided by the CMRE researchers, obtained by an expensive multi-beam sensor mounted in a fix place of the competition basin for the AUVs tracking.
Figure 4.30 shows the acoustic image obtained by the echo sounder data acquired by FeelHippo in the competition field. The grey scale has been modified, to be more understandable, into the scale shown on the left of the same figure (the green color corresponds to the low level of echo and the blue one to the maximum echo level). White pixels on the image are the points considered by the localization algorithm which belong to an edge of the basin. The center of the red circle represents the actual estimated position, whereas the red triangle represent the actual field of "view" of the echo sounder.

In Figure 4.31, a contemporary acoustic image of the competition field

Figure 4.28: Frames of the submersed structure acquired during the SAUC-e competition

Figure 4.29: Frames of the underwater anomaly acquired during the SAUC-e competition

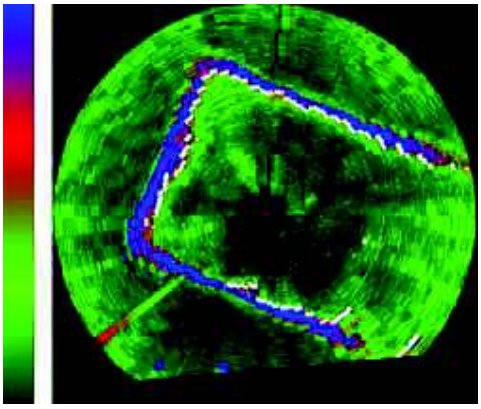

Figure 4.30: Acoustic image of the CMRE basin obtained by FeelHippo sensors

acquired by the CMRE multi-beam sensor for vehicle tracking is shown. The white shadow in the red square is FeelHippo, whereas the other visible big white shadow is the submerged structure.

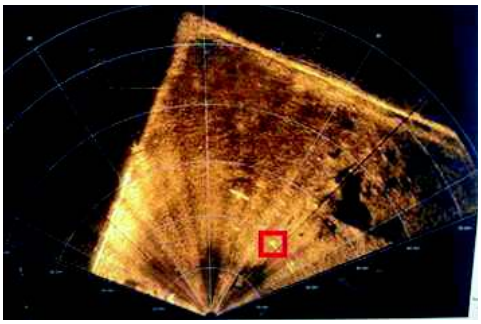

Figure 4.31: Acoustic image of the competition field obtained by the CMRE multi-beam

Overlapping the two images, as visible in Fig. 4.32, it is noticeable how they result similar. The "visible" structures are rightly identified. It is also worth to note that the localization algorithm is able to correctly identify the AUV position compared to the surrounding environment. The center of the red circle and the red square are quite coincident.

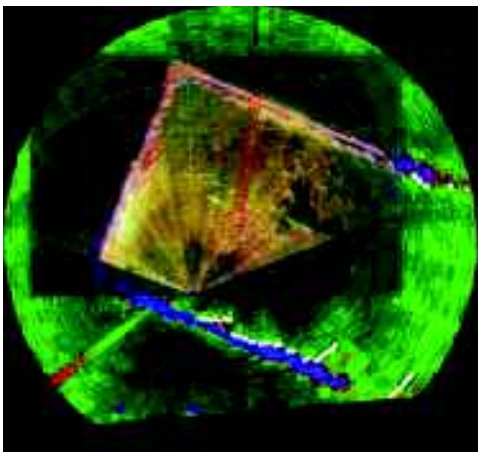

Figure 4.32: Overlapping of the two acoustic images

# Chapter 5

# Cooperative Mobile Manipulation: I-AUV model

The cooperative mobile manipulation represents a challenging field of autonomous robotics, especially in underwater environments. In the chapter, after a brief state of the art, the modelling techniques used for the Autonomous Underwater Vehicle-Manipulator System (A-UVMS) are described. In the following sections, both the kinematical and dynamical models and the control architecture of the A-UVMS will be better explained and analysed.

## 5.1 MDM I-AUV model

The cooperative mobile manipulation is one of the challenging field in robotics; this challenge involves different control problems but, in the underwater environment, the problems are also related to localization and communication issues. The presence of a swarm of autonomous vehicles equipped by robotic arms introduces different problems involving vehicle control, robotic arm control and swarm control. The main advantage stems from the capability for carrying out complex and dexterous tasks which cannot be simply made using a single robot. Main coordination schemes for multiple mobile manipulators in the literature are: Leader–follower control and hybrid position–force one.
The leader–follower control for mobile manipulator, where one or a group of mobile manipulators play the role of a leader, which track a preplanned trajectory, and the rest of the mobile manipulators form the follower group which move in conjunction with the leader mobile manipulators. To overcome parameter uncertainty in the model of the robot, a decentralized control law is applied to individual robots, in which an adaptive is used to model robot dynamics online. In literature many different contributions are expressed, but only few of these involve the swarm of I-AUVs for the technical problems ex-

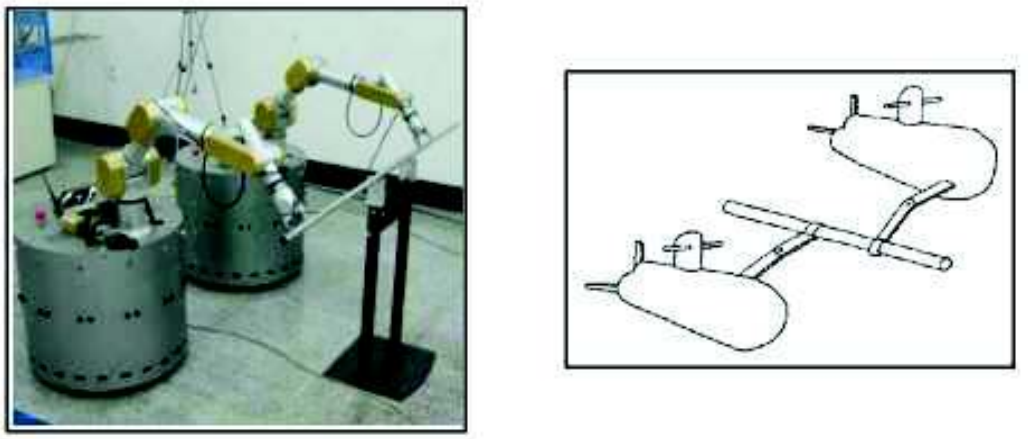

Figure 5.1: Application of Cooperative Mobile Manipulation for terrestrial robots and UVMSs

pressed before.
The I-AUV, usually characterized by lesser size and weight than the ROV system, can be easily managed by a surface vehicle reducing the cost of the mission. According to the recent development of battery technologies and the reduction of the human interventions from the control loop, these vehicles can perform autonomously manipulation tasks, in which the ship is only required in the stages of immersion and recovery of the vehicle. Despite the many benefits, mainly due to the complexity of implementation and control issues, only a few research centers are equipped with an I- AUV. The first project to carry out an autonomous underwater vehicle equipped with a robotic arm started at the 1990 and it is attributable to the development of the ODIN and Otter vehicles [15], respectively, at the University of Hawaii and at the Robotics Laboratory at Stanford University. Both vehicles were fully implemented and had a simple manipulator to a 1 DOF, designed for automatic recovery of submerged objects. In the same time, at the French Ifremer research center, a VORTEX (Versatile and Open subsea Robot for Technical Experiments) was presented. This vehicle was under-actuated with 5 DOFs and was provided with a 7DOF robotic arm. These vehicles were prototypes and they are only used in controlled environments and conditions; the importance of this primitive projects was in the possibility to study the hydrodynamic model of the UVMS and their control issues.
In 1997, the European project AMADEUS (Advanced DEep Manipulation for Underwater Sampling) [17], which involves various universities, analyse the coordinated control of two robotic arms 7 DOFs. These robotic arms were mounted on a teleoperated ROV to collect samples and perform complex manipulation tasks. The development of this project has led, in 2004, to the

implementation of SAUVIM (Semi- Autonomous Vehicle for Intervention Missions) at the University of Hawaii: this was the first underwater vehicle which operated manipulation tasks in open sea. SAUVIM is equipped with a manipulator arm with 7 DOF, the same used in the project AMADEUS, which is controlled in a decoupled manner with respect to the vehicle body [16]. The vehicle was fully controlled (6 DOFs) through the use of 8 thrusters and it had a high weight difference between the vehicle and the robotic arm. This characteristic allows the possibility to decouple the vehicle and the arm controls. The vehicle was only semi-autonomous because it was autonomous in

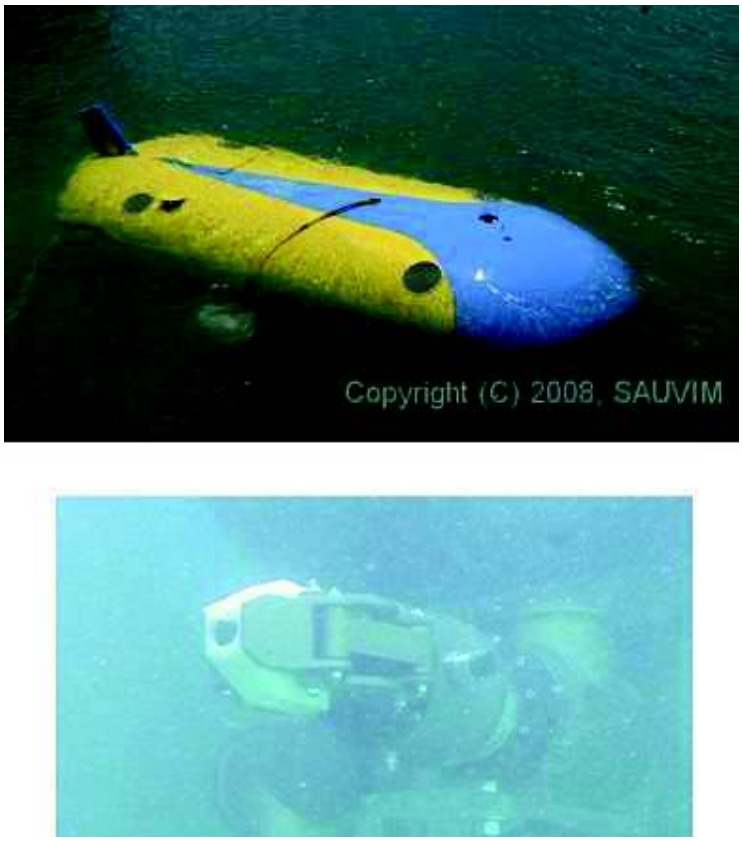


Figure 5.2: SAUVIM vehicle with the Ansaldo robotic arm

terms of electrical feed and low-level control, but it had a communication cable to perform the high control level. The user only specifies the high-level instructions, on the basis of the cameras and other on board sensors, while the robot autonomously operates the low-level commands necessary to complete the task. SAUVIM is today used for the recovery of objects from the seabed and other handling operations at a maximum depth of 4000m.
Recent researches in the field of I-AUV are mainly focused to the increase of the high-level autonomy, regarding the conduct of missions intervention. On the other part, the vehicles developed in the past projects were considerable

in terms of size and weight, suitable to work at great depths and in oceanic environments. Therefore, particular interest was focused to the development and implementation of smaller and lighter I-AUV (with mass less than 300 kg), used to interventions that require navigation of up to 500m depth, such as the vehicle ALIVE (Autonomous Light Intervention Vehicle) developed within the European FP5 GROWTH program. The main reached results obtained at the

Figure 5.3: ALIVE vehicle

end of the project can be synthetysed in the following:

- Localization using acoustic signals.
- Navigating to the proximity of the target.
- Finding the target and approaching.
- Visual servo control for station keeping.
- Disturbance rejection, compensating for underwater current.
- Visual servo control for manipulating/interacting with an ROV panel (valve operations).

A final contribution to the development of the state of the art in the field of I-AUV is the TRIDENT European project started in 2010 [19]. The objective of TRIDENT is to develop new methodologies to carry out handling tasks in unstructured underwater environments, through a cooperative team including an AUV equipped with a 7 DOFs robot arm and an ASC (Autonomous Surface Craft). The purpose of the ASC is to replace the ship required for the I- AUV operations. Through the ASC and a USBL (Ultra Short Baseline) acoustic modem, it is possible to communicate with the I- AUV allowing a further

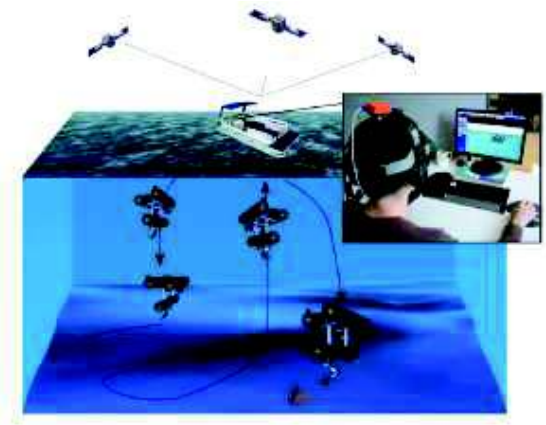

Figure 5.4: TRIDENT architecture

reduction of the costs. The main contribution of the TRIDENT project to this research field are:

- Surveying: simultaneous localization and mapping (SLAM).
- Localization using maps, INS, DVL.
- Navigating to the proximity of the target.
- Finding the target and approaching.
- Visual servo control for station keeping.
- Visual servo control for interacting with and retrieving a Black Box mock-up.
- Virtual/augmented reality for mission control.

The project involves several European partners, including the University of Heriot- Watt (Scotland) with the Nessie AUV and the University of Girona (Spain) with Sparus.

The previous projects started from the idea of a single I-AUV in which all the sensors and the dexterous capacities are centralized. The concept behind our research activity are the reduction of the single I-AUV characteristics and performance thanks to the implementation of a I-AUV swarm (the transition from the Autonomous mobile manipulation to the Cooperative Mobile Manipulation).

In the following sections, the AUV presented before (FeelHippo) will be modelled as Intervention-AUV (or UVMS) vehicle; this means the introduction of a 7-DOFs robotic arm on the vehicle. The main simplification hypotheses compared to the real MDM AUV are:

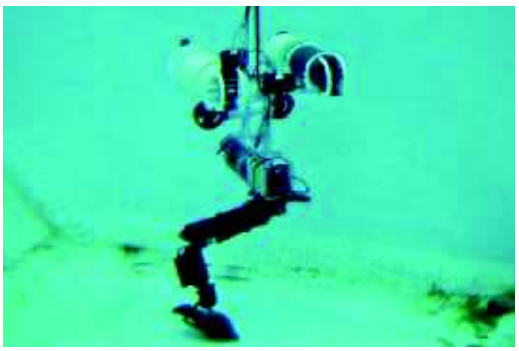

Figure 5.5: TRIDENT vehicle

- Introduction of the robotic arm with 7 Degree of Freedoms to use redundancy techniques;
- Increase of the vehicle DOFs to a fully controlled AUV: as can be seen from the literature, the use of fully controlled vehicle allows the solving of complex manipulation tasks;
- Increase of the autonomy: the MDM AUV is supposed to be increased in terms of energy autonomy to autonomously perform manipulation tasks;
- Vehicle gripper: it is supposed the rigid connection between the end-effector and the object (th problem of the grasping is not considered in this thesis).

### 5.1.1 Kinematical model of the UVMS

To complete the study of the whole kinematic system characterized by the AUV and by the robotic arm, it is necessary to better analyse the kinematic model of the manipulator arm. For this application, it is supposed to use a 7DOFs anthropomorphic robot with spherical wrist. This manipulator can be shown schematically (figure 5.7), such as a serial mechanism consisting of 7 rigid bodies linked through each others by the revolute kinematic constraints. The kinematic model of a serial robot can be treated by solving two problems: the direct kinematics and the inverse kinematics. After a brief description of the simplifying hypothesis, both kinematics problems are analysed.
In figure 5.6 is schematically shown the AUV and the robotic arm. The robotic arm is schematically connected to the vehicle in the front part (positioned in the central-bottom position) to minimize the motion disturbances and to maintain the center of mass of the vehicle under the thrust. The robotic arm relatively moves to the vehicle by rotating around two mutually perpendicular axes. The two links (arm and forearm ) can rotate with respect to the others around an orthogonal axis and have an end-effector with gripper manipulator.

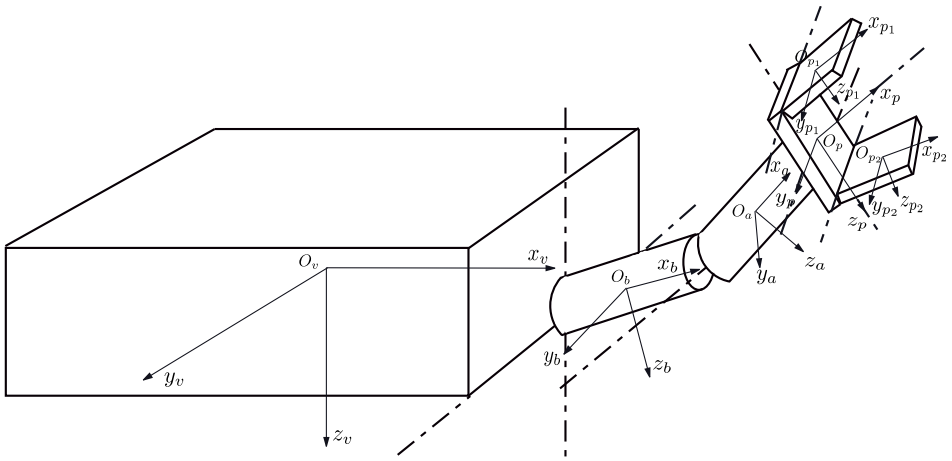


Figure 5.6: I-AUV schematic representation

In the following the gripper will be considered as a rigid connection between end-effector and object. In the figure, the center of the spherical wrist is in the point of intersection of the axes of rotation of the gripper relative to the forearm link.
Comparing this with the classical scheme of the anthropomorphic manipulator, it is worth to note that the first link is collapsed into a single point (the intersection of the two axes of rotation of the arm relative to the vehicle) and the three bodies of the spherical wrist also collapsed in the center of the wrist.

#### 5.1.1.1 Kinematical models

The objective of the direct kinematics is the determination of the pose of the end-effector, as function of the values assumed by the joint variables:

$$T_n^0 = T_n^0\left(\vec{q}\right) \ , \tag{5.1}$$

where $T_n^0 \in \mathbb{R}^{4x4}$ is the homogeneous transformation matrix between the base reference frame $< 0 >$ fixed to the AUV and the end-effector reference frame $< n >$ and $\vec{q} \in \mathbb{R}^{nx1}$ is the joint variables. The solution is always determined. Considering a manipulator having $n+1$ arms connected by $n$ joints, where each link is associated with the $< i >$ reference system. Assume that each joint provides a single degree of freedom to the mechanical structure, corresponding to the joint variable $q_i$. The overall transformation of coordinates, which expresses the position and orientation of the tern $< n >$ (end-effector) with respect to $< 0 >$ reference frame (vehicle), is given by:

$$T_n^0\left(\vec{q}\right) = \prod_{i=1}^{n} A_i^{i-1}\left(q_i\right) \ , \tag{5.2}$$

where $A_i^{i-1}\left(q_i\right)$ is the homogeneous transformation matrix between the $< i-1 >$ and the $< i >$ reference frames.

To generalize the calculation of the matrices appearing in (5.2), each reference system fixed to each link is defined according to Denavit-Hartenberg convention. In the case of 7DOFs anthropomorphic manipulator with spherical wrist, consisting of 7 links joined by seven revolute pairs, $n$ reference systems are chosen with $< i > i = 0, ..., 7$ (figure 5.7). Then, the position and orientation of the $< i >$ reference system is completely specified by four scalar parameters (Denavit-Hartenberg) $a_i$, $D_I$, $alpha_i$ and $\vartheta_i$, according to which the associated homogeneous transformation matrix as follows:

$$A_i^{i-1}(q_i) = \begin{bmatrix} c_{\vartheta_i} & -s_{\vartheta_i}c_{\alpha_i} & s_{\vartheta_i}s_{\alpha_i} & a_i c_{\vartheta_i} \\ s_{\vartheta_i} & c_{\vartheta_i}c_{\alpha_i} & -c_{\vartheta_i}s_{\alpha_i} & a_i s_{\vartheta_i} \\ 0 & s_{\alpha_i} & c_{\alpha_i} & d_i \\ 0 & 0 & 0 & 1 \end{bmatrix} . \tag{5.3}$$

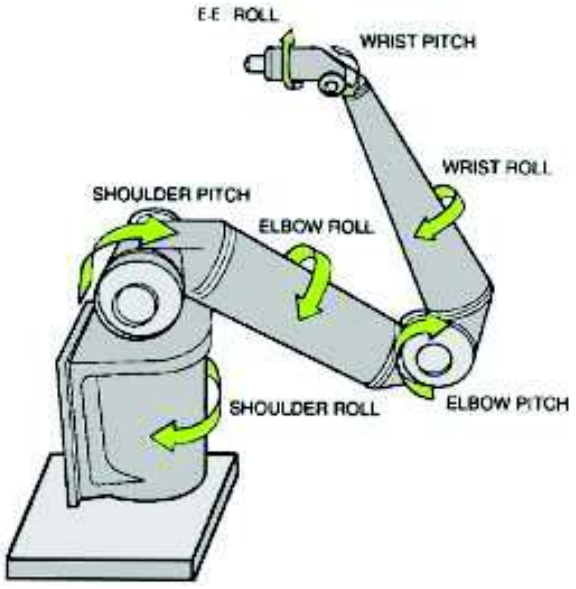


Figure 5.7: Kinematical scheme of the robotic arm

The D-H parameters are described in table 5.1. Using (5.2) and (5.3), the homogeneous transformation matrix is

$$T_n^0(\vec{q}) = \left[\begin{array}{ccc|c} \vec{n}_7^0 & \vec{s}_7^0 & \vec{a}_7^0 & \vec{p}_7^0 \\ \hline 0 & 0 & 0 & 1 \end{array}\right] , \tag{5.4}$$

where the $\vec{p}_7^0$ is the end-effector pose in the $< 0 >$ reference system and the unitary vectors *normal* (along $x_7$), *sliding* (along $y_7$) and *approach* (along $z_7$) are obtained through the successive product of the homogeneous transformation matrix (see 5.3). The inverse kinematics is used to determine the joint variables starting from the end-effector pose. Its resolution is crucial to

| Link | $a_i$ | $\alpha_i$ | $d_i$ | $\vartheta_i$ |
|---|---|---|---|---|
| 1 | 0 | $\pi/2$ | $d_1$ | $\vartheta_1$ |
| 2 | 0 | $\pi/2$ | 0 | $\vartheta_2 + \frac{\pi}{2}$ |
| 3 | 0 | $-\pi/2$ | $d_3$ | $\vartheta_3$ |
| 4 | 0 | $\pi/2$ | 0 | $\vartheta_4 + \frac{\pi}{2}$ |
| 5 | 0 | $-\pi/2$ | $d_5$ | $\vartheta_5$ |
| 6 | 0 | $\pi/2$ | 0 | $\vartheta_6$ |
| 7 | 0 | 0 | $d_7$ | $\vartheta_7$ |

Table 5.1: Denavit-Hartenberg parameters

translate the specific task, assigned in the workspace of the end- effector, to the corresponding motions in the joint space $\vec{p}_n^0 = \vec{p}_{n,\text{des}}^0(t)$ and $R_n^0 =_{n,\text{des}}^0(t)$, with $\vec{q} = \vec{q}_{\text{des}}(t)$.
In general, the inverse kinematic problem is more complex than the direct one, because the equations to be solved are highly non-linear and analytical solutions may exist or not . The use of a redundant manipulator (7DOFs) for underwater manipulation tasks is necessary to complete the task and to avoid singularities. Singularities are particular robot configuration in which the Jacobian matrix loss rank. When the manipulator is redundant, the Jacobian matrix has more columns than rows and infinite solution exist to the classical relation between velocity in the operative space and velocities of the joints:

$$\vec{v}_e = \begin{bmatrix} \dot{\vec{p}}_e \\ \vec{\omega}_e \end{bmatrix} = J\dot{\vec{q}} \tag{5.5}$$

An interesting method to use the redundant DOFs is to formulate the problem as a constrained linear optimization problem. Particularly, once the end effector velocity $\vec{v}_e$ and the Jacobian $J$ are given, it is desired to find the solutions $\dot{\vec{q}}$ that satisfy the linear equation 5.5 and minimize the quadratic cost functional of joint velocities. The problem can be solved through the Lagrange multipliers method.

$$\dot{\vec{q}} = J_r^\dagger \vec{v}_e \tag{5.6}$$

where

$$J_r^\dagger = J^T(JJ^T)^{-1} \tag{5.7}$$

is the right pseudo-inverse of Moore-Penrose. The obtained solution locally minimizes the norm of the joint velocities. Supposing $\dot{\vec{q}}$ a solution of (5.5); then also $\dot{\vec{q}} + N_J\dot{\vec{q}}_o$ is a solution in case that $N_J$ were a projection of the vector $\dot{\vec{q}}_o$ in the null space of $J$.

$$\dot{\vec{q}} = J_r^\dagger \vec{v}_e + (I_n - J_r^\dagger J)\dot{\vec{q}}_0 \tag{5.8}$$

The solution of this equation is composed of two terms: the first one is relative to the minimum norm joint velocities, and the second one, is the homogeneous

solution. This solution satisfies the additional constrain. A direct consequence is that in case of $\vec{v}_e = 0$ is possible to generate internal motions that reconfigure the manipulator structure without changing the end effector pose.
The $\dot{\vec{q}}$ satisfy the equation (5.5) and are very close to $\dot{\vec{q}}_0$. In literature, there are many possible choices of $\dot{\vec{q}}_0$ and one of these is:

$$\dot{\vec{q}}_0 = k_0 \left( \frac{\partial w(\vec{q})}{\partial \vec{q}} \right)^T \tag{5.9}$$

where $k_0 > 0$ and $w(\vec{q})$ is a secondary objective function of the joint variables. Since the solution moves along the direction of the gradient of the objective function, it attempts to maximize it locally compatible to the primary objective. A typical objective function $w(\vec{q})$ is the following:

$$w(\vec{q}) = \sqrt{det(J(\vec{q})J^T(\vec{q}))} \tag{5.10}$$

which vanishes at a singular configuration; thus, by maximizing this measure, redundancy is exploited to move away from singularities.
The inversion of the differential kinematics very close to a singularity can create many problems in terms of computational load. Therefore, it is useful to improve the robustness of the Jacobian $J$ (or $J_r^\dagger$) a damped least squares inverse, defined as:

$$J^\star = J^T(JJ^T + k^2 I)^{-1} \tag{5.11}$$

where $k^2 I$ is the the damping factor that renders the inversion better conditioned from a numerical viewpoint.

### 5.1.2 Dynamical model of the UVMS

The dynamical model of the system (I-AUV) consists in two different parts: an underwater vehicle (AUV) and a robotic arm. The hypotheses to study the models are to assume that both the vehicle and the various links of the manipulator can be considered as rigid bodies and connected by revolute kinematic joints. This whole mechanical system can be studied through classical multibody techniques.
The external forces and torques, i.e. the hydrodynamic effects and the buoyancy, are introduced into the model by means of generalized Lagrangian forces applied to each body constituting the multibody system (the body-vehicle, the links, the robotic manipulator arm and the gripper) in order to increase the reality of the system.
The multibody method used to model the hydrodynamic effects proposes to separate the dynamical study of the rigid system from the one of hydrodynamic and buoyancy effects.
The dynamical analysis of a multibody system can be addressed mainly following two methods: the Newtonian approach and the Lagrangian one. The

Newtonian method involves the description of the fundamental equations of dynamic for each rigid body and the introduction, among the external actions, of the reaction forces between the various links and the frame (not known a priori). This approach is quite general, and particularly suitable for the description of the serial mechanisms, due to the recursive nature of the approach. The second method consists, instead, in the introduction of a pseudo-energetic function and in the use of Lagrange's equations. In this thesis, the Lagrangian redundant approach is used to the study of the dynamics of the rigid bodies as it is more systematic and easily automatable (this method is mainly used in softwares able to model and simulate multibody systems).
To uniquely define the state of the system a set of redundant Lagrangian coordinates is introduced:

$$\vec{q} = \left(\vec{q}_1^T, ..., \vec{q}_N^T\right) \in \mathbb{R}^{6\text{Nx1}} \ , \quad \text{with} \quad \vec{q}_i = \begin{bmatrix} \vec{G}_i \\ \vec{\Phi}_i \end{bmatrix} \in \mathbb{R}^{6\text{x1}} \quad i = 1, ..., N \ , \tag{5.12}$$

where $\vec{G}_i$ and $\vec{\Phi}_i$ are respectively the coordinates of the CG and the Euler angles of the $i$-th rigid bodies.
It is assumed that the constraints are two-sided, sufficiently regular and independent, representable by algebraic equations in which it does not appear explicitly the time variable and holonomic (constraints on the configuration). It is also considered, for this application, the hypothesis that these constraints are smooth (ideal) although it is not strictly necessary for the approach.
With these assumptions the algebraic equation of the constraints can be written in a compact form, such as:

$$\vec{\psi}\left(\vec{q}\right) = \vec{0} \ , \tag{5.13}$$

with $\vec{\psi} \in \mathbb{R}^p$ ($p$ is the number of Degree of Freedoms DOFs taken out by the constrains).
The Lagrange equations for rigid body systems are obtained as a condition of stationarity (minimization) of the generalized Lagrangian function $\mathcal{L}^*$ estimated as:

$$\mathcal{L}^*\left(\dot{\vec{q}}, \vec{q}, \vec{\lambda}\right) = T\left(\dot{\vec{q}}, \vec{q}\right) - V\left(\vec{q}\right) - \vec{\lambda}^T \vec{\psi}\left(\vec{q}\right) \ , \tag{5.14}$$

where $T$ is the kinetic energy of the system, $V$ the potential energy and $\vec{\lambda} \in \mathbb{R}^p$ is the Lagrangian vector.
The complete differential-algebraic equation (DAE) system, which is obtained from the previous equation, can be described through a unique matrix equation:

$$\begin{bmatrix} M & \left(\frac{\partial \vec{\psi}}{\partial \vec{q}}\dot{\vec{q}}\right)^T \\ \frac{\partial \vec{\psi}}{\partial \vec{q}}\dot{\vec{q}} & 0_{pxp} \end{bmatrix} \begin{Bmatrix} \ddot{\vec{q}} \\ \vec{\lambda} \end{Bmatrix} = \begin{Bmatrix} \vec{Q} - C\dot{\vec{q}} - \left(\frac{\partial V}{\partial \vec{q}}\right)^T \\ \vec{\gamma} \end{Bmatrix} . \tag{5.15}$$

The use of the Lagrangian approach allows the study of the complete I-AUV model in terms of rigid dynamic equations.
In order to obtain the equations of motion of the whole I-AUV system, it is necessary to obtain, from the Newtonian formulation of the system, the external forces and torques acting on the various bodies of the multibody system. These actions, defined by $\vec{\tau}_{RB}$ in the equation of motion, are:

- control actions $\vec{\tau}$
- sea current disturbances $\vec{\tau}_E$
- hydrodynamic and buoyancy effects $\vec{\tau}_H$

The absolute velocity of the vehicle $\vec{\nu}$ written in the body reference frame is:

$$\vec{\nu} = \vec{\nu}_r + \vec{\nu}_c \ , \tag{5.16}$$

where $\vec{\nu}_r$ is the relative velocity and $\vec{\nu}_c$ is the current velocity. Using (5.16) with the linearity properties of the Coriolis and Damping matrices, it is possible to write the following equation of motion:

$$\begin{aligned} \vec{\tau}_E + \vec{\tau} = {} & (M_{RB} + M_A)\left(\dot{\vec{\nu}}_r + \dot{\vec{\nu}}_c\right) + \\ & + \left(C_{RB}\left(\vec{\nu}_r\right) + C_{RB}\left(\vec{\nu}_c\right) + C_A\left(\vec{\nu}_r\right) + C_A\left(\vec{\nu}_c\right)\right)\left(\vec{\nu}_r + \vec{\nu}_c\right) + \\ & + \left(D\left(\vec{\nu}_r\right) + D\left(\vec{\nu}_c\right)\right)\left(\vec{\nu}_r + \vec{\nu}_c\right) + \vec{g}\left(\vec{\eta}\right) \ . \end{aligned} \tag{5.17}$$

where $M_A$ is the added mass matrix, $M_{RB}$ is the rigid body mass matrix, $C_{RB}$ is the Coriolis rigid body matrix, $C_A$ is the added Coriolis matrix, $D$ is the damping matrix and $g$ is the gravity vector.
Through the same approach, it is possible to obtain the new definition of the Jacobian matrix between body $\vec{\nu}$ and fixed frame $\dot{\vec{\eta}}$ velocities:

$$\dot{\vec{\eta}} = J\left(\vec{\eta}\right)\vec{\nu}_r + J\left(\vec{\eta}\right)\vec{\nu}_c \ . \tag{5.18}$$

Replacing in (5.17) the description of the equation of motion in the current reference frame, the new expressions of the external forces and torques acting on the various bodies as function of current velocity $\vec{\nu}_c$ and relative velocity $\vec{\nu}_r$ are produced:

$$\begin{aligned}\vec{\tau}_H + \vec{\tau}_E = & M_{RB}\dot{\vec{\nu}}_c - M_A\dot{\vec{\nu}}_r + \\ & + C_{RB}\left(\vec{\nu}_r\right)\vec{\nu}_c + C_{RB}\left(\vec{\nu}_c\right)\vec{\nu}_r + C_{RB}\left(\vec{\nu}_c\right)\vec{\nu}_c - C_A\left(\vec{\nu}_r\right)\vec{\nu}_r + \\ & - D\left(\vec{\nu}_r\right)\vec{\nu}_r - \vec{g}\left(\vec{\eta}\right) \ .\end{aligned} \tag{5.19}$$

These actions are reduced and applied to the Center of Gravity (CG) of each rigid bodies. The advantage of the presented method is the possibility to split in two parts the study of the dynamics of rigid bodies immersed in a fluid; in this way it is possible to study the rigid body dynamics through a classical multibody method and evaluating the effects due to the fluid as external forces and torques. Therefore, the equations of motion to describe the whole system are:

$$\begin{aligned}\vec{\tau}_H + \vec{\tau}_E = & M_{RB}\dot{\vec{\nu}}_c - M_A\dot{\vec{\nu}}_r + \\ & + C_{RB}\left(\vec{\nu}_r\right)\vec{\nu}_c + C_{RB}\left(\vec{\nu}_c\right)\vec{\nu}_r + C_{RB}\left(\vec{\nu}_c\right)\vec{\nu}_c - C_A\left(\vec{\nu}_r\right)\vec{\nu}_r + \\ & - D\left(\vec{\nu}_r\right)\vec{\nu}_r - \vec{g}\left(\vec{\eta}\right) \ .\end{aligned} \tag{5.20}$$

and

$$\dot{\vec{\eta}} = J\left(\vec{\eta}\right)\vec{\nu}_r + J\left(\vec{\eta}\right)\vec{\nu}_c \ . \tag{5.21}$$

where $M_A$ is the added mass matrix, $M_{RB}$ is the rigid body mass matrix, $C_{RB}$ is the Coriolis rigid body matrix, $C_A$ is the added Coriolis matrix, $D$ is the damping matrix and $g$ is the gravity vector.
Thanks to Eq. 5.19 and to the knowledge of the control actions $\tau$, it is possible to take in account these effects through:

$$\vec{\tau}_{RB} = \vec{\tau} + \vec{\tau}_H + \vec{\tau}_E. \tag{5.22}$$

and to couple this contribute with the whole multibody system dynamics by means of Eq. 5.15. These actions are reduced and applied to the Center of Gravity (CG) of each rigid bodies. The advantage of the presented method is the possibility to split in two parts the study of the dynamics of rigid bodies immersed in a fluid; in this way it is possible to study the rigid body dynamics through a classical multibody method and considering the effects due to the fluid as external forces and torques.

#### 5.1.2.1 Hydrodynamics and buoyancy effects

The modelling of hydrodynamics and buoyancy effects is necessary to reproduce in a proper way the I-AUV during a navigation or a manipulation task. Particularly, we have implemented these actions in each bodies belonging to the I-AUV system (vehicle, links of the arm and gripper); the simulated effects are:

- hydrostatic effects due to the added masses;
- hydrodynamic effects due to the added masses;
- drag and lift forces;
- buoyancy effects.

For each body, these terms are described with respect to a reference frame system having its origin in the CG of the body, with axes parallel to the principal axes of inertia, vertical downhill z-axis, x-axis along the direction of the vehicle (when the robotic arm is stretched) and the y-axis accordingly in order to define a dexterous reference frame.
As regards the links of the robotic arm, the authors have supposed three assumptions: cylindrical shape, totally immersed bodies and characterized by three levels of symmetry. Assuming that the arm does not move at high velocities, the added mass matrix $M_A$ and the matrix of the centrifugal and Coriolis effects $C_A$ are respectively described in [1].
For a cylindrical body of mass $m$, length $L$ and radius $R$, which moves in a fluid of density $\rho_a$, the coefficients of the matrices $M_A$ and $C_A$ can be obtained according with the strip theory [1], and according with the hypothesis $R \ll L$, the following equations are obtained:

$$\begin{aligned} &X_{\dot{u}} = -0.1\pi\rho_a R^2 L, \quad Y_{\dot{v}} = -\pi\rho_a R^2 L, \quad Z_{\dot{w}} = -\pi\rho_a R^2 L \\ &K_{\dot{p}} = 0, \qquad\qquad M_{\dot{q}} = -\tfrac{1}{12}\pi\rho_a R^2 L^3, \quad N_{\dot{r}} = -\tfrac{1}{12}\pi\rho_a R^2 L^3 \ . \end{aligned} \tag{5.23}$$

As regards the effects of the hydrodynamic resistance, the elements of the damping matrix $D$ are evaluated, my means of CFD analysis [29], expressing the forces and torques through the following six dimensionless parameters:

- Frontal, lateral and vertical drag coefficient:

$$C_{Dx} = \frac{F_x}{\frac{1}{2}\rho_a A_f v^2} \quad C_{Dy} = \frac{F_y}{\frac{1}{2}\rho_a D L v^2} \quad C_{Dz} = \frac{F_z}{\frac{1}{2}\rho_a D L v^2} \tag{5.24}$$

- Roll, pitch and yaw resistance coefficient:

$$C_{Mx} = \frac{M_x}{\frac{1}{2}\rho_a A_f D^3 \omega^2} \quad C_{My} = \frac{M_y}{\frac{1}{2}\rho_a D L^4 \omega^2} \quad C_{Mz} = \frac{M_z}{\frac{1}{2}\rho_a D L^4 \omega^2} \ . \tag{5.25}$$

where the used symbols are: speed $v$, angular velocity $\omega$, frontal area $A_f$ , diameter $D$, fluid density $\rho_a$, length $L$.

### 5.1.3 Control of the UVMS

The equations of motion of UVMS (Underwater Vehicle-Manipulator System, that includes both ROVs and I- AUVs) are formally very similar to the equations of motion of the manipulators with fixed base. There is a wide literature dealing with the control problems for robotic manipulators; this similarity have suggested the development and adaptation of the same techniques and algorithms also in the case of UVMS. However, there are some additional difficulties: the dynamic coupling between the vehicle and the manipulator, the uncertainty in the knowledge of the whole dynamical model (mainly due to the characterization of hydrodynamical effects), the low controllability of the vehicle during the hovering phase(due to the limited performance of the commercial thruster), the kinematic redundancy of the system and the low bandwidth of the sensors typically used for navigation of such vehicles.
In conclusion, it is evident that the UVMSs are very complex systems, characterized by several limitations and control issues.
The algorithms developed for the ROV systems are various and allow the partial resolution of the just exposed difficulties through both robust control and adaptive control techniques. Usually, it is possible to find ROV based on PID controllers with self-calibrated gains (to easily handle the motion of the arm), or adaptive strategies, that guarantee an increasing of the performance compared with two separate controls. In other cases, the Sliding Mode approach is used (with terms of forward compensation to the effects caused by the dynamic coupling between the motion of the manipulator and that of the vehicle). As regards the I-AUVs, the philosophy adopted so far is the following: during the motion of the robotic arm, the vehicle is supposed to be fixed, and it is modeled as a passive joint. Whereas, when the AUV is moving, the manipulator is assimilated to a static element fixed to the body-vehicle. Therefore, all disturbances caused by the relative motion are compensated through the synthesis of control laws sufficiently robust. There are only a few examples of controllers (decentralized) that provide the feed-forward terms to model the dynamic coupling (vehicle ODIN) or adaptive algorithms (SAUVIM [7]). In the following, in order to increase the reliability of the I-AUV, it will be implemented a PID decoupled control technique (for the vehicle and for the manipulator). As regards the robotic arm control, a kinematic controller is preferred comparing with a more complicated dynamical control strategy. The idea is to use the classical algorithm for redundant manipulator, the Control Loop based on the Inverse Differential Kinematics.

#### 5.1.3.1 Vehicle control

The vehicle is supposed to have 6 DOFs in order to allows the manipulation phase. In this part, the classical control strategy based on SISO PID controllers

is used. where the classical transfer function is defined by:

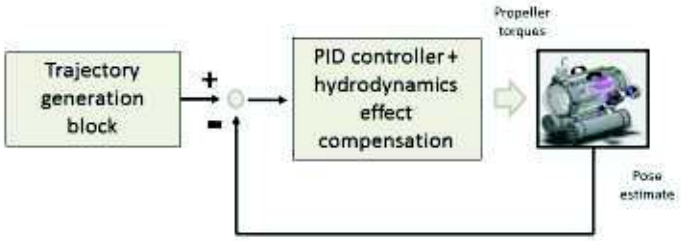


Figure 5.8: SISO PID scheme for the vehicle control based on a defined trajectory

$$G(s) = \frac{U(s)}{E(s)} = k_P + \frac{k_I}{s} + k_D s = \frac{k_D s^2 + k_P s + k_I}{s} \ , \tag{5.26}$$

where the input variable is $e(t)$ the error between the desired trajectory and the measured trajectory, and $k_P$, $k_D$, $k_I$ are the positive gains. Each PID will produce an action $u(t)$ composed by a proportional, derivative and integral components:

$$u(t) = k_P e(t) + k_D \dot{e}(t) + k_I \int_0^t e(T)\, dT \ , \tag{5.27}$$

In the control scheme the dynamic model of the manipulator is not considered because this control strategy is completely decoupled. The drawback is that the coupling effects are considered as disturbances, and after the designing the controller, it is necessary to test the robustness characteristics. Finally, the PID control law is, in vector form:

$$\vec{\tau}_{\text{PID}} = K_P \vec{e}(t) + K_D \dot{\vec{e}}(t) + K_I \int_0^t \vec{e}(T) dT \ , \tag{5.28}$$

where the $K_P$, $K_D$ and $K_I$ matrices are diagonal and positive defined and the variable $\vec{e} = \vec{\eta}_d - \vec{\eta}$ is defined the trajectory error in the NED convention. This variable is derived from the comparison between the desired trajectory, generated by a suitable motion planner algorithm and the state of the system feedback through the on board sensors.
A standard PID control can be improved from the partial knowledge of the vehicle motion laws: in this case, it is possible to introduce a compensation term for the hydrostatic effects; this way, a constant force opposite to the resultant force between the weight and buoyancy of the AUV. According to this strategy, the vector $\vec{\tau}_{\text{PID}}$ is modified:

$$\vec{\tau} = (J_b^n)^T \vec{\tau}_{\text{PID}} + \vec{\tau}_{\text{comp}}(\vec{\eta}) \ , \tag{5.29}$$

where $\vec{\tau}_{\text{comp}}$ is the compensation vector and $\vec{\tau}_{\text{PID}}$ is referred in the body reference frame $< b >$, through the kinematical relation (1.7).

#### 5.1.3.2 Robotic arm control

The control problem of robotic arm is to determine the generalized forces (forces and torques) that the joint actuators have to be applied to the joints by ensuring the reaching of the desired characteristics during both the transient and the steady state phases. Usually, the motion characteristics are specified in the operative space and the control actions are directly calculate in the joint space. The control techniques of a robotic manipulator are traditionally divided into two approaches: joint space control and operative space one. In both cases, the control structure present the feedback closure to guarantee the robustness of the control.
The control scheme of the robotic arm is schematically described in Figure 5.9: The blocks described in Figure 5.9 are:

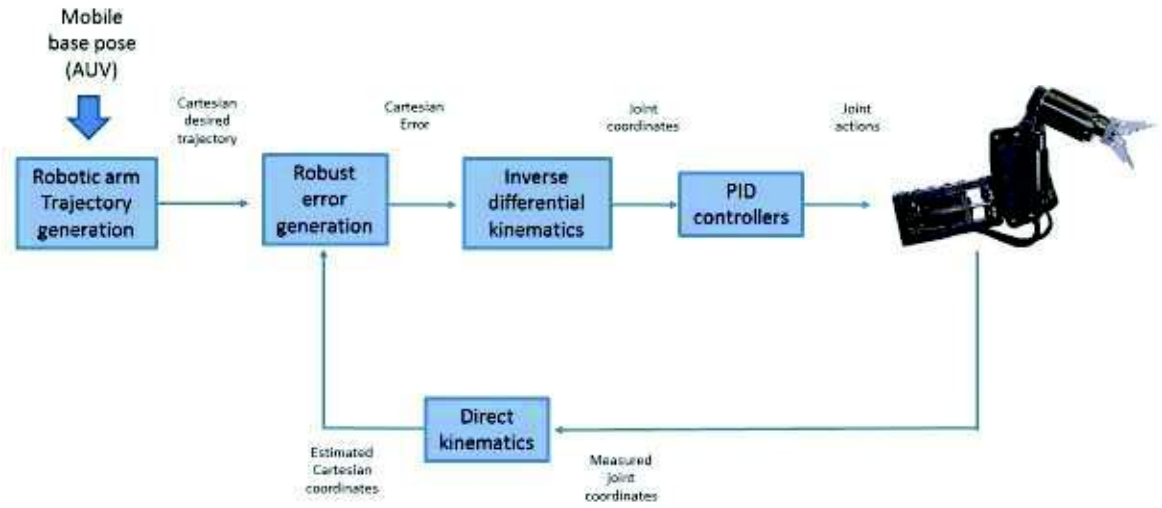


Figure 5.9: Inverse differential kinematics approach

- Robotic arm trajectory generation: this block allows the generation of the end-effector trajectory starting from the real pose (position and orientation) of the manipulator base (the AUV pose). The generation is performed according to the task to executed.

- Robust error generation: in this part the generation of the error in the Cartesian space is made. To increase the robustness of the kinematic control approach, a quaternion description of the orientation is implemented.

- Inverse differential kinematics: the inverse of the differential kinematics allows the change from the Cartesian space to the joint one. In this part, the use of the damped pseudo-inverse approach is used; the main task is to minimize the kinetic energy and the second one is to avoid singularity in the workspace (see section 5.1.1).
- PID controllers: they permit to obtain the joint actions starting from joint coordinates.
- Direct kinematics: this block is used to obtain from the real joint coordinates the estimated Cartesian coordinates of the end-effector.

# Chapter 6

# Cooperative Mobile Manipulation: control architecture

In this chapter, after a description of the potential field method theory, the cooperative control architecture for the mobile manipulation tasks is presented. The cooperative control architecture is based on the interaction between different potentials: Vehicle-Vehicle, Vehicle-Object, Vehicle-Obstacle. Usually, the potential field method is the base of the obstacle avoidance method: the main idea is to extend this approach also for the mobile manipulation of Intervention-AUV.
The proposed control architecture starts from the idea of reducing the number of necessary informations: it is supposed to decrease the necessity of expensive sensors and to use a decentralized approach. The approach can be seen as a classical decentralized approach because the knowledge of the vehicle is limited to few on board sensors; in section 6.2, this method is in detail explained.

## 6.1 Potential field method theory

In the potential field method, the vehicle is considered as a particle immersed in a potential field generated both by the goal and by the obstacles. The goal generates an attractive potential and each obstacle generates a repulsive potential. A potential field can be viewed as an energy field and its gradient at each point is a force. Therefore, the vehicle immersed in the potential field is subjected to two contributes: the target force action that drives it to the goal (due to the attractive potential gradient generated by the goal) and the obstacle force actions that repulses the vehicle from the obstacles (due to the repulsive potential gradient produced by the obstacles). In potential field based methods, the vehicle motion can be interpreted as the particle motion

in a gradient vector field generated by positive and negative electric particles. In this analogy, the vehicle is a positive charge, the target is a negative charge and the obstacles in order to repulse the vehicle are seen as positive charges. Gradients in this context can be interpreted as forces that attract the positively charged vehicle particle to a negative particle that acts as the target. The obstacles act as positive charges that generate repulsive forces. The superposition of the target attractive force and the obstacle repulsive forces drive the vehicle in a safe path to the target. The vehicle follows the path along the negative gradient of the potential function which means moving downhill towards the lowest point of the potential. Through this analogy, it is clear that the vehicle may be trapped in local minima away from the goal, this being a known drawback of the original version of potential field based methods.
Considering the tri-dimensional problem applied to a vehicle in which $\vec{q} = [xyz]^T$ is the position of the vehicle. The artificial potential field method defines a scalar function $U(\vec{q})$ generated by the superposition of attractive and the sum of repulsive potentials.

$$U(\vec{q}) = U_{att}(\vec{q}) + \sum U^i_{rep}(\vec{q}) \tag{6.1}$$

where $U^i_{rep}(\vec{q})$ is the repulsive potential generated by the i-th obstacle. Consider $U(\vec{q})$ is differentiable: at each $\vec{q}$, the gradient of the potential field, denoted by $\vec{\nabla}U(\vec{q})$, is a vector that points in the direction that locally maximally increases $U(\vec{q})$. In the potential field methods, the attractive potential is chosen to be zero at the target and to increase as the robot is far away from the goal. The repulsive potential, associated with each obstacle, is very high near to the obstacles and decreases when the distance to the obstacle increases. Along these principles, different attractive potentials may be chosen. Furthermore, the force that drives the robot is the negative gradient of the artificial potential, i.e.,

$$\vec{F}(\vec{q}) = \vec{F}_{att}(\vec{q}) + \vec{F}_{rep}(\vec{q}) = -\nabla U_{att}(\vec{q}) - \nabla U_{rep}(\vec{q}) \tag{6.2}$$

The force $\vec{F}(\vec{q})$ is a vector that points in the direction that, at each $(\vec{q})$, locally decreases $U$.

**Attractive potential**

Usually, the attractive potential is defined by the parabolic function that grows quadratically with the distance to the target:

$$U_{att}(\vec{q}) = \frac{1}{2} k_{att} d^2_{target}(\vec{q}) \tag{6.3}$$

where $d_{target}(\vec{q}) = \|(\vec{q} - \vec{q}_{target})\|$ is the Euclidean distance of the vehicle from the target $\vec{q}_{target}$ and $k_{att}$ is the scaling factor. The gradient,

$$\vec{\nabla}U_{att}(\vec{q}) = k_{att}(\vec{q} - \vec{q}_{target}) \tag{6.4}$$

is a vector field proportional to the difference $(\vec{q}-\vec{q}_{target})$ that points away from $\vec{q}_{target}$. The farther away the vehicle is from the goal, the bigger the magnitude of the attractive field. The attractive force considered in the Potential Field method is the negative gradient of the attractive potential

$$\vec{F}_{att}(\vec{q}) = -\vec{\nabla}U_{att}(\vec{q}) = -k_{att}(\vec{q} - \vec{q}_{target}) \tag{6.5}$$

According to the hypothesis that the vehicle velocity vector is proportional to the vector field force, the force $\vec{F}_{att}(\vec{q})$ drives the vehicle to the target with a velocity that decreases when the vehicle approaches the target. The force

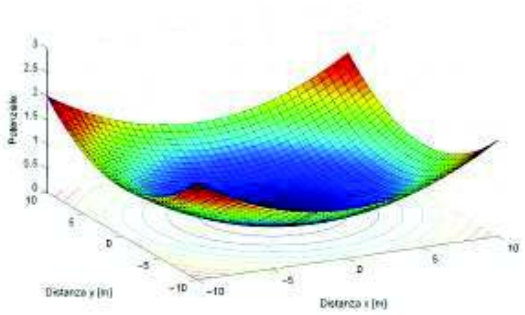


Figure 6.1: Target attractive potential

$\vec{F}_{att}(\vec{q})$ represents a linear dependence to the target, which means that it grows with no bound as $\vec{q}$ moves away from the goal which may determine a fast vehicle velocity whenever far from the $\vec{q}_{target}$. When the vehicle is far away from the target, this force imposes that it quickly approaches the goal, i.e., that it moves directly to the goal with a high velocity. On the contrary, the force and the vehicle velocity tend to zero, when the robot approaches the target. Therefore the target slowly approaches the target which is a useful feature to reduce target overshoot.

**Repulsive potential**

The repulsive potential allows the keeping of the vehicle position away from the obstacles, both those a priori known or those detected by the on-board sensors. The concept is the same of the attractive potential: the repulsive potential is stronger when the vehicle is closer to the obstacle and has a decreasing influence when the vehicle is far away. Given the linear nature of the problem, the repulsive potential is obtained from the sum of the repulsive effects of all the obstacles, i.e. $U_{rep}(\vec{q}) = \sum U^i_{rep}(\vec{q})$. It is reasonable to consider that the obstacle influence is limited to a bounded space near the object. An obstacle very far from the vehicle is not necessary felt by the vehicle. However, the magnitude of repulsive potential should increase when the robot approaches to the obstacle. To take into account this effect and the space bounded influence,

a possible repulsive potential generated by the $i-th$ obstacle is:

$$U^i{}_{rep}(\vec{q}) = \begin{cases} \frac{1}{2}k_{obst}\left(\frac{1}{d^i{}_{obs}(\vec{q})} - \frac{1}{d_0}\right)^2 \; if \; d^i{}_{obs}(\vec{q}) < d_0 \\ 0 \quad if \; d^i{}_{obs}(\vec{q}) \geq d_0 \end{cases} \tag{6.6}$$

where $d^i{}_{obs}$ is the minimal distance from $\vec{q}$ to the obstacle i, $k^i_{obst}$ is a scaling constant and $d_0$ is the obstacle influence threshold. The repulsive potential gradient $\vec{F}_{rep}(\vec{q}) = -\vec{\nabla}U_{rep}(\vec{q})$ is given by:

$$\vec{F}^i_{rep}(\vec{q}) = \begin{cases} k_{obst}\left(\frac{1}{d^i{}_{obs}(\vec{q})} - \frac{1}{d_0}\right)\frac{(\vec{q}-\vec{q}_{obs})}{d^3{}_{obs}(\vec{q})} \; if \; d^i{}_{obs}(\vec{q}) < d_0 \\ 0 \; if \; d^i{}_{obs}(\vec{q}) \geq d_0 \end{cases} \tag{6.7}$$

The presented potential field method is a simple path planning technique that has an intuitive operation principle based on potential fields. This method can be applied both in off-line version and in on-line one. One of the main drawback of this method is its high sensitivity to local minima that usually arise due to the symmetry of the environment and to concave obstacles.

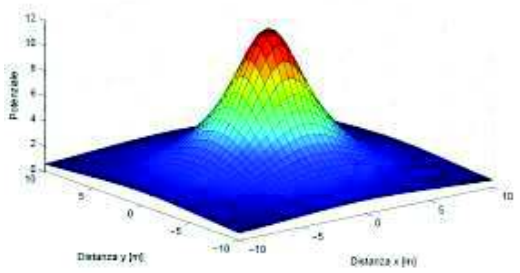


Figure 6.2: Obstacle repulsive potential

## 6.2 Control strategy

The control strategy for mobile manipulation is one of the challenging field in mobile robotics. The classical approaches for these control strategies can be synthetically divided into two main parts:

- Centralized approaches: these methods are used when a single robot is able to organize and to know the real pose of the whole swarm. There are different levels of centralized approach but in all cases, it is supposed to be known a high number of external variables; moreover, these approaches can include force control loop.

- Decentralized approaches: in these cases, the knowledge of each vehicle is limited to few information mainly coming from the on board sensors.

Usually, these methods presuppose a high number of mobile manipulators to overcome the limited knowledge. Also in these approaches, the force control loop can be performed.

Many researches are interested in this problem especially for terrestrial mobile robots but, in the underwater field, the classical approaches are more difficult because, both the localization and the communication, are more complex and less reliable. In the proposed case, the target application can be seen as the transportation of a generic object along an unstructured environment.
Since the characteristics of the considered I-AUVs, the proposed control architecture born from the idea of using the minimum number of parameters; the potential field method is very interesting from this point of view. Moreover, the potential field method is also suitable in unstructured and dynamic environments because it presupposes the reaching of the target position without the a priori knowledge of the trajectory. As briefly described in section 6.1, the advantages of the potential field method are that is usually based on the distance estimate and the exact knowledge of vehicle position is not necessary. Therefore, this method can be studied to evaluate the advantages and drawbacks for the mobile manipulation. Some simplification hypotheses could be made:

- the communication between acoustic modems is always possible and the delays are negligible;
- the I-AUVs vehicle control points the vehicle in the attractive target direction;
- the approaching phase is not considered.

The control architecture considers three main subjects: the I-AUVs, the object to be transported and the external environments (obstacles). In Figure 6.4,

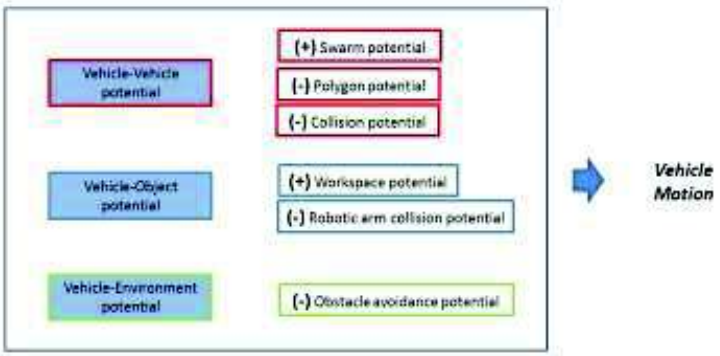


Figure 6.3: Control architecture scheme: potential interactions

the interactions between vehicles, object and environment are shown. The

interactions between vehicles (in order to avoid collisions) are coloured in black; the interaction between vehicle and the swarm formation are in green. The environment (with the possible obstacles) is coloured in red and the four arrows indicate the interaction with vehicles. The object to be manipulated is in blue and the four arrows show the connections between vehicles and object. Finally, on the right part of the figure also the interaction between environment and object is highlighted; this relation is an indirect connection (dotted line) because it is only obtained supposing the knowledge both of the object and of the obstacle shape.

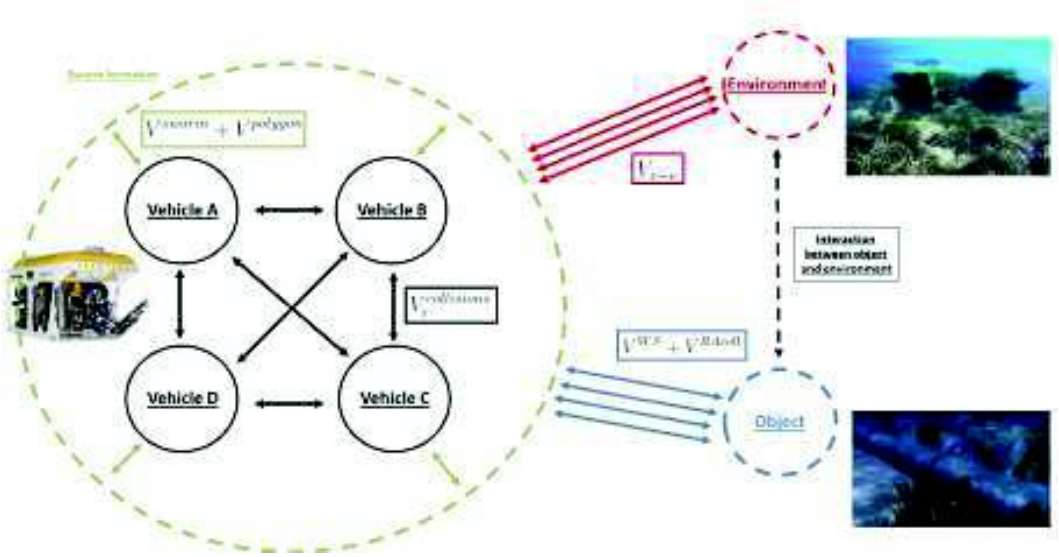


Figure 6.4: Interactions between potentials

### 6.2.1 Vehicle-Vehicle potential

The Vehicle-Vehicle potential $V_{v-v}$ consists of three main parts: the attractive potential to keep the vehicles in formation, the repulsive potential to keep the vehicles in a predefined shape (e.g. the vertices of a regular polygon) and the repulsive potential to avoid collisions between vehicles:

$$V_{v-v} = V^{swarm} + V^{polygon} + V_i^{collisions} \tag{6.8}$$

where $V_{v-v}$ is the total Vehicle-Vehicle potential acting on each vehicle, $V^{swarm}$ is the vehicle swarm potential, $V^{polygon}$ is vehicle polygon potential and $V_i^{collisions}$ is the vehicle collision potential (see Figure 6.5). The input of these three potential functions are obtained from the acoustic modems using the TDOA algorithms. As regards the vehicle distance estimation, the concept is to use the acoustic modem as range sensors (in terms of modulus) using the classical Time Difference Of Arrival (TDOA). The distance vector (position of

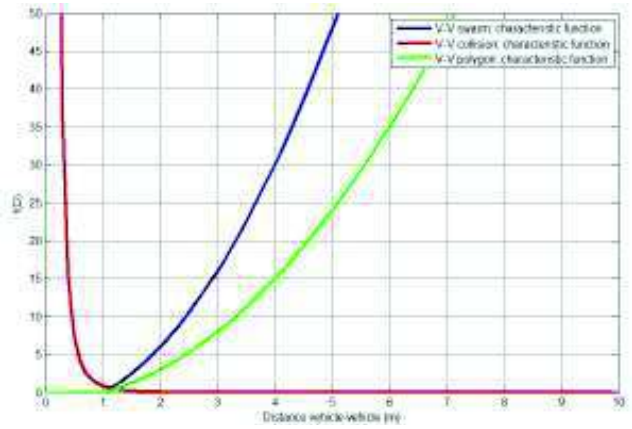


Figure 6.5: Vehicle-Vehicle potentials

I-AUVs) is externally provided by a supply vehicle probably equipped of an USBL device. This approach is based on the time slot architecture for the communication of each vehicle.
The vehicle swarm potential is based on the attractive potential and it is carried out both to keep within a spherical shape the I-AUVs and to attract the vehicles to the target position. In this case, the considered distance $d_i = \left\|\vec{x}_i - \vec{G}_d(t)\right\|$ is the distance between the vehicle position $\vec{x}_i$ and the center of the spherical shape $\vec{G}_d(t)$ (which can be time variable). This measurement can be made through the localization algorithm installed on board to the vehicle. Therefore, the force $\vec{F}_i^{swarm}$ acting on the vehicle is:

$$\vec{F}_i^{swarm} = -f_i^{swarm}(\left\|\vec{d}_i\right\|)\frac{(\vec{x}_i - \vec{G}_d(t))}{\left\|\vec{x}_i - \vec{G}_d(t)\right\|} \tag{6.9}$$

where $f_i^{swarm}(\left\|\vec{d}_i\right\|)$ is a defined function of the distance. In this case, the function has to consider a low boundary equal to the radius of the spherical shape in order to attract the vehicle outside the shape and to keep free the inside vehicles:

$$f_i^{swarm}(\left\|\vec{d}_i\right\|) = -k_s((\left\|\vec{d}_i\right\|)^2 - R^2), \tag{6.10}$$

where $k_s$ is the shape parameter to increase the tilt of the curve and $R$ is the spherical shape radius.
According to the section 6.1, the attractive potential is a vector field proportional to the difference $(\vec{x}_i - \vec{G}_d(t))$ that points away from $\vec{G}_d(t)$. The farther away the vehicle is from the target, then bigger the magnitude of the attractive field. Moreover, according to the hypothesis that the vehicle velocity vector is proportional to the vector field force, the force $\vec{F}_i^{swarm}$ drives the vehicle to the target with a velocity that decreases when the vehicle approaches the target.
The vehicle polygon potential $V^{polygon}$ is a repulsive potential and its objective

is to keep the vehicles at the vertices of a regular polygon (depending on the number of vehicles). This potential is necessary to send away from a same vertix two or more vehicles and to properly set the vehicles inside the spherical shape. In this repulsive potential, the distance to be considered is the reciprocal distance among two vehicles $d_{i,j} = \|\vec{x}_i(t) - \vec{x}_j(t)\|$ where $\vec{x}_i$ is the $i-th$ vehicle position and $\vec{x}_j$ is the $j-th$ vehicle position (in this case, the positions are time variable). The distance among two vehicles can be made using the acoustic modems and the TDOA algorithm (which using the IMU measurement can provide an estimation of the direction). Therefore, the force $\vec{F}_{i,j}^{polygon}$ acting on the $i-th$ vehicle is the sum of the contributes for each vehicles:

$$\vec{F}_{i,j}^{polygon} = +f_{i,j}^{polygon}(\left\|\vec{d}_{i,j}\right\|)\frac{(\vec{x}_i(t) - \vec{x}_j(t))}{\|\vec{x}_i(t) - \vec{x}_j(t)\|} \tag{6.11}$$

where $f_{i,j}^{polygon}(\left\|\vec{d}_{i,j}\right\|)$ is a characteristic function of the distance. For this case, the repulsive function has to consider an upper bound equal to the radius of the spherical shape in order to not overcome the spherical shape and to keep on the edge the vehicles:

$$f_{i,j}^{polygon}(\left\|\vec{d}_{i,j}\right\|) = +k_p\left(\frac{1}{\left\|\vec{d}_{i,j}\right\|^2} - \frac{1}{R^2}\right), \tag{6.12}$$

where $k_p$ is the repulsive shape parameter to increase the tilt of the curve and $R$ is the spherical shape radius.
According to section 6.1, the repulsive potential is stronger when the vehicle is closer to another vehicle and it has a decreasing influence when the vehicle is far away. In this case, the repulsive potential is obtained from the sum of the repulsive effect of all the vehicle, i.e. $U_i^{polygon}(\left\|\vec{d}_{i,j}\right\|) = \sum U_{i,j}^{polygon}(\left\|\vec{d}_{i,j}\right\|)$. It is reasonable to consider that the vehicle influence is limited to a bounded space near the object.
Finally, the vehicle collision potential $V_i^{collisions}$ is a repulsive potential and prevents collisions between the vehicles. This potential is calculated for each vehicles and is useful when the object to be transported is quite small compared with the vehicle workspaces and there is the possibility of vehicle collisions. Also in this potential, the distance to be considered is the reciprocal distance among two vehicles $d_{i,j} = \|\vec{x}_i(t) - \vec{x}_j(t)\|$ which is described before. The force $\vec{F}_{i,j}^{collisions}$ acting on the $i-th$ vehicle is the sum of the contributes for each vehicles:

$$\vec{F}_{i,j}^{collisions} = +f_{i,j}^{collisions}(\left\|\vec{d}_{i,j}\right\|)\frac{(\vec{x}_i(t) - \vec{x}_j(t))}{\|\vec{x}_i(t) - \vec{x}_j(t)\|} \tag{6.13}$$

where $f_{i,j}^{collisions}(\left\|\vec{d}_{i,j}\right\|)$ is a characteristic function of the distance. For this case, the repulsive function has to consider an upper bound equal to a radius

belonging of a spherical shape doubling the vehicle sizes. This approximation permits to not collide the vehicles:

$$f_{i,j}^{collisions}(\left\|\vec{d}_{i,j}\right\|) = +k_c \left( \frac{1}{\left\|\vec{d}_{i,j}\right\|^2} - \frac{1}{d_c^2} \right), \tag{6.14}$$

where $k_c$ is the repulsive shape parameter to increase the tilt of the curve and $d_1$ is the radius belonging of a spherical shape doubling the vehicle sizes.
The repulsive potential allows the keeping of the vehicle far from the the other vehicles; moreover, the potential is stronger when the vehicle is closer to another vehicle and it has a decreasing influence when the vehicle is far away. Also in this case, the repulsive potential applied to a vehicle is obtained from the sum of the repulsive effect of all the vehicles, i.e. $U_i^{collision}(\left\|\vec{d}_{i,j}\right\|) = \sum U_{i,j}^{collision}(\left\|\vec{d}_{i,j}\right\|)$.

### 6.2.2 Vehicle-Object potential

The Vehicle-Object potential $V_{v-obj}$ allows the motion of the vehicle to maintain a correct position of the end-effector compared to the vehicle position. Particularly, in this case, the robotic arm controller explained in section 5.1.3 is partially replaced from this potential function: through the equilibrium of this potential function, the end-effector and the vehicle can react to changes of the external conditions. The vehicle-object potential can be carried out both on the vehicle and on the robotic arm; in the proposed approach, this potential function is applied to the vehicle motion in order to easily changes the vehicle motion to reject a robotic arm disturbance. The followed approach allows that the vehicle navigation is also function of the object position. The kinematic controller presented in section 5.1.3 can be activated when the potential function is not suitable for a task, e.g. when you consider a precise manipulation task. In addition, it allows the estimation of the best working condition for the robotic arm position. The concept of using potential function rather than a classical kinematical controller is to keep less stiff the interactions among vehicle and robotic arm: this way, the dynamical coupling these two systems are reduced.
The vehicle-object potential consists of two contributes: the workspace potential function $V^{WS}$ and the robotic arm collision potential function $V^{RAcoll}$.

$$V_{v-o} = V^{WS} + V^{RAcoll} \tag{6.15}$$

where $V_{v-o}$ is the whole Vehicle-Object potential acting on the vehicle, $V^{WS}$ is the workspace potential, which permits to maintain the end-effector position within the robotic arm workspace, and $V^{RAcoll}$ is the robotic arm collision potential which avoids collisions among vehicle and end-effector (see Figure

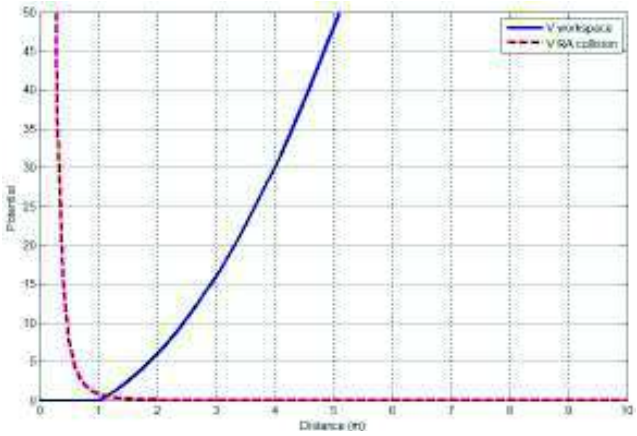


Figure 6.6: Vehicle-Vehicle potentials

6.6). The workspace potential is based on the attractive potential function and is necessary to maintain the end-effector position within the workspace of the robotic arm. As regards the considered distance, $d_{ee,v} = \|\vec{x}_v - \vec{x}_{ee}\|$ is the distance between the robotic arm position $\vec{x}_v$ and the end-effector position $\vec{x}_{ee}$. This distance measurement can be made through direct kinematics algorithm: knowing the joint variables, it is possible to obtain a single solution to the direct kinematic problem. The force $\vec{F}_i^{WS}$ acting on the vehicle is:

$$\vec{F}^{WS} = -f^{WS}(\|d_{ee,v}\|)\frac{(\vec{x}_v - \vec{x}_{ee})}{\|\vec{x}_v - \vec{x}_{ee}\|} \tag{6.16}$$

where $f^{WS}(\left\|\vec{d}_{ee,v}\right\|)$ is a characteristic function of the distance. This function can be realized through a quadratic curve limited with upper and lower bounds respectively defined by the maximum extension of the robotic arm and by the minimum one:

$$\begin{cases} f^{WS}\left(\|d_{ee,v}\|\right) = -k_{WS}\left(\left(\|d_{ee,v}\|\right)^2 - R_{max}^2\right) & if\ R_{min} \leq \left(\|d_{ee,v}\|\right) \leq R_{max} \\ f^{WS}\left(\|d_{ee,v}\|\right) = 0 & \|d_{ee,v}\| < R_{min} \end{cases} \tag{6.17}$$

where $k_{WS}$ is the shape parameter to increase the tilt of the curve, $R_{max}$ is the maximum extension of the robotic arm and $R_{min}$ is the minimum extension of the robotic arm. The function has also a saturation in force depending on the manipulator characteristics.
The attractive potential is a vector field proportional to the difference $(\vec{x}_v - \vec{x}_{ee})$ that points away from $\vec{x}_{ee}$. The concept is to maintain the best end-effector position.
The robotic arm collision potential is a repulsive potential and its objective is to keep the end-effector away from the vehicle. This potential is required to

change the vehicle trajectory when the manipulator are moving in a different position. In this repulsive potential, the distance to be considered is the same of the previous case: $d_{ee,v} = \|\vec{x}_v - \vec{x}_{ee}\|$ is the distance between the robotic arm position $\vec{x}_v$ and the end-effector position $\vec{x}_{ee}$. This distance measurement can be made through direct kinematics algorithm: knowing the joint variables, it is possible to obtain a single solution to the direct kinematic problem. The force $\vec{F}^{RAcoll}$ acting on the vehicle is:

$$\vec{F}^{RAcoll} = +f^{RAcoll}(\|d_{ee,v}\|)\frac{(\vec{x}_v - \vec{x}_{ee})}{\|\vec{x}_v - \vec{x}_{ee}\|} \tag{6.18}$$

where $f^{RAcoll}(\left\|\vec{d}_{ee,v}\right\|)$ is a characteristic function of the distance. The repulsive function has an upper bound equal to the minimum extension of the robotic arm:

$$f^{RAcoll}(\left\|\vec{d}_{ee,v}\right\|) = +k_{RA}\left(\frac{1}{\left\|\vec{d}_{ee,v}\right\|^2} - \frac{1}{R_{min}^2}\right), \tag{6.19}$$

where $k_{RA}$ is the repulsive shape parameter to increase the tilt of the curve and $R_{min}$ is the minimum extension of the robotic arm.

### 6.2.3 Vehicle-Environments potential

The Vehicle-Environment potential $V_{v-e}$ is necessary to avoid obstacles during the transportation of the object. This potential is a repulsive potential because it has to modify the vehicle trajectories to avoid the obstacle. The input necessary to the repulsive potential function are only provided by the on board sensors (echo-sounder and IMU). In addition, the $V_{v-e}$ potential, knowing an estimate of the object position can carries out at the object the obstacle avoidance (maintaining the connections with the object).
The Vehicle-Environment potential $V_{v-e}$ is calculated for each obstacles. In this potential, the distance to be considered is the reciprocal distance among a vehicle and the obstacle $d_{i,o} = \|\vec{x}_i(t) - \vec{x}_o(t)\|$ where $\vec{x}_i$ is the $i-th$ vehicle position and $\vec{x}_o$ is the obstacle position. The force $\vec{F}_{i,o}^{v-e}$ acting on the $i-th$ vehicle is the sum of the contributes for each obstacles:

$$\vec{F}_{i,o}^{v-e} = +f_{i,o}^{v-e}(\left\|\vec{d}_{i,o}\right\|)\frac{(\vec{x}_i(t) - \vec{x}_o(t))}{\|\vec{x}_i(t) - \vec{x}_o(t)\|} \tag{6.20}$$

where $f_{i,o}^{v-e}(\left\|\vec{d}_{i,o}\right\|)$ is a characteristic function of the distance. The considered repulsive function has an upper bound equal to a radius belonging of a spherical shape doubling the vehicle sizes. This way, the vehicle has the margin to avoid the obstacle. The characteristic function is :

$$f_{i,o}^{v-e}(\left\|\vec{d}_{i,o}\right\|) = +k_O\left(\frac{1}{\left\|\vec{d}_{i,o}\right\|^2} - \frac{1}{d_O^2}\right), \tag{6.21}$$

where $k_O$ is the repulsive shape parameter to increase the tilt of the curve and $d_O$ is the radius belonging of a spherical shape doubling the vehicle sizes.
The repulsive potential allows the keeping of the vehicle far from the the other obstacles. The potential is stronger when the vehicle is closer to an obstacle and it has a decreasing influence when the vehicle is far away. In case of many obstacles, the repulsive potential applied to a vehicle is obtained from the sum of the repulsive effects of each obstacle, i.e. $U_i^{v-e}(\left\|\vec{d}_{i,o}\right\|) = \sum U_{i,o}^{v-e}(\left\|\vec{d}_{i,o}\right\|)$.

## 6.3 UVMS control architecture

The cooperative control control architecture described in the previous section also modifies the control architecture of the UVMS (both of the vehicle and of the robotic arm). The new control strategy based on the potential field method uses only few information coming from the external part of the vehicle; most of these are obtained by the on board sensors. As can be seen from the

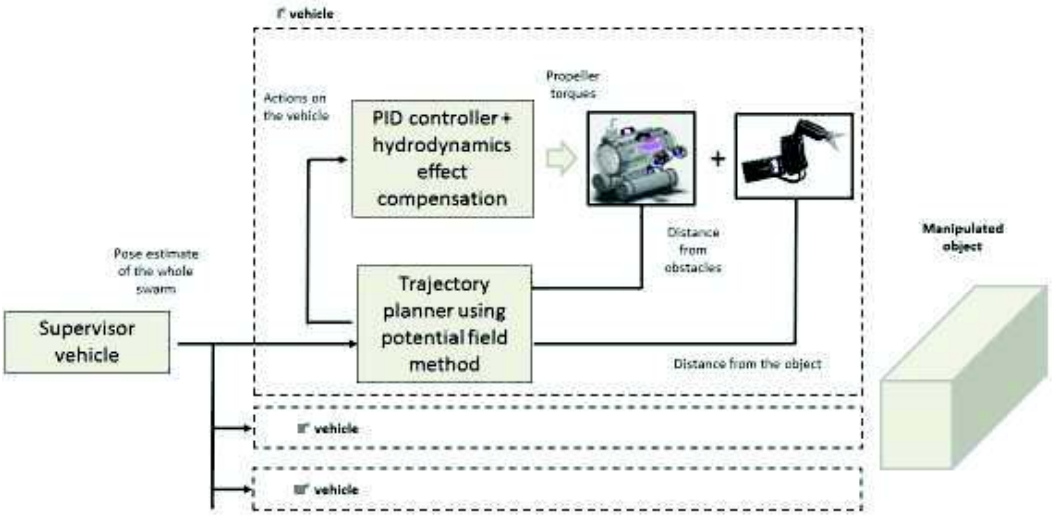


Figure 6.7: UVMS control strategy based on potential field approach

UVMS control architecture (Figure 6.7), each vehicle is controlled through the trajectory planner in which the three potential contributes (Vehicle-Vehicle, Vehicle-Object, Vehicle-Environment) are calculated to obtain the best trajectory satisfying all the constrains. The effects of the potential field are only applied on the vehicle; therefore, the redundant DOFs of the UVMS are used to keep in formation the vehicles. Concerning the control strategy presented in section 5.1.1, the robotic arm continue to use the redundant DOFs to keep the correct pose and to avoid singularity configurations.
As regard the supervisor vehicle, the necessity to properly localize the vehicles is caused to calculate the distance vectors between all the vehicles and it will probably use a Ultra Short Base Line (USBL) device.

# Chapter 7

# Cooperative Mobile Manipulation: simulations and results

In this chapter, the results of the numerical simulations are analysed. The objective of this analysis is to prove the proposed cooperative strategy for a swarm of Intervention-Autonomous Underwater Vehicle, highlighting advantages and drawbacks. The simulated tasks are referred to potential functions shown in section 6.2:

- Vehicle-Vehicle potential function: the interactions between vehicles are based on the classical attractive and repulsive potential functions and consist of three contributes. The first one is the swarm potential function (attractive) able to keep the vehicles within a spherical shape; the second one is the polygon potential function (repulsive) that allows the vehicle distribution on the polygon vertices. The last one is the collision potential function (repulsive) that avoids the collision between vehicles.

- Vehicle-Object potential function: the control of the robotic arm is partially replaced from this potential function control. The vehicle is subjected to two contributes: the workspace potential function, in which the end-effector is controlled to remain within the robotic arm workspace, and the robotic arm collision potential function, that allows the changes of the vehicle trajectory to avoid collision between vehicle and object.

- Vehicle-Environment potential function: this is the classical obstacle avoidance technique able to dynamically avoid obstacles during the vehicle trajectories.

The sum of all these contributes carries out the I-AUVs swarm trajectory. The analysed task is a classical transportation task in which the swarm is composed by four-five I-AUVs with 6DOFs. Each vehicle has a single robotic arm

with 7DOFs and a gripper that is (for hypothesis) rigidly connected with the object. In this simulation the approaching phase is neglected. The simulation environment is MATLAB®- Simulink (Simmechanics tool) where the I-AUVs are modelled using the multibody approach explained in section 5.1.2. The used integrator is the fixed step ODE 5 Dormand-Prince with a step-size of $1e-4$ s.

## 7.1 Swarm control

In this section will be better analysed the behaviour of the I-AUVs swarm when the Vehicle-Vehicle potential function is activated. The simulations started from a generic configuration of the I-AUVs are attracted from a spherical shape which is performing a straight line trajectory. In the performed simulation, the I-AUVs are not rigidly connected to the object in order to emphasize the potential fields effects. The enabled potential functions are the swarm potential function, the polygon potential function and the collision one. The potential functions are mainly used to control X-Y-Z DOFs. In Figure 7.1, the initial conditions of the swarm are shown.

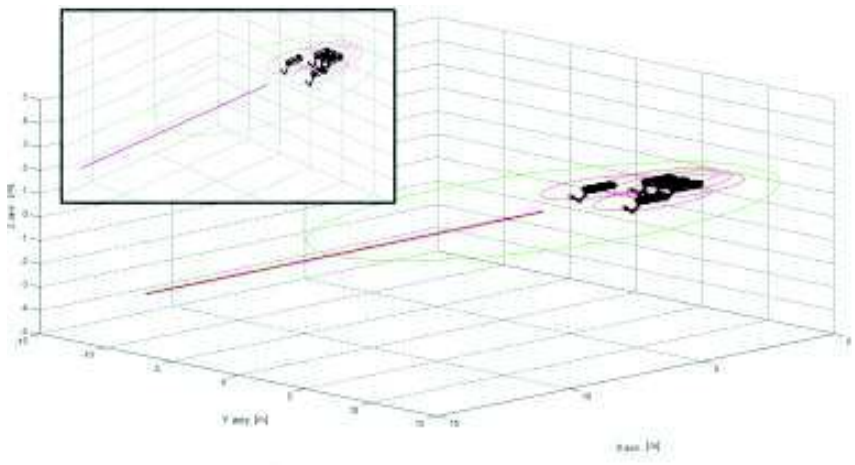

Figure 7.1: Initial conditions of the I-AUVs swarm

In Figures from 7.2 to 7.6, the behaviour of the vehicle in terms of $\vec{\eta} = [x\ y\ z\ \rho\ \phi\ \psi]$ is shown.
All graphics show the efficiency of the roll-pitch-yaw control; in fact, the angular coordinates are quite stable and the error are very low.

As can be seen from these graphics, the behaviour of the vehicles after a brief transient is quiet calm. In the transient, the collision potential functions generate force actions to keep the vehicle at a correct distance. Finally, the control actions go to zero because the vehicles have reached their stable con-

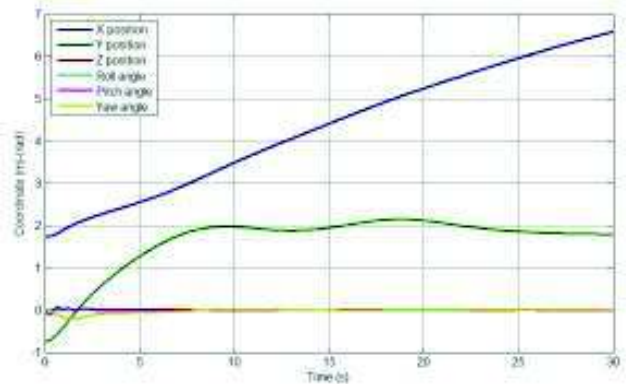


Figure 7.2: Vehicle 1: position and orientation

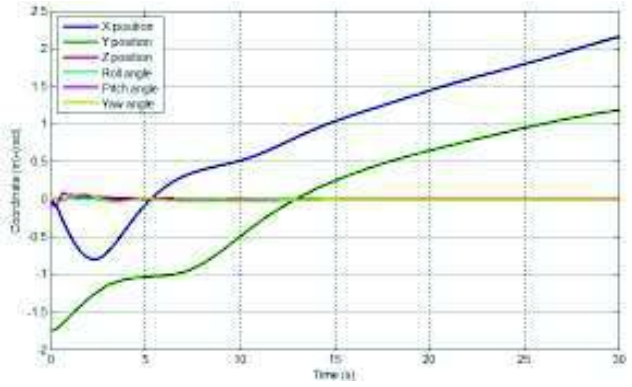


Figure 7.3: Vehicle 2: position and orientation

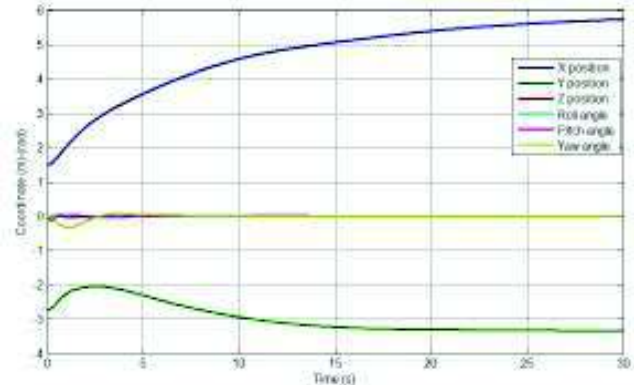


Figure 7.4: Vehicle 3: position and orientation

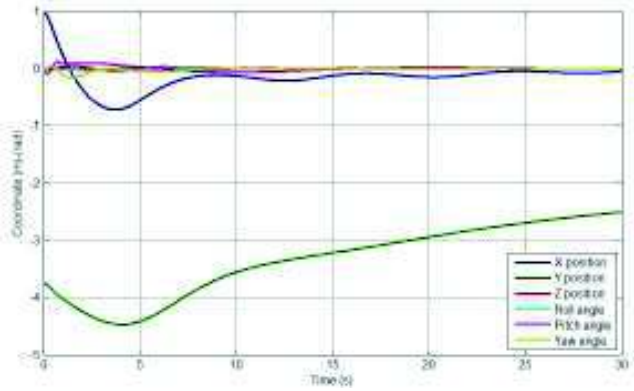


Figure 7.5: Vehicle 4: position and orientation

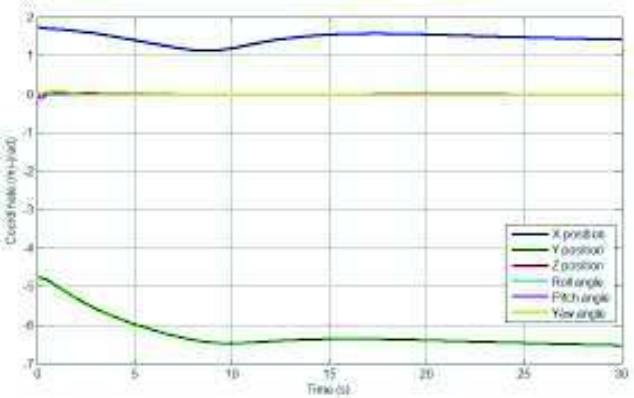


Figure 7.6: Vehicle 5: position and orientation

figuration at the regular polygon vertices. In the following, the final position of the I-AUVs swarm is shown.

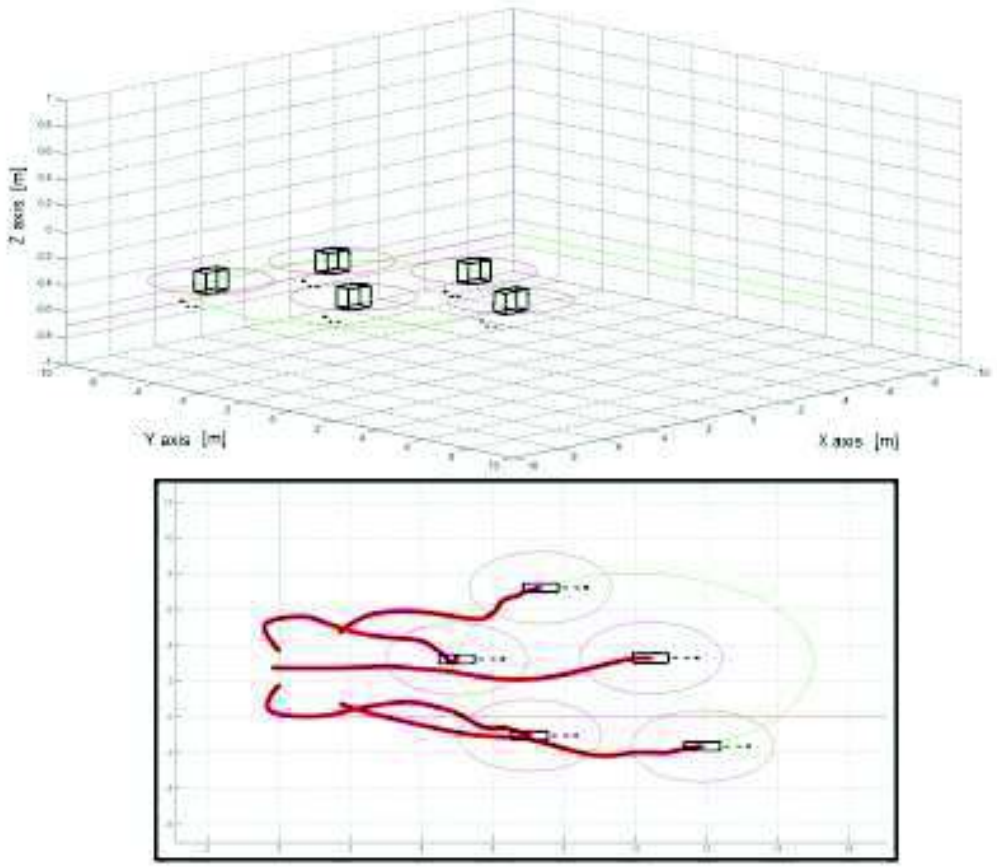


Figure 7.7: Final conditions of the I-AUVs swarm

## 7.2 Swarm obstacle avoidance

In this second section, the I-AUVs swarm behaviour is analysed when the swarm deal an obstacle. In this simulation, it is considered the contributes due to both the Vehicle-Vehicle potential function and the Vehicle-Environment one. Therefore, the behaviour of the vehicles is obtained as the sum of four different potential functions: the swarm potential function, the polygon one, the collision one and the obstacle avoidance function. The obstacle is modelled as a spherical shape. The initial conditions of the simulation are the same of the previous simulation.
In this case, in the vehicle navigation control, a useful feature for the next steps of mobile manipulation is introduced: the desired yaw angle is given by the time-derivative of the longitudinal direction. This way, the vehicle is constrained to always point out towards the longitudinal direction of the vehicle, reducing the hydrodynamics effects. In Figure 7.8, the initial positions of the vehicles are represented. Figures from 7.9 to 7.13 describe the dynamical

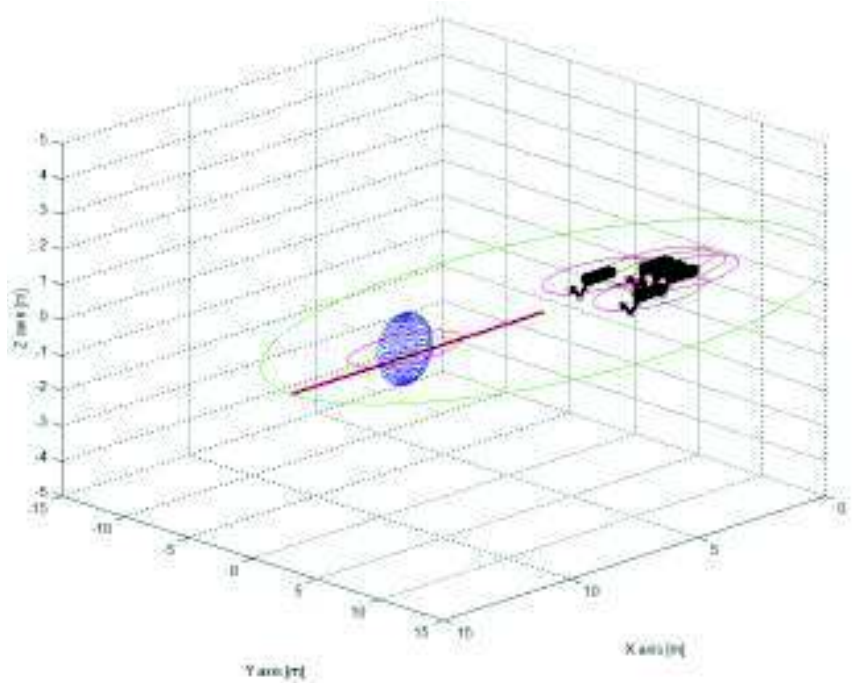

Figure 7.8: Initial conditions of the I-AUVs swarm

behaviour of each vehicles in presence of an obstacle: as can be seen, the swarm is still started from the same initial conditions but the interactions with the obstacle modify the vehicle trajectories. In particular, in each vehicle, the yaw angle is quite nervous which is due to the obstacle's presence and of the close initial conditions between vehicles. The changes in the yaw angles after 10 s are caused by the circumnavigation of the obstacle.

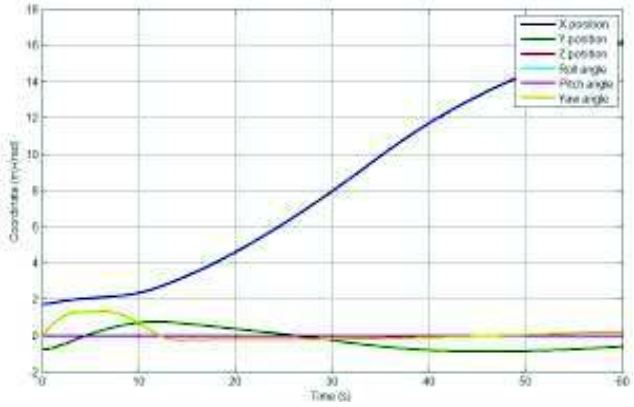


Figure 7.9: Vehicle 1: position and orientation

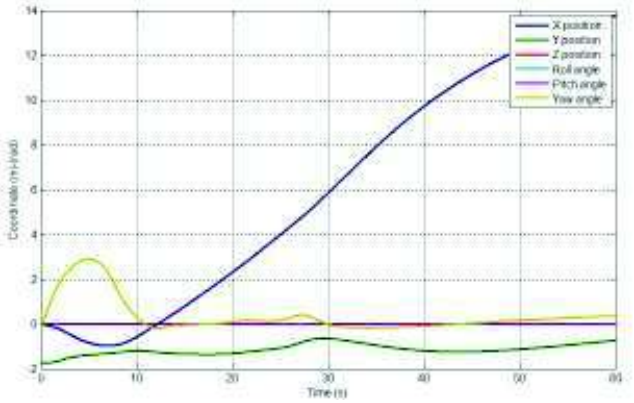


Figure 7.10: Vehicle 2: position and orientation

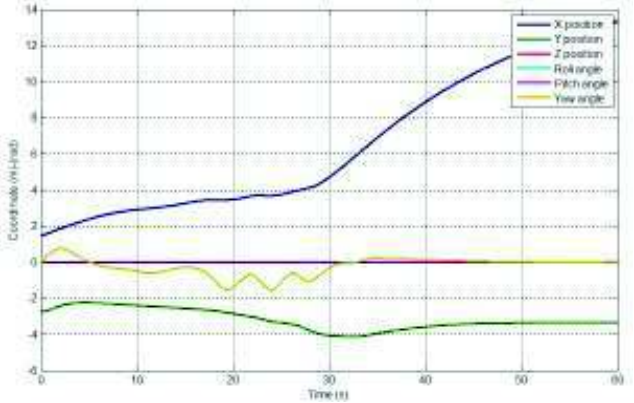


Figure 7.11: Vehicle 3: position and orientation

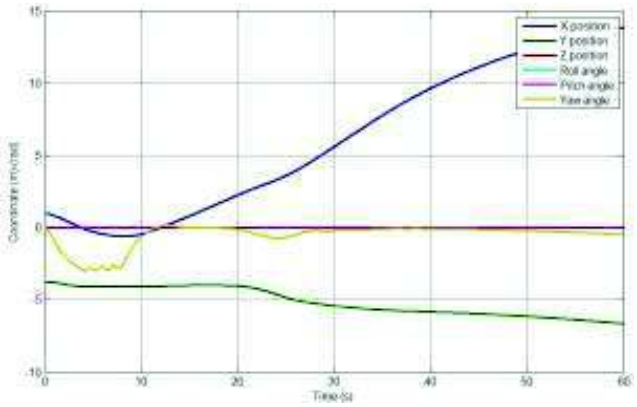


Figure 7.12: Vehicle 4: position and orientation

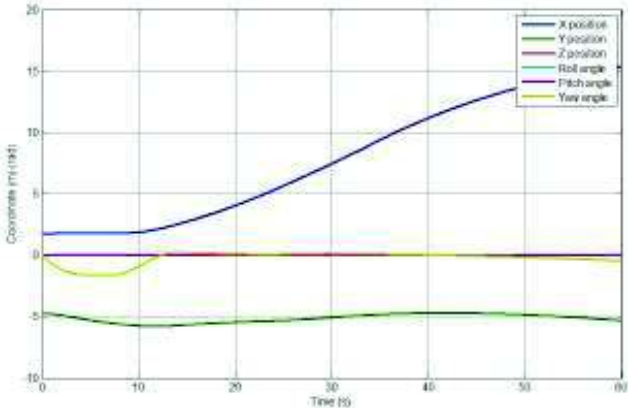


Figure 7.13: Vehicle 5: position and orientation

Finally, Figure 7.14 represents the final condition of the I-AUVs swarm, after the circumnavigation of the obstacle. It is worth to note the position of the vehicle in the XY plane: since the spherical shape of the swarm is moving, the vehicles are disposed along the semicircle.

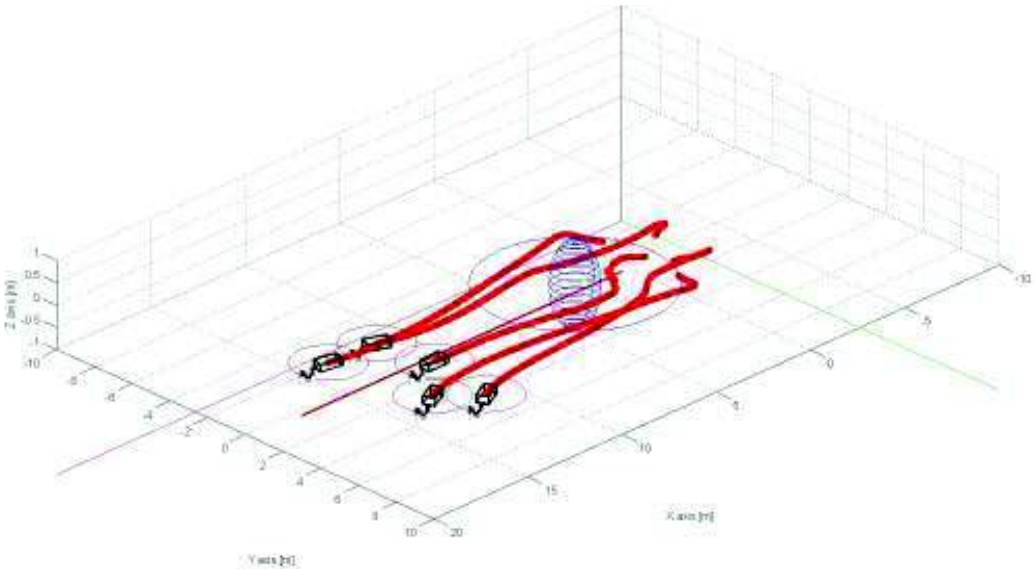

Figure 7.14: Final conditions of the I-AUVs swarm

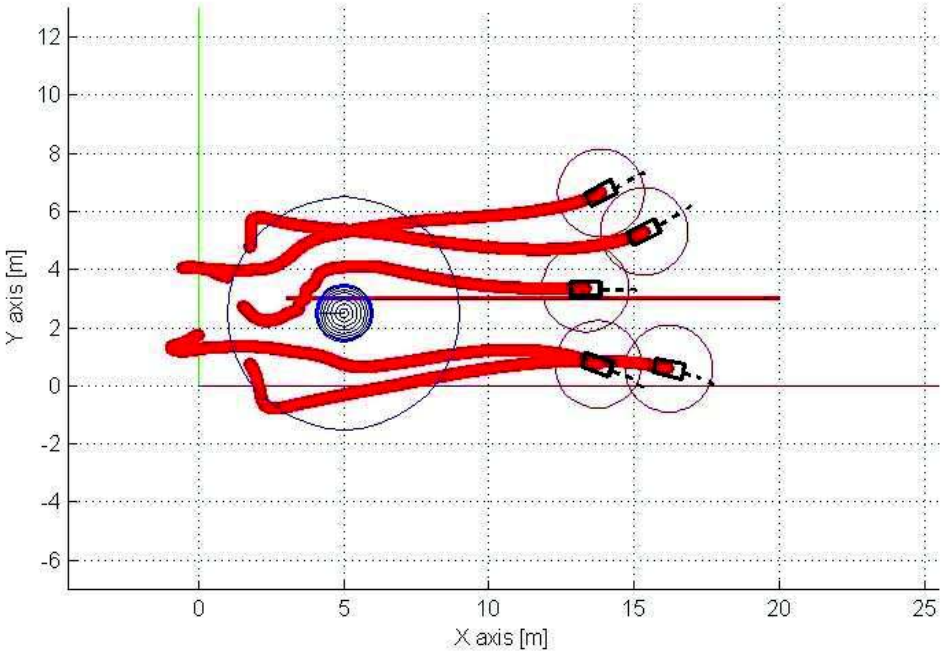


Figure 7.15: Final conditions of the I-AUVs swarm in the XY plane

## 7.3 Cooperative manipulation with obstacle avoidance

In this section, the preliminarily results of the cooperative manipulation with obstacle avoidance are shown. The cooperative mobile manipulation is performed by four I-AUVs placed at the four corners of the object. The trajectory is calculated by the sum of all contributes (Vehicle-Vehicle, Vehicle-Object, Vehicle-Environment potentials). The obstacle is modelled as a spherical shape. The robotic arms started from an initial position computed by the inverse differential kinematics algorithm to avoid singularity positions; the contribution of the Vehicle-Object potential is used to keep the end-effector pose in the proper workspace. In Figure 7.16, the initial positions of the vehicles are represented; in addition, the influence of the potentials are shown (the red circle is the Vehicle-Object potential and the green circle is the Vehicle-Vehicle one). The red line is the trajectory of the swarm caused by the swarm potential function.

Figure 7.17 shows a zoom of the initial poses of the vehicles.

Figures 7.18 to 7.21 describe the dynamical behaviour of each vehicles in presence both of an obstacle and of the object: the swarm is started from the initial conditions presented in Figure 7.16. It is worth to note the effect of the the obstacle presence: the y-coordinates are quite constant but in presence of

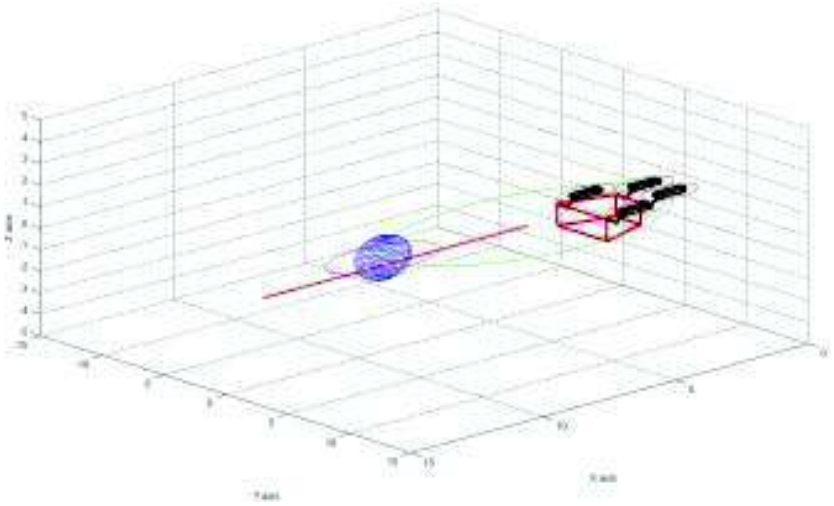

Figure 7.16: Initial conditions of the I-AUVs swarm with the object

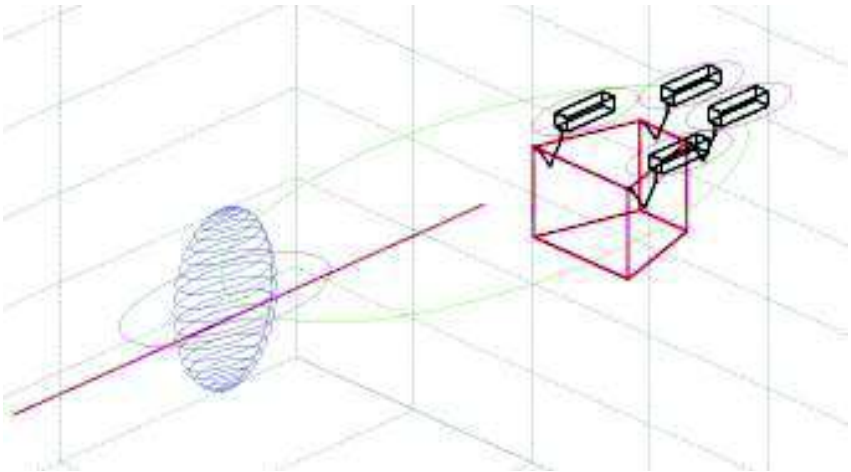

Figure 7.17: Zoom on the initial conditions of the I-AUVs swarm

the obstacle increase to keep away from the obstacle. The angular coordinates (roll, pitch and yaw) show the effect of the angular controllers; the results are quite encouraging because the errors are very low.

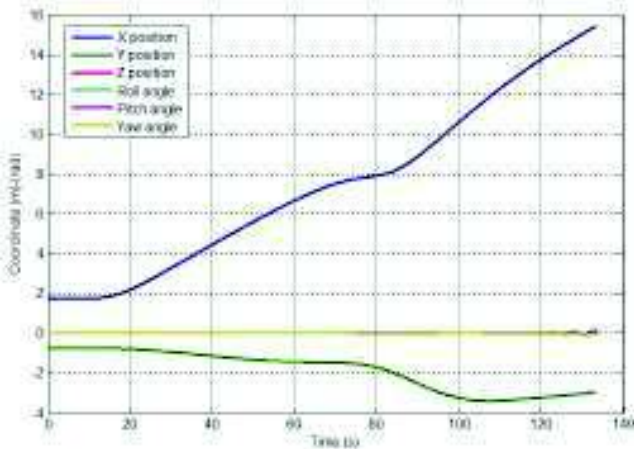


Figure 7.18: Vehicle 1: position and orientation

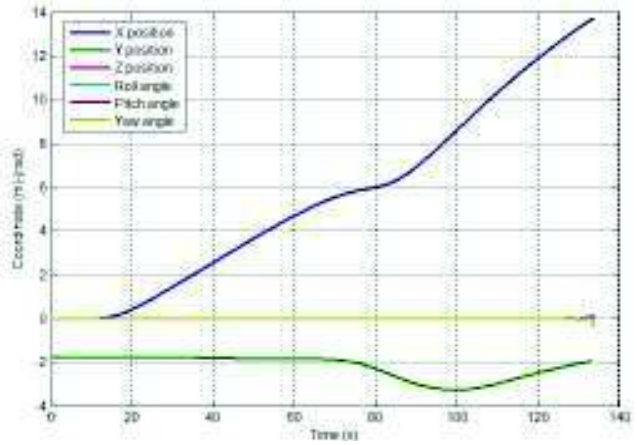


Figure 7.19: Vehicle 2: position and orientation

In conclusion, the Figure 7.22 represents the final condition of the I-AUVs swarm, after the obstacle avoidance phase; in addition, in Figure 7.23 it is worth to note the trajectory of the vehicles in the XY plane. The vehicles have not yet reached the swarm formation (the green circle). In addition, it is possible to evaluate the behaviour of the manipulated object, there are three different time instant shown on this figure: the blue object is at the beginning of the obstacle avoidance phase, the black object is at the maximum effect of the $V_{v-e}$ potential and, finally, the red object at the final situation of the swarm. As can be seen, in this case, also the interaction between object and obstacle is created due to the knowledge of the object and obstacle shapes.

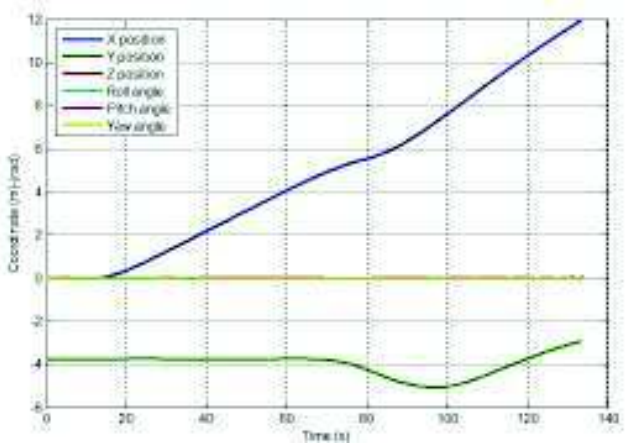


Figure 7.20: Vehicle 4: position and orientation

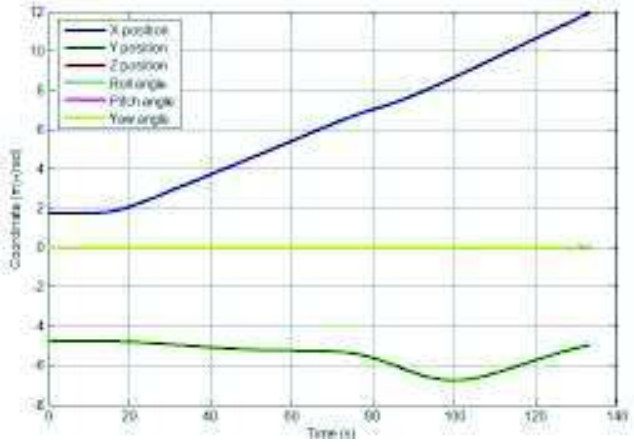


Figure 7.21: Vehicle 5: position and orientation

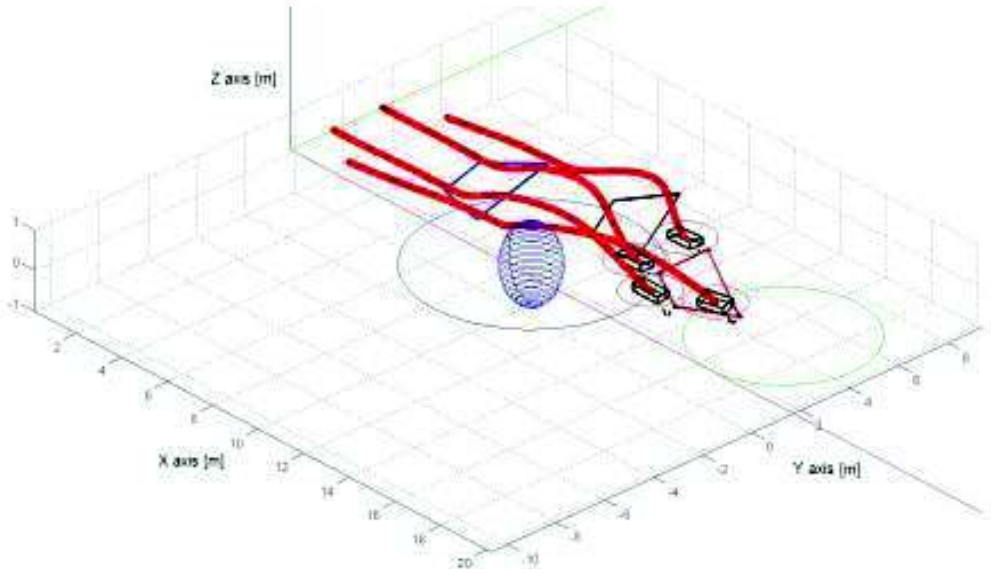


Figure 7.22: Final conditions of the I-AUVs swarm

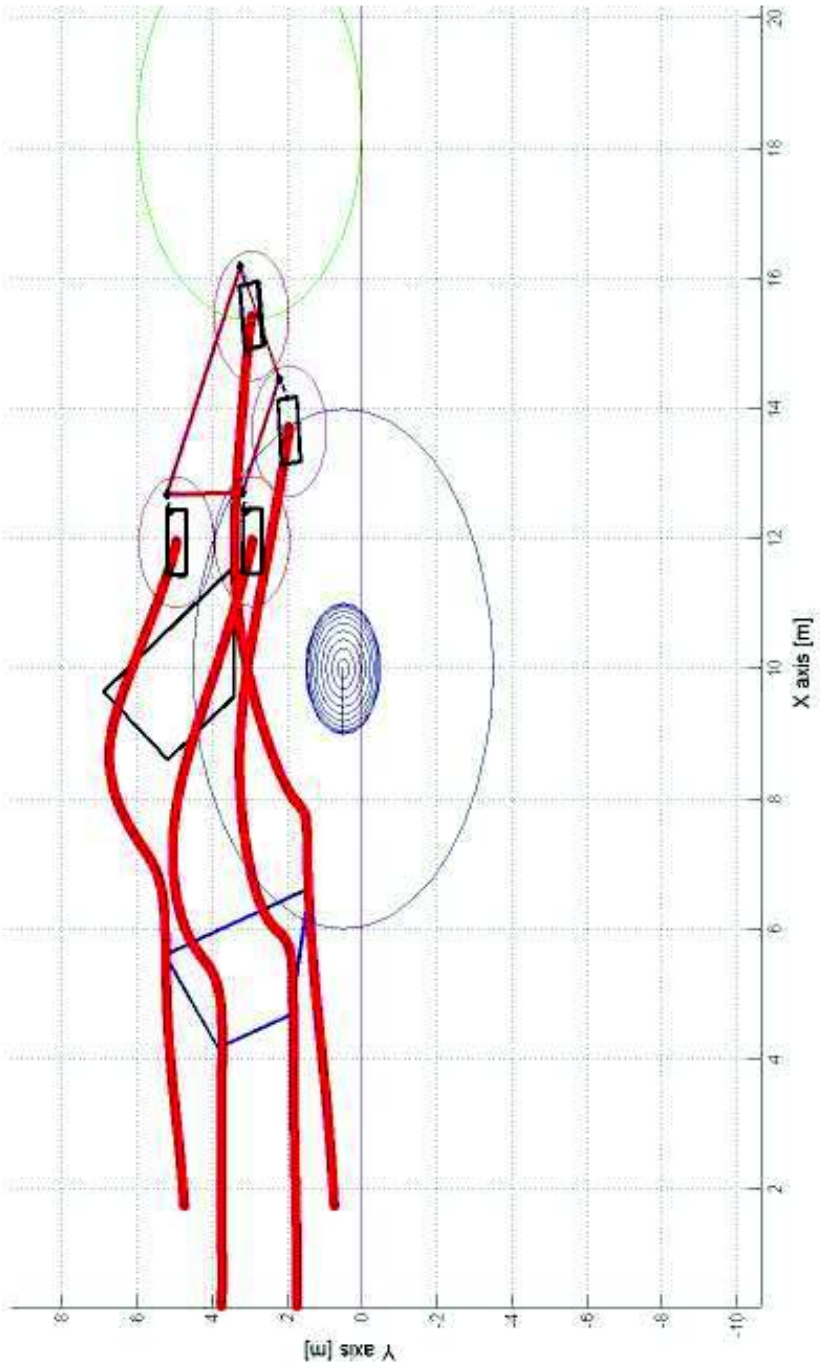


Figure 7.23: Final conditions of the I-AUVs swarm: XY plane

# Chapter 8

# Conclusions and future developments

The research activity presented in this Ph.D. dissertation concerned the development and control of a small and low cost AUV able to carry out both inspection and cooperative tasks. The main research fields of this thesis deals with both the Autonomous Underwater Vehicles (AUVs), in particular Intervention AUVs (I-AUVs) or Autonomous-Underwater Vehicle-Manipulator Systems (A-UVMSs), and the cooperative control strategy for mobile manipulation applied to the underwater environment. After a brief overview of the state of the art regarding I-AUVs and the cooperative architecture for mobile manipulation, the thesis can be conceptually divided into two main parts: the development and testing of the real AUV carried out at the Mechatronics and Dynamical Modelling Lab (University of Florence) and the analysis and simulation of an innovative cooperative control strategy based on the potential field method. The main idea that connects these two parts is the possibility to perform, through a completely decentralized approach (both in terms of control, of manipulation characteristics and of sensors), the same tasks carried out by a complex and expensive I-AUV. The second part can be seen as the possible evolution of the AUV presented in the first part which presupposes a re-design phase to introduce the robotic arm. This part is focused on the innovative control architecture based on the reduction of the necessary informations.
In the first part, the whole development of the small AUV is presented. The development of a complete simulation model (Chapter 1) is in parallel performed with the development of the real vehicle (Chapter 2) in order to test the control architecture and different control strategies (Chapter 3). The design of the vehicle in terms of mechanical analysis, of electronic devices and control systems is carried out. The vehicle is very compact and it is able to perform the following tasks:

- observation missions: the vehicle is provided of two fixed cameras (in front of the vehicle and in the bottom part) and a single beam echo-

sounder able to evaluate the distance from the objects;

- localization in structured environment: the vehicle allows the auto-localization in structured environment, e.g harbours, coastal areas, etc. through a relatively low cost system. The localization system is based on a single beam echo-sounder installed on a rotative shaft and on a localization algorithm;

- cooperative tasks: the vehicle is endowed by an acoustic modem able to communicate and to calculate the flying time.

The simulations for the testing phase are based on the European competition SAUC-e 2013, in which autonomous underwater vehicles developed by European universities and research centers, compete in different tasks. This year, the competition proposed four tasks: the validation task, the inspection of an underwater structure, the wall tracking in cooperation with an other AUV and an acoustic localization task. All these tasks are preliminarily simulated in order to test the control strategies and to analyse the real behaviour of the vehicle (Chapter 4). The modelling and simulation phase is realized through two steps using two different simulation environments: MATLAB®- Simulink environment, to easily test the control strategies, and ROS-UWsim one, to analyse the behaviour of the ROS control architecture.
The second part of the thesis deals with the development of cooperative control strategy for mobile manipulation. As introduced before, the thesis started from the idea to reduce both the complexity and the costs of the AUV parts; therefore, the same concept is applied to the study of an innovative cooperative mobile manipulation architecture where the reduction of the costs, of the sensors and of the controlled DOFs have more impact compared to a single I-AUV. In this context, using the knowledge acquired in the first part, some hypotheses are made to define the kinematical and the dynamical model of the A-UVMS (Chapter 5). In chapter 6, the innovative cooperative control strategy for mobile manipulation is presented. The cooperative control architecture is mainly based on the potential field method. Usually, the potential field method is used for obstacle avoidance tasks; the main idea of our innovative approach is to define different potential functions able to permit the cooperative manipulation of different I-AUVs. Finally, the whole manipulation task is performed as the sum of different contributions. The main advantages of this approach are the low number of necessary information coming from the other vehicles, the ability to dynamically react to the external environment changes and the possibility to scale the approach to a variable number of vehicles. This strategy is completely decentralized because it is only based on the local parameter knowledge: the idea is to use the acoustic modem capacity to approximatively calculate the distance from the other vehicles. Probably to obtain the distance vector, the vehicles will be equipped of acoustic modems able to communicate

and to localize with respect of a fixed vehicle (supervisor vehicle). The potential functions used in this strategy can be synthetically summarized into the following interactions: vehicle-vehicle interaction (based on the distance measurement between vehicles), vehicle-object interaction (based on the kinematical model of the robotic arm) and vehicle-environment interaction (based on both the rotating echo-sounder system and the localization algorithm). The interactions among these contributions allow the transportation of a generic object into an unknown environment. The preliminar results of the performed simulations have shown interesting features (Chapter 7).
As regards the future developments, one of this will be the introduction of a force algorithm able to better evaluate the proper actions on the object. Moreover, the advantages of the force feedback introduction are the improvement of the performed manipulation tasks, but the drawback is the difficulties in the measuring phase. The investigations about the manipulation tasks will be probably performed in a future National project started at the beginning of the 2014, in which the MDM Lab has to realize two cooperative robotic arms installed on an underwater vehicle. Currently, we can only test the algorithm for a single AUV; however, the cooperative control strategy based on potential field method can be better analysed through an experimental test campaign (not for mobile manipulation) carried out with the small MDM AUV and another AUV of the MDM Lab. In conclusion, numerical simulations with realistic modelling of the environment, of the object and of the vehicles can be made to better investigate this approach.

# Bibliography


[1] Fossen T., *Guidance and Control of Ocean Vehicles*, I Ed., John Wiley & Sons, Chichester UK, 1994.

[2] T. Tarn, G. Shoults. and S. Yang, *A dynamic model of an underwater vehicle with a robotic manipulator using kane's method*, Autonomous Robots, pp. 195- 282, 1996.

[3] Hildebrandt M., Christensen L., Kerdels J. et al., *Realtime Motion Compensation for ROV-based Tele-operated Underwater Manipulators*, IEEE Robotics & Automation Magazine, Bremen, 2009.

[4] G. Shoults, *Dynamics and Control of an Underwater Robotic Vehicle with an N-axis Manipulator*, Washington University: Ph.D Thesis, 1996.

[5] Christensen L., Kampmann P. et al., *Hardware ROV Simulation Facility for the Evaluation of novel Underwater Manipulation Techniques*, IEEE Robotics & Automation Magazine, Bremen, 2009.

[6] Siciliano B., Khatib O., *Handbook of Robotics*, Springer Handbooks, Napoli and Stanford, 2008.

[7] J. Kim, W. K. Chung, and J. Yuh, *Dynamic analysis and two-time scale control for Underwater vehicle manipulator systems*, in IEEE/RSJ Int. Conf on Intelligent Robots and Systems,pp. 577-582, 2003. Vol. 1.

[8] G. Antonelli, F. Caccavale, S. Chiaverini, and L. Villani, *Tracking control for underwater vehicle manipulator systems with velocity estimation*, IEEE Journal of Oceanic Engineering, vol. 25, no. 3, pp. 399-413, 2000.

[9] Y. Cui and N. Sarkar, *A unified force control approach to autonomous underwater manipulation*, Robotica, vol. 19, pp. 255-266, 2001.

[10] Y. Cui and J. Yuh, *A unified adaptive force control of underwater vehicle-manipulator systems (uvms)*, IEEE/RSJ Int. Conf on the Intelligent Robots and Systems,pp. 553-558, 2003.

[11] G. Antonelli, S. Chiaverini, *Fuzzy redundancy resolution and motion coordination for underwater vehicle-manipulator systems*, IEEE Transactions on Fuzzy Systems, vol. 11, no. 1, pp. 109-120, 2003.

[12] N. Sarkar and T. K. Podder, *Coordinated motion planning and control of autonomous underwater vehicle-manipulator systems subject to drag optimization*, IEEE Journal of Oceanic Engineering, vol. 26, no. 2, pp. 228-239, 2001.

[13] C. C. de Wit, E. O. Diaz, and M. Perrier, *Control of an underwater vehicle manipulator with composite dynamics*, Proc. of the American Control Conference,(Philadelphia, Pennsylvania), pp. 389-393, 1998.

[14] G. Antonelli, S. Chiaverini, *Adaptive tracking control of underwater vehicle-manipulator systems*, IEEE Int. Conf. on Control Applications, (Trieste, Italy), pp. 1089-1093, 1998.

[15] Antonelli G., *Underwater Robots*, Springer Tracts in Advanced Robotics, Springer-Verlag, 2nd edition, Heidelberg, 2006.

[16] Marani G., Choi S. K., Yuh J., *Underwater autonomous manipulation for intervention missions AUVs*, Ocean Engineering Journal, University of Hawaii, 2008.

[17] D. M. Lane, J. B. C. Davies, G. Casalino et al., *AMADEUS: Advanced MAnipulation for DEep Underwater Sampling*, IEEE Robotics & Automation Magazine, Universitat de Barcelona, 2009.

[18] Breivik M., Fossen T. I., *Giudance-Based Path Following for Autonomous Underwater Vehicles*, in Proceedings of the OCEANS'05, Washington D.C., USA, 2005.

[19] P. J. Sanz, P. Ridao, G. Oliver et al., *TRIDENT: a Framework for Autonomous Underwater Intervention Missions with Dexterous Manipulation Capabilities*, in the 7th Symposium on Intelligent Autonomous Vehicles, Lecce, 2010.

[20] O. Khatib, K. Yokoi, K. Chang, D. Ruspini, R. Holmberg, and A. Casal, *Vehicle/Arm Coordination and Multiple Mobile Manipulator*, Intelligent Robots and Systems, pp. 546 - 553 vol.2, 1996.

[21] H. G. Tanner, S. Loizou, and K. J. Kyriakopoulos, *Nonholonomic navigation and control of cooperating mobile manipulators*, IEEE Trans. Robot. Autom., vol. 19, no. 1, pp. 53–64, Feb. 2003.

[22] Yasuhisa Hirata, Youhei Kume, Zhi-Dong Wang, Kszuhiro Kosiige, *Coordinated Motion Control of Multiple Mobile Manipulators based on Virtual 3-D Caster*, International Conference on Robotics,Intelligent Systems and Signal Processing, pp. 19-24, October 2003.

[23] Y. Hirata, Y. Kume, T. Sawada, Z.Wang, and K. Kosuge, *Handling of an object by multiple mobile manipulators in coordination based on casterlike dynamics*, Proc. IEEE Int. Conf. Robot. Autom., vol. 26, pp. 807–812, 2004.

[24] Thomas G. Sugar and Vijay Kumar, *Vehicle/Arm Coordination and Multiple Mobile Manipulator*, IEEE Transactions on Robotics and Automation, vol. 18, no. 1, pp. 94-103, 2002.

[25] Xin Chen and Yangmin Li, *Cooperative Transportation by Multiple Mobile Manipulators Using Adaptive NN Control*, International Joint Conference on Neural Networks, pp. 4193-4200, 2006.

[26] Zhijun Lia, b, Shuzhi Sam Gea, , and Zhuping Wanga, *Robust adaptive control of coordinated multiple mobile manipulators*, Mechatronics Volume 18, Issues 5-6, Pages 239-250, June 2008.

[27] Zhijun Li, Pey Y. Tao, Shuzhi S. Ge, Martin Adams, and Wijerupage S, *Robust Adaptive Control of Cooperating Mobile Manipulators With Relative Motion*, IEEE Transactions on Systems, Man, and Cybernetics, Part B: Cybernetics, vol. 39, no. 1, pp. 103-116, 2009.

[28] Hao Su and Venkat Krovi, *Decentralized Dynamic Control of a Nonholonomic Mobile Manipulator Collective: a Simulation Study*, ASME Dynamic Systems and Control Conference, pp.1-8, USA 2008.

[29] Benedetto Allotta, Roberto Conti, Riccardo Costanzi, Francesca Giardi, Enrico Meli, Alessandro Ridolfi, *Modelling and Control of an Autonomous Underwater Vehicle for Mobile Manipulation*, proceedings of ECCOMAS World Conference 2013, Vienna 2013.

# List of Figures